Nonlinear Ship Motions by a Rankine Panel Method

by

Yifeng Huang

B.E., Naval Architecture & Ocean Engineering,
Shanghai Jiao Tong University, China, 1987
M.E., Mechanical Engineering, Florida Atlantic University, 1991

Submitted to the Department of Ocean Engineering
in partial fulfillment of the requirements for the degree of

Doctor of Philosophy in Hydrodynamics

at the

MASSACHUSETTS INSTITUTE OF TECHNOLOGY

February 1997

© Massachusetts Institute of Technology 1997. All rights reserved.

Author .....
Department of Ocean Engineering
December 16, 1996

Certified by .....
Paul D. Sclavounos
Professor of Naval Architecture
Thesis Supervisor

Accepted by .....
Professor J. Kim Vandiver
Chairman, Departmental Committee on Graduate Students

MASSACHUSETTS INSTITUTE
OF TECHNOLOGY

APR 29 1997

ARCHIVES

LIBRARIES

Nonlinear Ship Motions by a Rankine Panel Method

by

Yifeng Huang

Submitted to the Department of Ocean Engineering
on December 16, 1996, in partial fulfillment of the
requirements for the degree of
Doctor of Philosophy in Hydrodynamics

Abstract

A Weak-Scatterer theory for the calculation of motion responses of a ship traveling with a mean velocity in a heavy sea state is developed. In contrast to the classical linear theory, the amplitude of the incoming wave and the body motion is not restricted, while the ship-generated disturbances are assumed to be comparatively small. A boundary-integral formulation, based on the Rankine source Green function, is studied with focus on the treatment of large ambient waves and ship motions. A nonlinear equation of rigid body motion is derived.

A Rankine panel method, which has been developed for the frequency- and time-domain solution of three-dimensional ship flows, is improved and implemented for the study of nonlinear seakeeping problems. The enforcement of the exact body boundary conditions and the evaluation of the partial time-derivatives in the free surface conditions are examined. The free surface conditions are integrated with an Emplicit (Explicit-Implicit) Euler scheme and the nonlinear equation of motion is solved by a fourth-order predictor-corrector method. Founded upon a solid understanding of the numerical error propagation and stability properties, the numerical method has proven to be convergent, stable and accurate. Schemes necessary to make the method more efficient are also discussed.

Numerical computations of ship motions are performed for a variety of ships: a Series60 hull for method validation, two conventional containerships for practical applications. The numerical solutions offer a clear improvement over the linear theory and a quasi-nonlinear method, and are found to agree well with experiment measurements. The nonlinearities associated with steep ambient waves and ship hydrostatics are shown to be important in accurate predictions of ship motion responses.

Thesis Supervisor: Paul D. Sclavounos
Title: Professor of Naval Architecture

To Wen

Acknowledgments

This thesis is dedicated to my wife, Wen, for the unconditional love she has offered me since that miraculous November day, the unique perspective she has provided me as a woman, and the unwavering support she has given me. Without her company through all the triumphs and failures during the past five years, it would have been difficult for me to come this far. I am also deeply indebted to my parents, Deshuang Huang and Qiange Hong, and my brother, Yiming Huang, for their uplifting spirit and continuing concerns throughout all these years.

I am very thankful to my advisor, Professor Pavlos(Paul) D. Sclavounos, for his keen insight, clear guidance and warm encouragement. I hope I could one day emulate his professionalism and acquire his scientific research ability. His offer of a research assistantship five years ago also made it possible for me to pursue my dreams at this great Institution. I would like to thank Professors T. Francis Ogilvie and Dick K.P. Yue for serving on my thesis committee and showing interest in this research. Dr. David C. Kring deserves my special gratitude for his constant help and many good suggestions. My sincere appreciation goes to Drs. F. Thomas Korsmeyer and Torgeir Vada for taking pains to proofread the early drafts of this thesis. The excellent classes taught by Professor J. Nicholas Newman laid a solid foundation for me as a hydrodynamicist.

I wish to thank all the friends I have had for their help now and then. Especially, Dr. Zhiyong Xia is due my gratitude for the friendship we have enjoyed since our days in college. My thanks are directed to Dr. Yuming Liu, for the interesting discussions, sometimes heated arguments, we have had. People at the Department of Ocean Engineering of MIT, particularly at the Laboratory of Ship and Platform Flows, provide a great environment for scientific research and studies, and, I say thank you. Many thanks are extended to the basketball "gang", who let me slip away from the strenuous MIT life once a while and I hope we will continue our fun games.

Financial support has been provided by A.S. Veritas Research and the Office of Naval Research and is greatly appreciated.

Contents

1 Introduction **12**

1.1 Background 12

1.1.1 Linear Theory 15

1.1.2 Nonlinear Theory 18

1.2 Overview 21

2 Mathematical Formulation **23**

2.1 The Exact Boundary Value Problem 23

2.2 The Weak-Scatterer Formulation 27

2.2.1 Decompositions 28

2.2.2 Free Surface Conditions 29

2.2.3 Body Boundary Conditions 31

2.2.4 Boundary Value Problems 32

2.2.5 The Resultant Forces 34

2.2.6 The Equation of Motion 36

2.2.7 Time Derivatives 39

3 Numerical Algorithms **42**

3.1 Rankine Panel Method 42

3.1.1 Geometric Approximation 44

3.1.2 Oval-Type Grid Approximation 47

3.1.3 Numerical Issues 50

3.1.4 Temporal Integration 54

3.1.5 Numerical Filtering 60

4 Numerical Results **63**

4.1 Computer Implementation 63

4.2 Feasibility Study 66

4.2.1 Series60 (Block Coefficient 0.7) 67

4.2.2 SnowDrift (Ballast) 70

4.2.3 Steady Sinkage/Trim and Wave Elevation 74

4.3 Weak-Scatterer Computation 77

4.3.1 Validation of Body Boundary Conditions 77

4.3.2 Convergence Studies 81

4.3.3 Oval-Type Grid 88

4.3.4 Series60 (Block Coefficient 0.7) 94

4.3.5 SnowDrift (Ballast) 97

4.3.6 S7-175 Containership 100

4.3.7 Nonlinearities and Wave Patterns 103

5 Conclusions and Future Work **109**

A Discrete Integration Schemes and their Dispersion Relations **113**

B Generation of the Oval-Type Grid **115**

List of Figures

1-1 Counter Stern and Flared Bow Ship 14

2-1 Coordinate System 23

3-1 Typical Rectangular Computational Grid 46

3-2 Oval and rectangular grid. 48

3-3 Typical Oval-Type Computational Grid 49

3-4 Low-pass filters for spatial smoothing. The 7-point-modified filter is used in the present study 62

4-1 Work Flow Chart for the Weak-Scatterer Version of the SWAN2 Program. 65

4-2 Amplitude and phase of the heave response amplitude operator (RAO) for a Series60 ($C_b = 0.7$) hull at $\mathcal{F} = 0.2$ in head seas. 68

4-3 Amplitude and phase of the pitch response amplitude operator (RAO) for a Series60 ($C_b = 0.7$) hull at $\mathcal{F} = 0.2$ in head seas. 69

4-4 Body Plan for a Slender Container Vessel: SnowDrift. 71

4-5 Body Plan for a Container Vessel: S7-175. 71

4-6 Amplitude and phase of the heave response amplitude operator (RAO) for the SnowDrift ($D = 8(m)$) hull at $\mathcal{F} = 0.325$ in head seas. Demonstrates the importance of the nonlinearities associated with the nonlinear hydrostatic and Froude-Krylov forces. 72

4-7 Amplitude and phase of the pitch response amplitude operator (RAO) for the SnowDrift ($D = 8(m)$) hull at $\mathcal{F} = 0.325$ in head seas. Demonstrates the importance of the nonlinearities associated with the nonlinear hydrostatic and Froude-Krylov forces. 73

4-8 Amplitude and phase of the heave response amplitude operator (RAO) for the SnowDrift ($D = 8(m)$) hull at $\mathcal{F} = 0.325$ in head seas. Demonstrates the importance of the steady sinkage/trim and wave elevation. 75

4-9 Amplitude and phase of the pitch response amplitude operator (RAO) for the SnowDrift ($D = 8(m)$) hull at $\mathcal{F} = 0.325$ in head seas. Demonstrates the importance of the steady sinkage/trim and wave elevation. 76

4-10 Diagonal added mass and damping coefficients for the Series60 ($C_B = 0.7$) at $\mathcal{F} = 0.2$. 79

4-11 Cross-coupling added mass and damping coefficients for the Series60 ($C_B = 0.7$) at $\mathcal{F} = 0.2$. 80

4-12 Spatial convergence of heave and pitch motions for the SnowDrift hull (D=8m) at $\mathcal{F} = 0.325$ in incident head seas, at an encounter frequency of $\omega(L/g)^{1/2} = 3.408$. 83

4-13 Temporal convergence of heave and pitch motions for the SnowDrift hull (D=8m) at $\mathcal{F} = 0.325$ in incident head seas, at an encounter frequency of $\omega(L/g)^{1/2} = 3.408$. 84

4-14 Convergence of heave and pitch motions with respect to filtering frequency for S7-175 at $\mathcal{F} = 0.275$ in incident head seas, at an encounter frequency of $\omega(L/g)^{1/2} = 3.628$. 85

4-15 Convergence of heave and pitch motions with respect to beach size for S7-175 at $\mathcal{F} = 0.275$ in incident head seas, at an encounter frequency of $\omega(L/g)^{1/2} = 3.628$. 86

4-16 Convergence of heave and pitch motions with respect to beach starting point for S7-175 at $\mathcal{F} = 0.275$ in incident head seas, at an encounter frequency of $\omega(L/g)^{1/2} = 3.628$. 87

4-17 Constant domain width convergence of heave and pitch motions for the SnowDrift hull (D=8m) at $\mathcal{F} = 0.325$ in incident head seas, at an encounter frequency of $\omega(L/g)^{1/2} = 3.408$. 89
4-18 Whole domain width convergence of heave and pitch motions for the SnowDrift hull (D=8m) at $\mathcal{F} = 0.325$ in incident head seas, at an encounter frequency of $\omega(L/g)^{1/2} = 3.408$. 90
4-19 Constant domain spacing convergence of heave and pitch motions for the SnowDrift hull (D=8m) at $\mathcal{F} = 0.325$ in incident head seas at an encounter frequency of $\omega(L/g)^{1/2} = 3.408$. 91
4-20 Comparison between rectangular and oval free surface grid of heave motions for the SnowDrift hull (D=8m) at $\mathcal{F} = 0.325$ in incident head seas at an encounter frequency of $\omega(L/g)^{1/2} = 3.408$. 92
4-21 Comparison between rectangular and oval free surface grid of pitch motions for the SnowDrift hull (D=8m) at $\mathcal{F} = 0.325$ in incident head seas at an encounter frequency of $\omega(L/g)^{1/2} = 3.408$. 93
4-22 Amplitude and phase of the heave response amplitude operator (RAO) for the Series60 ($C_b = 0.7$) hull at $\mathcal{F} = 0.2$ in head seas. 95
4-23 Amplitude and phase of the pitch response amplitude operator (RAO) for the Series60 ($C_b = 0.7$) hull at $\mathcal{F} = 0.2$ in head seas. 96
4-24 Amplitude and phase of the heave response amplitude operator (RAO) for the SnowDrift ($D = 8(m)$) hull at $\mathcal{F} = 0.325$ in head seas. 98
4-25 Amplitude and phase of the pitch response amplitude operator (RAO) for the SnowDrift ($D = 8(m)$) hull at $\mathcal{F} = 0.325$ in head seas. 99
4-26 Amplitude and phase of the heave response amplitude operator (RAO) for the S7-175 Containership at $\mathcal{F} = 0.275$ in head seas. 101
4-27 Amplitude and phase of the pitch response amplitude operator (RAO) for the S7-175 Containership at $\mathcal{F} = 0.275$ in head seas. 102
4-28 Snapshots of hull positions for the S7-175 containership at $\mathcal{F} = 0.275$ in head seas. 104

4-29 Nonlinearities of motion RAO's for the S7-175 containership at $\mathcal{F} = 0.275$ at different incoming wave slopes. In head seas with the ratio of the wavelength over ship length at 1.25. 105

4-30 Disturbance wave patterns for the SnowDrift (ballast) containership at $\mathcal{F} = 0.325$. In head seas with the ratio of the wavelength over ship length $\lambda/L = 1.50$. 106

4-31 Disturbance wave patterns history for the SnowDrift (ballast) containership at $\mathcal{F} = 0.325$. In head seas with the ratio of the wavelength over ship length $\lambda/L = 1.50$. 107

4-32 Disturbance wave patterns history for the SnowDrift (ballast) containership at $\mathcal{F} = 0.325$. In head seas with the ratio of the wavelength over ship length $\lambda/L = 1.50$. 108

List of Tables

3.1 Savings of CPU hours and Memory storage between oval-type grid and rectangular grid. 48

Chapter 1

Introduction

1.1 Background

The ultimate criterion for a successful ship hull design is how economically and safely the ship travels in an unpredictable, sometimes hostile, ocean environment since any accident could mean a disaster for life, property and the environment. In practise, however, the design process for ships still relies primarily on semi-empirical rules and the designer's experience. These empirical designs do not always produce the most efficient ships. Furthermore, a semi-empirical approach would fail for a new ship concept since there is not much design experience available for such a ship. Therefore, a good naval architect should have a thorough understanding of ship motion responses.

Froude [14] and Krylov [31] were the first few scientists who studied hydrodynamic aspects of ship motions. But the equation of motion they derived consisted of only mass, linearized restoring forces, and the Froude-Krylov excitation force. This excitation force was obtained by integrating just the incident wave pressure over the still-water submerged ship surface. They did not or could not analyze the hydrodynamic disturbances associated with the presence of the ship hull because the theoretical understanding and computational capabilities available today did not exist at that time. A century later with increasingly powerful computers and sophisticated linear theory of ship motions (cf. Cummins [7], Wehausen [72], Ogilvie [53] and Newman

[51]), this thesis approaches the complete nonlinear problem of ship motions in steep ambient waves.

The complete problem of ship motions is fully nonlinear and strong nonlinearities exist in almost every phase of the problem.

- **Free Surface Nonlinearities**

  1. The free surface conditions are strongly nonlinear containing combination of nonlinear terms of unknown quantities and are applied on an unknown surface, which itself is a part of the solution.
  2. There may be nonlinear interactions among different wave frequency components in the form of energy inter-exchanges, that might result in the amplification of the amplitude of existing waves and/or the creation of new wave components.
  3. Nonlinear free surface dynamics sometimes corrects an unphysical behavior predicted by linear solutions. For instance, at the critical frequency $\tau_{cr} = \frac{1}{4}$, linear theory predicts that there would be energy concentration near the ship with disturbance waves possibly of infinite amplitude.

- **Body Nonlinearities**

  1. Inhomogeneous body boundary conditions imposed upon an unknown body surface introduce important nonlinear effects such as the interactions between the steady and unsteady wave flows. The leading order effects are approximated in linear theory in the form of the so-called m-term.
  2. Non-slender body shapes often induce non-negligible ship-generated disturbances. Oil tankers are the obvious examples that have large ratio of beam over length, which may cause large disturbances and sometimes flow separations.
  3. Abrupt geometric changes near the calm waterline such as prominently flared bow and overhanging counter-top stern as shown in Figure 1-1 add

nonlinear effects that may not be adequately accounted for by linear theory.

Geometric Nonlinearity

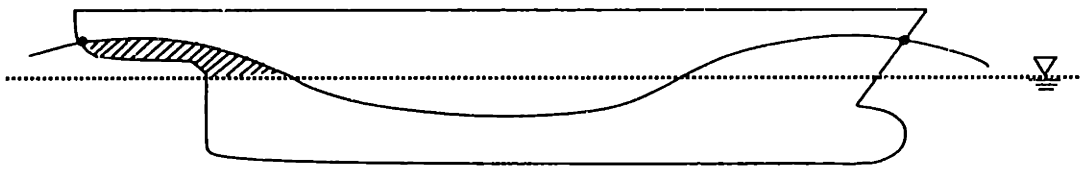

Counter Stern

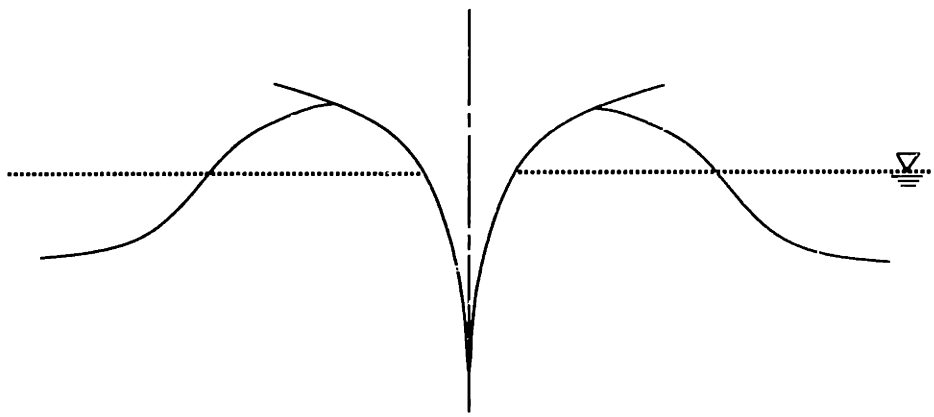

Flared Bow

Figure 1-1: Counter Stern and Flared Bow Ship

- **Other Nonlinearities**

  1. Bernoulli's equation used for calculating the hydrodynamic pressure contains quadratic terms of the gradients of the velocity potential.
  2. A ship traveling at speed of above 50 knots has long been the dream of naval architects and its study has been proposed around the industry

recently. Designing such a fast vessel requires sufficient understanding of the nonlinearities associated with high speed, slamming in particular.

3. The effect of viscosity on most water wave flows is negligible compared to that of the fluid inertia and gravity, and is therefore neglected in most hydrodynamics studies. But viscous damping could be very important in certain cases such as roll motions, especially at resonance in beam seas.

4. Shallow water makes surface waves non-dispersive and consequently causes a steep wave to steepen as it moves closer to sea shore. This introduces strong nonlinearities.

Summarizing the above, it is concluded that nonlinearities are essential in studies and designs of modern ships which often travel in heavy sea states and possess variety of geometric protrusions which cause linear theory to fail.

In occasions when a slender ship travels in a mild sea-state, linearization is nonetheless justifiable and linear theory produces reasonably accurate and practical predictions for ship motion responses, for example: the strip theory work by Korvin-Kroukovsky & Jacobs [26], Salvesen, Tuck & Faltinsen [59] and the linear numerical methods by Liapis [33], King, Beck & Magee [24], Bingham, Korsmeyer, Newman & Osborne [4], Sclavounos, Nakos & Huang [63].

In the following sections, the history of linear theory will be briefly reviewed along with the development of nonlinear ship wave theory. And finally, the structure of this thesis is outlined.

1.1.1 Linear Theory

The study of the linear theory of ship motion is founded upon the brilliant hypothesis of St. Denis and Pierson [11], namely the principle of superposition. They postulate that, at least for a long crested sea, the ship response to a random sea state may be represented by the summation of the ship response to each individual component wave. This theory allows us to reduce the stochastic ship motion problem in an

irregular sea to the deterministic ship motion problem in regular waves and thus greatly simplifies the problem.

Not satisfied with the simplistic approach of Froude [14] and Krylov [31], Michell [40] took the first significant step towards an account for the hydrodynamic disturbance due to a steadily translating vessel in his steady-state wave resistance theory. He drew his inspiration from thin-wing aerodynamics and developed a **thin ship theory**, where the ship is assumed to have vanishingly small beam compared to the ship length, draft, and ambient wavelength ($B \ll L, D, \lambda$). Peters and Stoker [57] extended this theory to include unsteady motions only to find non-resonant behavior of ship responses. Newman [47] adopted a more systematic perturbation scheme, which was able to reconcile the unphysical motion response predicted by Peters and Stoker's thin ship theory.

A typical ship or an aircraft is usually elongated with a beam and draft of the same order of magnitude and of one order smaller than the ship length ($B, D \ll L$). With the same geometric characteristics, both ship and aircraft may be considered slender bodies. It is possible to simplify the problem further by taking advantage of this unique shape.

Assuming short waves ($\lambda \ll L$), Lewis in 1929 [32] derived a **strip theory** to integrate the hydrodynamic forces longitudinally in terms of the two-dimensional quantities of each transverse section. This is another way to include the ship-generated disturbances that Froude and Krylov had neglected. Kovin-Kroukovsky and Jacobs [26] used numerical schemes to carry out the Lewis' integration and studied the ship motions for realistic ships. A systematic analysis of strip theory was carried out by Ogilvie and Tuck [54] and a rational approximation provided for the effects of the ship's forward speed.

Inspired by the development of the **slender body theory** in aerodynamics, Ursell [69], Newman & Tuck [48] and Maruo [37] studied the unsteady seakeeping problems

based on the assumption of long waves ($\lambda \ll L$).

In order to bridge the gap between the short wave approximation (strip theory) and long wave approximation (slender body theory), Newman [50] and Sclavounos [60] developed a unified theory, which accounts for three dimensionality in a more consistent manner than pure strip theory and slender-body theory.

Modern computer technology enables simulations of free surface flows around a realistic ship hull and greatly improves the accuracy of the predictions of linear ship motions. With the schemes of finite difference, finite element, and boundary element as the choices for the numerical algorithm, the boundary element method (panel method) has been established as a popular approach for free surface wave computations owing to its efficiency, accuracy and flexibility. Potential-flow-based panel methods are based on Green's theorem which relates properties of flows within the domain to domain boundary conditions. The pioneering work of Hess and Smith [18] broke the ground of panel methods in the numerical calculation and simulation of potential flows for bodies of general shapes. There are normally two types of approaches towards the numerical solution of free surface flows. The first one is to adopt linearized free surface wave Green function as the singularities distributed on the submerged hull surface and the uniform stream as the basis flow (cf. Liapis [33], King [23], Beck and Magee [2], Korsmeyer [25] and Bingham [5]). While this method is elegant in enforcing free surface conditions and radiation conditions (the linearized free surface conditions are satisfied automatically and there is no need to discretize the free surface domain), it is computationally expensive and difficult to extend the scheme to nonlinear solutions, due to the complexity of nonlinear free surface Green function (cf. Sclavounos [62]). The other approach, the Rankine Panel Method, was first introduced by Gadd [15] and Dawson [10], who employed the double-body flow as the basis for linearization, chosen primarily through physical intuition. The free surface is discretized into quadrilateral panels and covered by the Rankine sources and dipoles. This so-called Rankine Panel Method (RPM) provides much flexibility for different kinds of free surface formulations and numerical algorithms, and enjoys

great success in dealing with realistic ship hulls for the solution of both steady and unsteady wave flows (cf. Nakos [42], Raven [58], Jensen, Bertram and Söding [20], and Kring [27]). This thesis work is a continuation of the work by Nakos and Kring, an endeavor started a decade ago with the objective to simulate free surface flows around a realistic hull and produce accurate predictions for the steady and unsteady ship flow characteristics.

1.1.2 Nonlinear Theory

Despite the success linear theory has had, the linear dynamic-hydrodynamic analysis is only suitable for the design of geometrically simple ship hulls which sail in mild seas. If the concerned ships are equipped with prominent bow flares and overhanging counter-top sterns moving in a severe sea state with large amplitude of motion, neglecting nonlinearities might lead to large errors, if not grossly wrong predictions. Numerous authors have studied various nonlinear aspects of the problem with considerable success even though there has not been yet an exact three-dimensional solution.

The theoretical solution of the nonlinear ship motion problem falls, as well, into two categories: analytical approach and numerical method. The analytical approach is mainly based on a systematic expansion of power series in wave amplitude or other relatively small quantities such as the beam/length ratio. The free surface conditions are grouped in terms of the order of ε, denoting the small quantity in the expansion. By equating terms with the same order of magnitude on both sides of the equations, the free surface conditions, that are valid up to that specific order of ε, are obtained. The classical linear theory is the first-order approximation. Sclavounos [62] used this approach and derived second-order radiation and diffraction free surface Green functions which are the fundamental quantities in the solution of boundary element methods. Kim and Yue [21] [22] took the same path and rendered the complete second-order diffraction solution of axisymmetric body in monochromatic and bichromatic incident waves. For more detailed development on the second-order wave-body interaction theory prior to these two papers, Ogilvie's review in 1983 [55] is a good

reference. This series expansion approach is mainly used in the investigations of the interactions between waves and zero-speed or slow-speed translating bodies because it is only possible to reduce the complexity of the second-order free surface conditions that consist of quadratic terms of linear velocity potential and its gradients in the slow-speed regime, and there are needs for the study of slow drift motion and drift damping in the offshore industry. In problems with significant forward speed, a direct numerical method seems to be a more promising scheme for both steady wave resistance and unsteady seakeeping studies.

In their seminal work, Longuet-Higgins and Cokelet [36] carried out two-dimensional, fully nonlinear free surface wave simulations by use of the so-called Mixed-Eulerian-Lagrangian (MEL) method. This tracks the fluid particles on the free surface with the time evolution and solves an Eulerian boundary value problem for the flow quantities. Vinje and Brevig [71] followed with the extension of the method to two-dimensional wave-body nonlinear interactions. The two-dimensional nonlinear bow flows were studied in the same spirit by Grosenbaugh and Yeung [17]. With the rapid advance in computer capabilities and development in numerical algorithms, Xü and Yue [73] adopted a similar initial boundary element method (IBEM) and successfully conducted a three-dimensional, fully overturning, breaking wave simulation. The scheme was further developed to study the nonlinear three-dimensional interaction between water waves and a surface-piercing body by Xue and Yue [74]. While the Mixed-Eulerian-Lagrangian method has enjoyed success in the simulations of detailed and localized flows such as wave overturning and breaking, it might be prohibitively expensive in terms of computational cost and difficult to deal with bodies of general shapes translating with forward speeds.

The Eulerian Rankine Panel Method however offers an alternative method for the solution of nonlinear seakeeping problems. It retains a large degree of computation efficiency and obtains accurate predictions of global fluid flows and force quantities with the limitation that it is not able to simulate some extreme events such as slamming and deck wetness. van Daalen [8] wrote a thesis about the numerical and theoretical

studies of water waves and floating bodies. The study by Beck, Cao, and Lee [3] pointed out the importance of working in the time domain for the nonlinear problems. Maskew [38] has obtained some interesting results in the time-domain nonlinear simulations for ship motions. Lin and Yue [34] implemented a so-called body-exact numerical method to simulate free surface flows with large-amplitude body motions. They used LINEARIZED free surface Green function with the enforcement of the exact body boundary conditions and produced some good results. But their approach does not account for the nonlinear hydrodynamic effects.

High-order spectral method has also been used by many researchers (cf. Dommermuth & Yue [12], Zakharov [75], Fornberg & Whitham [13], and Liu & Yue [35]), for solving nonlinear free surface wave problems. The spectral method is very efficient and accurate, but it requires a periodical free surface conditions and relatively simple geometries.

Pawlowski [56] proposed a Weak-Scatterer hypothesis to treat the large amplitude ship motions in heavy seas. In the hypothesis, only the ship-generated disturbances are assumed to be small and linearizable about the **large** amplitude SHIP MOTIONS and INCOMING WAVES. This theory is practical and useful, because it allows us to isolate and quantify the nonlinearities associated with steep ambient waves and large body motions. The advantage of this approach is that it offers a more exact solution, but one that is still simplified enough to retain some degree of linearity in the free surface conditions. In view of these, this thesis is going to adopt this hypothesis and address primarily the nonlinearities associated with large body motions and steep incoming waves while keeping some linear aspects of the formulation, in order to improve motion response predictions. Even though it does not include all nonlinearities mentioned above and is not a fully nonlinear solution of the ship motion problem, this model captures most significant nonlinearities affecting ship motions. Moreover, it achieves a good solution with numerical efficiency and control. And also, most ships are designed to be slender and therefore not to cause large wave disturbances even for large motions. The computer program derived from this theory will be a

valuable tool for computational analysis in contemporary conventional ship designs. Evidently, this Weak-Scatterer hypothesis is violated in the vicinity of the ship waterline where strong spray roots are often seen to form, caused by the ship forward motion or slamming. These effects are however not treated in this thesis.

1.2 Overview

The aim of this thesis is to study three-dimensional nonlinear ship waves based on the Weak-Scatterer hypothesis and produce a numerical method that simulates time domain nonlinear free surface flows for wide range of ships and predicts the motions in random sea state. Practical needs are emphasized, but with thorough investigation of theoretical and numerical aspects of the problem.

Building upon the solid foundation of the linear free surface flow simulation, and numerical error analysis, the solution of nonlinear hydrodynamic problems is sought in this work, in order to compute the motion amplitude and the external force on the ship, which is translating with a uniform speed and oscillating in six-degrees-of-freedom. The sea state, unlike linear theory, is not limited to small incoming wave amplitude and the ship motion is not necessarily small, as long as the disturbance waves remain linearizable. This is the essence of the so-called Weak-Scatterer theory. Under this interpretation of free surface flows, some degree of efficiency and simplicity are retained, while the nonlinearities associated with steep ambient waves and large ship motions are included.

Chapter 2 covers the analytical formulation of the problem, beginning with the exact (within the potential theory context) formulation for the free surface ship wave problem. The rationale of the Weak-Scatterer theory is then described and the corresponding approximate formulations for the free surface ship wave problem are stated. After carefully examining the boundary conditions, the boundary integral equation is formulated along with the expression for the forces acting on the ship. The nonlinear equation of motion is integrated numerically to obtain the motion responses of the

ship in a sea state.

Chapter 3 discusses the numerical aspects of the solution. The comparison of two different free surface discretizations: rectangular and oval-type, is investigated. Because of the discretization and truncation of the free surface, wave absorbing beaches at all edges of the computational domain are implemented and related issues are examined. A special filtering device is designed to take out the spurious numerical wave components in order to prevent those waves from polluting the real physical solution. The temporal integration algorithms for the free surface conditions and the equation of motion are analyzed. The criteria of stability and accuracy are considered.

Chapter 4 illustrates the results obtained by the aforementioned analytical formulations and numerical methods. Forced motion computations are first conducted to validate the treatment of the body boundary conditions. Then free motion simulations are carried out for three different hulls: a Series60 huli for method validation, containerships SnowDrift and S7-175 for practical applications. Comparisons with experimental measurements are shown.

Chapter 5 outlines the contributions of this thesis work and future topics of research.

Chapter 2

Mathematical Formulation

2.1 The Exact Boundary Value Problem

This thesis considers the solution of the problem of a freely floating ship advancing steadily in the presence of ambient waves.

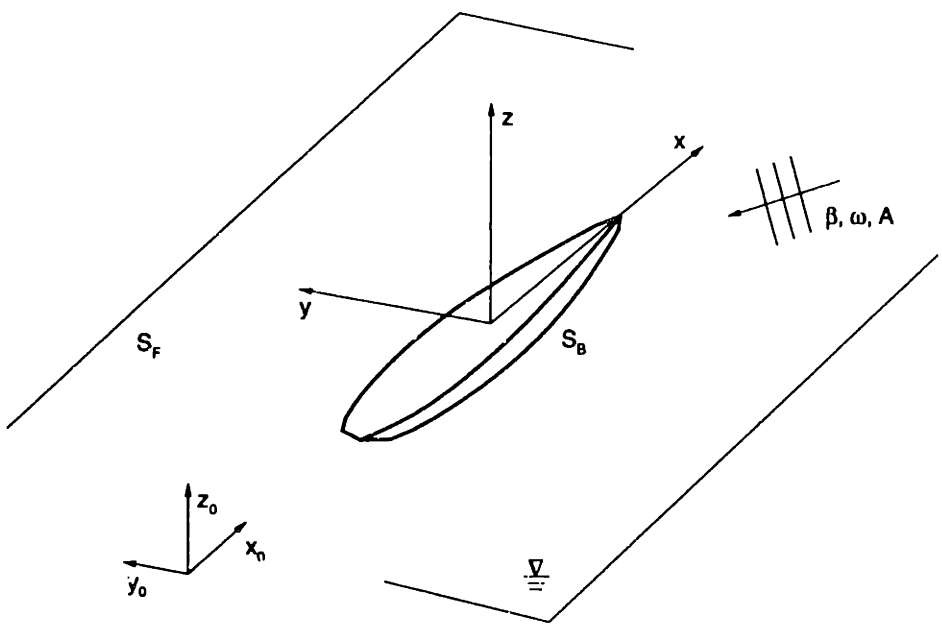

Figure 2-1: Coordinate System

Two reference systems will be utilized in this study of ship wave flows, as illustrated in Figure 2-1. The Cartesian coordinate system $\vec{x}_0 = (x_0, y_0, z_0)$ is fixed in space with the positive x_0-axis pointing upstream and the positive z_0-axis upwards. In this frame, the ship is translating with a constant speed U, while undergoing oscillatory motions about its calm water mean position. The other Cartesian coordinate system $\vec{x} = (x, y, z)$ has the same orientation as $\vec{x}_0$, but is fixed on the ship. Hereinafter, the physical problem will be described primarily in the coordinate system $\vec{x}$, and limited use of the system $\vec{x}_0$ will be made where appropriate.

The fluid is assumed to be ideal, so that it is inviscid and incompressible, and also the flow to be irrotational, so that there are no fluid separation and lifting effects. A total disturbance velocity potential $\Psi(\vec{x}, t)$ is hence introduced which is harmonic in the fluid domain. In accordance with the law of conservation of mass, the velocity potential Ψ is governed by the Laplace equation within the fluid,

$$\nabla^2\Psi(\vec{x}, t) = 0, \qquad \text{in the fluid domain.} \tag{2.1}$$

The disturbance flow velocity field $\vec{V}(\vec{x}, t)$ may be expressed as the gradient of the potential Ψ,

$$\begin{aligned} \vec{V}(\vec{x}, t) = \nabla\Psi(\vec{x}, t) &= \frac{\partial\Psi}{\partial x}\vec{i} + \frac{\partial\Psi}{\partial y}\vec{j} + \frac{\partial\Psi}{\partial z}\vec{k} \\ &= V_x\vec{i} + V_y\vec{j} + V_z\vec{k}. \end{aligned} \tag{2.2}$$

Here $\vec{i}, \vec{j}$ and $\vec{k}$ are the unit vectors corresponding to the Cartesian coordinate system $\vec{x}$. V_x, V_y, and V_z are the velocity components in the $\vec{i}, \vec{j}$ and $\vec{k}$ directions, respectively.

Applying the principle of conservation of momentum, the pressure field $p(\vec{x}, t)$ may be related to the flow kinematics. Bernoulli's equation, takes the form,

$$p - p_a = -\rho\left(\frac{\partial\Psi}{\partial t} + \frac{1}{2}\nabla\Psi \cdot \nabla\Psi + gz\right), \tag{2.3}$$

where ρ is the density of the fluid, g is the acceleration of gravity, and p_a is the

atmospheric pressure, which is taken as the reference pressure and assumed to be equal to zero because any constant would vanish after integration.

On all solid boundaries, the no-flux boundary conditions will be imposed. Without the fluid viscosity, the no-slip condition is not guaranteed. Thus on the submerged part of the ship, the normal component of the flow velocity is equal to that of the ship at the same location,

$$\frac{\partial \Psi}{\partial n} = \vec{V} \cdot \vec{n}, \tag{2.4}$$

where the normal vector $\vec{n}$ is defined by convention to point out of the fluid and into the body, and $\vec{V}$ is the total ship velocity.

In addition to the body boundaries, there is a free surface boundary. The free surface is considered as a 'material' surface, such that fluid particles, which are originally on the free surface, will remain on the surface for all later times. The Eulerian description of the flow is adopted in this thesis, so no overturning and breaking waves are allowed to exist. The total wave elevation $\eta(x, y, t)$, which defines the free surface position, is therefore a single-valued function of the coordinates x, y and time t. With this, a kinematic boundary condition is imposed on the free surface,

$$\frac{D}{Dt}[z - \eta(x_0, y_0, t)] = 0, \qquad \text{on the exact free surface.} \tag{2.5}$$

The dynamic condition on the free surface is that the fluid pressure is equal to the atmospheric pressure, i.e. zero. Surface tension effects are neglected for the length scale of interest in this study. By virtue of Bernoulli's equation (2.3), the condition is stated in the form,

$$\frac{\partial \Psi}{\partial t} + \frac{1}{2}\nabla\Psi \cdot \nabla\Psi + g\eta = 0, \qquad \text{on the exact free surface.} \tag{2.6}$$

Equations (2.5) and (2.6) need initially to be stated relative to the earth-fixed coordinate system $\vec{x}_0$, but in practise, the equations relative to the ship-fixed coordinate system $\vec{x}$ might be more useful. Thus via a Galilean transformation, the kinematic

and dynamic conditions (2.5) and (2.6) are transformed to as follows, respectively,

$$\left[\frac{\partial}{\partial t} - (\vec{U} - \nabla\Psi)\cdot\nabla\right]\eta = \frac{\partial\Psi}{\partial z}, \qquad \text{on the exact free surface.} \quad (2.7)$$

$$\left[\frac{\partial}{\partial t} - (\vec{U} - \nabla\Psi)\cdot\nabla\right]\Psi = \frac{1}{2}\nabla\Psi\cdot\nabla\Psi - g\eta, \qquad \text{on the exact free surface,} \quad (2.8)$$

where $\vec{U}$ is the translational speed of the ship.

In the far field, appropriate radiation conditions are necessary to ensure that the ship-generated waves propagate outwards. There have been no rigorous mathematical expression of the radiation conditions. Conventional hydrodynamics prescribes that the fluid flow is quiescent for *finite* time.

$$\nabla\Psi \longrightarrow 0, \qquad \text{at spatial infinity.} \quad (2.9)$$

The response of the physical system governed by the equations derived above should be causal and the solutions of these equations require initial conditions (cf. Wehausen & Laitone [72]). In this study, the initial state is defined so that the ship and fluid are at rest at the initial time, $t = 0$, such that:

$$\Psi = 0, \qquad z = 0, \quad (2.10)$$

$$\frac{\partial\Psi}{\partial t} = 0, \qquad z = 0. \quad (2.11)$$

And, this completes the exact formulation of the physical problem of a ship starting from rest and reaching a uniform speed in the presence of ambient waves. A more detailed discussion of the exact initial boundary value problem is presented in Wehausen & Laitone [72].

2.2 The Weak-Scatterer Formulation

The formulation derived in the previous section is exact within the scope of potential theory. It is however difficult and expensive at this point to solve this fully nonlinear free surface flow problem, because the free surface conditions are highly nonlinear, and worse yet, are imposed upon an unknown surface. So from the days of Michell in the late 19th century, researchers have been trying to find a linearized scheme that could produce the best simulation for realistic flows and be solvable. Many linear models have been developed with varied degrees of sophistication and success. But as described in the Introduction, pure linear theory often gives inadequate predictions of wave resistance, ship motions, and ship global structural loads. This work adopts the Weak-Scatterer hypothesis, as a balance between the exact and linear theories.

The so-called Weak-Scatterer hypothesis, in which the ship-generated disturbances due to forward translation and the ship's interactions with the ambient waves are much smaller than the ambient waves and the ship motions, was first proposed by Pawlowski [56] and has been inspired by numerous experimental observations. Most ships are designed to be slender in order to reduce wave resistance, in the sense that the longitudinal dimensions and their derivatives are much larger than the transverse ones, it is therefore physically justifiable to assume that the ship-generated disturbances are comparatively small, even with large amplitude ambient waves and ship motions. This is evident when looking at ship waves in a towing tank or in the ocean. This weakly-nonlinear approach improves upon the classical linear theory in that the magnitudes of incident waves and ship motions are no longer prescribed at the onset of the solution. Incident waves are primarily driven by the environmental conditions. The more severe the weather is, the larger the incident wave amplitude becomes. Hence it is not very reasonable in linear theory to restrict the magnitude of incident wave. For a slender ship, the disturbance caused by its movement could still be small even when the ship is undergoing a large motion. And this is obvious if imagining a knife-like ship moving up-down in the ocean. Those large disturbances that do exist, spray for instance, do not contribute significantly to global forces. Founded upon

this physical intuition, the Weak-Scatterer theory is therefore adopted in this thesis to linearize the ship-generated disturbances over the *steep* incoming waves with the *exact* statement of the body boundary conditions.

2.2.1 Decompositions

Under the assumptions of Weak-Scatterer hypothesis, the following decompositions for the total disturbance velocity potential Ψ and the total wave elevation η are postulated,

$$\Psi(\vec{x},t) = \Phi(\vec{x},t) + \phi(\vec{x},t) + \varphi_0(\vec{x},t) + \varphi(\vec{x},t), \tag{2.12}$$

$$\eta(x,y,t) = \zeta_0(x,y,t) + \zeta(x,y,t). \tag{2.13}$$

The double-body basis flow, Φ, is taken as the solution of the ship moving through a wavy solid boundary (no-flux on the surface), which is defined by the incoming incident wave. It is more or less related to the steady translation of the ship, nevertheless it is an *unsteady* quantity. This is in contrast to linear theory. The time-local flow, ϕ, is the solution of a pressure release problem and is used to take out the impulsive part of the problem. Its introduction is entirely motivated by the consideration of numerical stability and will be addressed more carefully in later sections. This quantity is mostly associated with the radiation part of the problem. φ_0 denotes the incident wave potential and ζ_0 is the incident wave elevation. φ and ζ stand for the remaining part of the total disturbance quantities: wave disturbance velocity potential and wave elevation, respectively. And, they are closely related to the wave generation and scattering due to the body.

In accordance with the Weak-Scatterer hypothesis, the basis flow, Φ, the time-local flow, ϕ, and the incident wave (φ_0, ζ_0) are assumed to be the dominant parts of the solution and the corrections (φ, ζ) to be small.

$$\Phi \sim \mathcal{O}(1); \quad \varphi_0 \sim \mathcal{O}(1); \quad \phi \sim \mathcal{O}(1); \quad \varphi \sim \mathcal{O}(\epsilon), \tag{2.14}$$

$$\zeta_0 \sim \mathcal{O}(1); \quad \zeta \sim \mathcal{O}(\epsilon), \tag{2.15}$$

where $\varepsilon \ll 1$, with ε denoting some form of small quantity, for example, the ratio of the ship beam over the ship length.

2.2.2 Free Surface Conditions

Applying the above decompositions (2.12,2.13) to the free surface conditions (2.7,2.8) and dropping the terms of $\mathcal{O}(\varepsilon^2)$, the free surface conditions become linearized over ε.

$$\begin{aligned}[\frac{\partial}{\partial t} - (\vec{U} - \nabla\Phi - \nabla\phi - \nabla\varphi_0)\cdot\nabla]\,\zeta = &-[\frac{\partial}{\partial t} - (\vec{U} - \nabla\Phi - \nabla\phi - \nabla\varphi_0)\cdot\nabla]\,\zeta_0 + \frac{\partial\varphi_0}{\partial z} \\ &+\frac{\partial\Phi}{\partial z} + \frac{\partial\phi}{\partial z} + \frac{\partial\varphi}{\partial z} - \nabla\varphi\cdot\nabla\zeta_0, \\ &\text{on} \quad z = \eta(x,y,t),\end{aligned} \tag{2.16}$$

$$\begin{aligned}[\frac{\partial}{\partial t} - (\vec{U} - \nabla\Phi - \nabla\phi - \nabla\varphi_0)\cdot\nabla]\,\varphi = &-[\frac{\partial}{\partial t} - (\vec{U} - \nabla\Phi - \nabla\phi - \nabla\varphi_0)\cdot\nabla]\,\varphi_0 \\ &+\frac{1}{2}\nabla\varphi_0\cdot\nabla\varphi_0 - g\zeta_0 \\ &-[\frac{\partial}{\partial t} - (\vec{U} - \nabla\Phi)\cdot\nabla]\,\Phi + \frac{1}{2}\nabla\Phi\cdot\nabla\Phi \\ &-[\frac{\partial}{\partial t} - (\vec{U} - \nabla\Phi - \nabla\phi)\cdot\nabla]\,\phi \\ &+\frac{1}{2}\nabla\phi\cdot\nabla\phi - g\zeta, \\ &\text{on} \quad z = \eta(x,y,t).\end{aligned} \tag{2.17}$$

Note that the conditions are applied on the surface of $z = \eta$. Since the scattered waves are assumed to be small and the boundary value problem is solved on an incident wave free surface, another step is needed to transfer the conditions from $z = \eta(x,y,t)$ to $z = \zeta_0(x,y,t)$, using Taylor expansion. Thus it reads,

$$
\begin{aligned}
[\frac{\partial}{\partial t} - (\vec{U} - \nabla\Phi - \nabla\phi - \nabla\varphi_0)\cdot\nabla]\,\zeta = & -[\frac{\partial}{\partial t} - (\vec{U} - \nabla\Phi - \nabla\phi - \nabla\varphi_0)\cdot\nabla]\,\zeta_0 + \frac{\partial\varphi_0}{\partial z} \\
& + \frac{\partial\Phi}{\partial z} + \frac{\partial\phi}{\partial z} + \frac{\partial\varphi}{\partial z} - \nabla\varphi\cdot\nabla\zeta_0 \\
& + [\frac{\partial^2\Phi}{\partial z^2} + \frac{\partial^2\varphi_0}{\partial z^2} - \nabla(\frac{\partial\Phi}{\partial z} + \frac{\partial\varphi_0}{\partial z})\cdot\nabla\zeta_0]\,\zeta, \\
& \qquad\qquad \text{on} \quad z = \zeta_0(x,y,t),
\end{aligned}
\tag{2.18}
$$

$$
\begin{aligned}
[\frac{\partial}{\partial t} - (\vec{U} - \nabla\Phi - \nabla\phi - \nabla\varphi_0)\cdot\nabla]\,\varphi = & -[\frac{\partial}{\partial t} - (\vec{U} - \nabla\Phi - \nabla\phi - \nabla\varphi_0)\cdot\nabla]\,\varphi_0 \\
& + \frac{1}{2}\nabla\varphi_0\cdot\nabla\varphi_0 - g\zeta_0 \\
& - [\frac{\partial}{\partial t} - (\vec{U} - \nabla\Phi)\cdot\nabla]\,\Phi + \frac{1}{2}\nabla\Phi\cdot\nabla\Phi \\
& - [\frac{\partial}{\partial t} - (\vec{U} - \nabla\Phi - \nabla\phi)\cdot\nabla]\,\phi \\
& + \frac{1}{2}\nabla\phi\cdot\nabla\phi - g\zeta \\
& - [\frac{\partial}{\partial t} - (\vec{U} - \nabla\Phi - \nabla\phi - \nabla\varphi_0)\cdot\nabla]\,\frac{\partial\Phi}{\partial z}\zeta \\
& - [\frac{\partial}{\partial t} - (\vec{U} - \nabla\Phi - \nabla\phi - \nabla\varphi_0)\cdot\nabla]\,\frac{\partial\phi}{\partial z}\zeta \\
& - [\frac{\partial}{\partial t} - (\vec{U} - \nabla\Phi - \nabla\phi - \nabla\varphi_0)\cdot\nabla]\,\frac{\partial\varphi_0}{\partial z}\zeta, \\
& \qquad\qquad \text{on} \quad z = \zeta_0(x,y,t).
\end{aligned}
\tag{2.19}
$$

Omitting all terms of $\mathcal{O}(\varepsilon^2)$, and transferring the conditions further from the free surface of $z = \zeta_0$ to the calm surface $z = 0$, it is easily seen that the above conditions reduce to the linearized free surface conditions based on the double-body linearization. Note that setting $\Phi = 0$ simplifies the equations further to the Neumann-Kelvin formulation, if also transferring the conditions from the surface of $z = \zeta_0$ to $z = 0$. These free surface conditions are valid for any incoming waves, plane progressive wave or Stokes wave. The kinematic free surface condition (2.18) could be further simplified for plane progressive waves.

2.2.3 Body Boundary Conditions

The body boundary conditions are applied on the instantaneous position of the submerged body surface, determined by the intersection of incident wave profile and the instantaneous position of body boundary. The boundary conditions are stated so that the normal component of the fluid velocity is equal to that of the body velocity, which is composed of steady velocity U and oscillatory velocity $\partial\delta/\partial t$,

$$\frac{\partial \Psi}{\partial n} = \vec{U} \cdot \vec{n} + \frac{\partial \vec{\delta}}{\partial t} \cdot \vec{n}, \qquad \text{on } S_B, \tag{2.20}$$

where $\vec{\delta}$ is the oscillatory displacement of the ship and is defined as follows,

$$\vec{\delta} = \vec{\xi}_T + \vec{\xi}_R \times \vec{x}, \tag{2.21}$$

where $\vec{\xi}_T$ is the translational displacement and $\vec{\xi}_R$ is the rotational displacement. $\vec{x}$ is the position vectors of a point on the ship relative to the ship-fixed coordinate system $\vec{x}$.

Plugging in the velocity potential decomposition (2.12) leads to,

$$\frac{\partial \Phi}{\partial n} = \vec{U} \cdot \vec{n}, \qquad \text{on } S_B, \tag{2.22}$$

$$\frac{\partial \phi}{\partial n} = \frac{\partial \vec{\delta}}{\partial t} \cdot \vec{n}, \qquad \text{on } S_B, \tag{2.23}$$

$$\frac{\partial \varphi}{\partial n} = -\frac{\partial \varphi_0}{\partial n}, \qquad \text{on } S_B. \tag{2.24}$$

From these equations, it is clear that the basis flow Φ mostly takes care of the "steady" (not time-independent since the normal vector $\vec{n}$ is time-dependent) part of the flow, the time-local flow ϕ deals with the radiation part and the disturbance flow φ accounts for the scattering part. Please note that these categorizations are not as clear-cut as in the classical linear theory because of the nonlinearity. In free motion simulations, it is very important to have the time-local flow extract the impulsive part of the flow

so that the numerical stability is ensured.

The so-called m-terms in the linear theory, resulting from the linearization of the body boundary conditions and accounting for the interactions between the steady and the oscillatory flows, do not explicitly appear in this formulation, because the satisfaction of the exact body boundary conditions *automatically* includes the m-term effects. In Chapter 4, computations will be shown confirming that this statement is indeed valid.

2.2.4 Boundary Value Problems

All velocity potentials should satisfy the Laplace equation and this will be enforced through Green's second identity, that leads to a boundary integral equation consisting of the integration of unknowns. The Rankine source is chosen in this work as the Green function,

$$G(\vec{x},\vec{\xi}) = \frac{1}{2\pi}\frac{1}{|\vec{x}-\vec{\xi}|}. \tag{2.25}$$

The nonlinear free surface Green function would satisfy the free surface conditions and radiation conditions, and eliminate the need to discretize the free surface. However, this Green function would be complicated and the integral kernel would be too difficult and expensive to evaluate. Just looking at the second order free surface conditions (cf. Sclavounos [62]) is more than enough to deter us from taking this route. In contrast, the panel method based upon the Rankine source is much simpler and more straightforward due to its flexibility in different free surface formulations and its ease to evaluate the integral, albeit panels have to be distributed on the free surface and numerical beaches implemented to enforce the radiation conditions.

The resulting integral equation reads as follows,

$$\Psi(\vec{x}) + \iint_{S_F \cup S_B} \Psi(\vec{\xi})\frac{G(\vec{x},\vec{\xi})}{\partial n_{\vec{\xi}}} - \iint_{S_F \cup S_B} \frac{\partial \Psi(\vec{\xi})}{\partial n_{\vec{\xi}}} G(\vec{x},\vec{\xi}) = 0, \tag{2.26}$$

where $\vec{x}$ denotes the coordinates of the field point and $\vec{\xi}$ the coordinates of the source point, S_F indicates the truncated free surface and S_B the submerged body surface.

Note that Ψ is not just the total flow, rather it symbolizes all the velocity potentials involved.

There are three separate boundary value problems, which must be solved for the basis flow, Φ, the time-local flow, ϕ, and the disturbance flow, φ. They are outlined below.

Basis Flow

The double-body basis flow is actually a free-surface-no-flux basis flow. It is the solution of the boundary value problem, which allows for no normal velocity cross the free surface. It is named as a double-body flow because it is historically related to the flow associated with a body with its image above the free surface advancing through an infinite fluid in linear theory. The free surface condition for this flow is,

$$\frac{\partial \Phi}{\partial n} = 0, \qquad \text{on} \quad z = \zeta_0, \tag{2.27}$$

and the body boundary condition is shown as in (2.22).

Time-Local Flow

The time-local flow must be solved when free floating simulations are of interest. This flow takes care of the impulsive and accelerative nature of the entire physical flow and accounts for the radiated waves from the body due to body motions. It could be included in the disturbance correction potential φ, but the numerical stability analysis by Kring [27] concludes that this impulsive nature of the fluid must be separated from the entire flow to avoid numerical instability in the integration of the equation of motion. For forced motion simulations, the separation of the time-local flow from the total flow, albeit not necessary, improves the conditioning of the resulting matrix, and in turn, the accuracy of solutions. Details will be discussed in the next chapter.

The boundary condition on the free surface is the pressure release condition — zero velocity potential.

$$\phi = 0, \qquad \text{on} \quad z = \zeta_0, \tag{2.28}$$

and the body boundary condition has been stated in the preceding section as shown in (2.23).

Disturbance Flow

The disturbance flow φ is solved as a solution of a mixed boundary value problem. The velocity potential on the free surface is obtained by the integration of the dynamic free surface condition (2.19) and the normal velocity on the submerged surface is prescribed by the body boundary condition (2.24). Therefore the boundary value problem is solved for the normal velocity on the free surface and the velocity potential on the submerged body surface.

2.2.5 The Resultant Forces

The velocity potentials and the normal velocities can be obtained either from the boundary conditions or from the solutions of the boundary value problems, outlined in the preceding subsection. The tangential velocities can be obtained analytically by a B-spline representation of the velocity potentials, which will be described in Chapter 3. Then the pressure can be easily derived from Bernoulli's equation (2.3), assuming the atmospheric pressure p_a to be zero,

$$p = -\rho\left(\frac{\partial \Psi}{\partial t} + \frac{1}{2}\nabla\Psi \cdot \nabla\Psi + gz\right). \tag{2.29}$$

Substituting in the decomposition of the velocity potential (2.12), it becomes,

$$p = p_l + p_m + p_c, \tag{2.30}$$

with each component written separately as,

$$p_l = -\rho\left\{\left[\frac{\partial}{\partial t} - (\vec{U} - \nabla\Phi - \nabla\phi - \nabla\varphi_0)\cdot\nabla\right]\phi - \frac{1}{2}\nabla\phi\cdot\nabla\phi\right\}, \tag{2.31}$$

$$p_m = -\rho \left[\frac{\partial}{\partial t} - (\vec{U} - \nabla\Phi - \nabla\phi - \nabla\varphi_0)\cdot\nabla\right]\varphi$$
$$-\rho\left\{\left[\frac{\partial}{\partial t} - (\vec{U} - \nabla\Phi - \nabla\varphi_0)\cdot\nabla\right]\varphi_0 - \frac{1}{2}\nabla\varphi_0\cdot\nabla\varphi_0\right\}$$
$$-\rho\left\{\left[\frac{\partial}{\partial t} - (\vec{U} - \nabla\Phi)\cdot\nabla\right]\Phi - \frac{1}{2}\nabla\Phi\cdot\nabla\Phi\right\}, \tag{2.32}$$

$$p_c = -\rho g z. \tag{2.33}$$

p_l, p_m and p_c denote local flow pressure, memory flow pressure and hydrostatic pressure, respectively. Again, the quadratic terms of φ and ζ have been dropped out in accordance with the Weak-Scatterer spirit. Thus the resultant generalized forces F_j, which include the forces F_1, F_2, F_3 along (x, y, z) respectively, and the moments F_4, F_5, F_6 about (x, y, z) respectively, can be obtained by integrating the pressure on the submerged part of the body surface. Of course, a momentum conservation analysis could have been used to calculate the generalized forces, but it would be complicated and inaccurate because of the use of numerical beaches in the far field. And it would be unnecessary as well since we have the pressure integration performed over the *exact* submerged surface of the ship, that should give us accurate results.

$$F_j = \iint_{S_B} p\, n_j\, dS, \qquad j = 1, 2, \ldots, 6, \tag{2.34}$$

where n_j is the generalized normal and defined as,

$$(n_1, n_2, n_3) = \vec{n},$$
$$(n_4, n_5, n_6) = \vec{x} \times \vec{n}. \tag{2.35}$$

The steady hydrostatic force, arising from part of the integration of p_c, is balanced by the propulsion force and the buoyancy force, and will not be used in the calculation. The unsteady hydrostatic force is known as the restoring force. The hydrodynamic force, integration of p_l and p_m, include the excitation force, resulting from the diffraction of incident waves, and the radiation force, originated from the free surface memory effects.

2.2.6 The Equation of Motion

Newton's law must initially be stated about the earth-fixed reference frame $\vec{x}_0$ and later be transferred to the desired reference frame. The conservation of linear momentum takes the form

$$\mathbf{M}\frac{d^2}{dt^2}(\vec{\xi}_T + \mathbf{T}\vec{x}_G) + \mathbf{C}(\vec{\xi}_T + \mathbf{T}\vec{x}_G) = \vec{F}, \tag{2.36}$$

where $\mathbf{M}$ is the mass matrix of the ship, $\mathbf{C}$ is the linearized restoring coefficient matrix, and the nonlinear components will be included in the force calculation. $\vec{x}_G$ is the coordinate of the center of gravity in the ship-fixed system $\vec{x}$ and $\vec{F}$ is the generalized force. $\vec{\xi}_T = (\xi_1, \xi_2, \xi_3)$ and $\vec{\xi}_R = (\xi_4, \xi_5, \xi_6)$ are formed by the translation and rotation of the body respectively. Sometimes $\vec{\xi}_R$ are also called the Euler angles. Then the nonlinear rotational matrix $\mathbf{T}$ is defined with the order of the Euler angles as (ξ_6, ξ_5, ξ_4),

$$\mathbf{T} = \begin{Bmatrix} \cos\xi_5\cos\xi_6 & -\cos\xi_4\sin\xi_6 + \sin\xi_4\sin\xi_5\cos\xi_6 & \sin\xi_4\sin\xi_6 + \cos\xi_4\sin\xi_5\cos\xi_6 \\ \cos\xi_5\sin\xi_6 & \cos\xi_4\cos\xi_6 + \sin\xi_4\sin\xi_5\sin\xi_6 & -\sin\xi_4\cos\xi_6 + \cos\xi_4\sin\xi_5\sin\xi_6 \\ -\sin\xi_5 & \sin\xi_4\cos\xi_5 & \cos\xi_4\cos\xi_6 \end{Bmatrix}, \tag{2.37}$$

and this matrix $\mathbf{T}$ is normal, such that its inverse is equal to its transpose, or

$$\mathbf{T}^{-1} = \mathbf{T}^T, \tag{2.38}$$

and for linearized rotation, i.e. small $\vec{\xi}_R$, the matrix $\mathbf{T}$ is reduced to

$$\mathbf{T} = \begin{Bmatrix} 1 & -\xi_6 & \xi_5 \\ \xi_6 & 1 & -\xi_4 \\ -\xi_5 & \xi_4 & 1 \end{Bmatrix}. \tag{2.39}$$

Denoting by $\vec{H}_G$ the angular momentum about the ship-fixed frame and by $\vec{M}_G$

the corresponding moment exerted by the fluid, the angular momentum conservation principle states that

$$\frac{d\vec{H}_G}{dt} = \frac{\partial \vec{H}_G}{\partial t} + \vec{\omega} \times \vec{H}_G = \vec{M}_G, \tag{2.40}$$

where ω is the angular velocity vector relative to the body-fixed axes and is defined as

$$\vec{\omega} = \mathbf{B}\vec{\alpha}, \tag{2.41}$$

with $\vec{\alpha}$ be the vector of the Euler angular velocities,

$$\vec{\alpha} = [\dot{\xi}_4,\ \dot{\xi}_5,\ \dot{\xi}_6]^T. \tag{2.42}$$

The matrix $\mathbf{B}$ is

$$\mathbf{B} = \begin{Bmatrix} \cos\xi_5 \cos\xi_6 & \sin\xi_6 & 0 \\ \cos\xi_5 \sin\xi_6 & \cos\xi_6 & 0 \\ -\sin\xi_5 & 0 & 1 \end{Bmatrix}, \tag{2.43}$$

and for small rotation, the matrix $\mathbf{B}$ becomes the unit matrix $\mathbf{I}$. The angular momentum principle may therefore be cast in the form

$$\mathbf{I}\frac{\partial \vec{\omega}}{\partial t} + \vec{\omega} \times \mathbf{I}\vec{\omega} + \mathbf{C}\mathbf{T}^T\vec{\xi}_R = \mathbf{T}^T\vec{M}_G, \tag{2.44}$$

where $\mathbf{C}$ represents the linearized rotational restoring coefficients. (2.36) and (2.44) thus complete the exact nonlinear statements of the linear and angular momentum conservation principles and from which the equations of motion can be derived to solve for the motion responses of the ship.

A displacement vector $\xi = (\vec{\xi}_T, \vec{\xi}_R)^T$ may be defined and the principle of conservation of momentum is restated in a more concise form,

$$\mathbf{M_N}\ \ddot{\vec{\xi}}(t) + \mathbf{C_N}\ \vec{\xi}(t) = \vec{F}(\ddot{\vec{\xi}}, \dot{\vec{\xi}}, \vec{\xi}, t), \tag{2.45}$$

where $\mathbf{M_N}$ and $\mathbf{C_N}$ indicate the nonlinear matrices for mass and restoring coefficients respectively and are reduced to their linear counterpart when the ship motions are

small. The numerical stability analysis presented in the next chapter dictates that the impulsive forces (the forces proportional to the acceleration) must be separated from the total force $\vec{F}$ (the right-hand-side of (2.45)). Consequently the velocity potential is decomposed into the time-local part and memory part as carried out in the previous formulation of the boundary value problems, and in turn, the total force is broken into a time-local force and a memory force. The time-local force is associated with the instantaneous fluid motion while the memory force results from the history of the wave propagation. With these considerations the equation of motion becomes,

$$(\mathbf{M_N} + a_0)\ddot{\vec{\xi}}(t) + b_0\dot{\vec{\xi}} + (\mathbf{C_N} + c_0)\vec{\xi}(t) = \vec{F}_m(\dot{\vec{\xi}}, \vec{\xi}, t), \tag{2.46}$$

where the matrix coefficients a_0, b_0 and c_0 represent the nonlinear time-local forces proportional to the acceleration $\ddot{\vec{\xi}}$, the velocity $\dot{\vec{\xi}}$ and the displacement $\vec{\xi}$, respectively.

Some previous work states the memory force $\vec{F}_m$ in a canonical form (cf. King [23], Bingham [5]), which uses the convolution integral to illustrate the wave propagation, or the memory effects in wave flows.

$$\vec{F}_m = \vec{X}(t) - \int_{-\infty}^{t} d\tau K(t-\tau)\dot{\vec{\xi}}(\tau), \tag{2.47}$$

where $\vec{X}(t)$ is the excitation force and $K(t)$ is the velocity impulse response function. The displacement impulse response function or acceleration impulse response function may also be used. In this nonlinear formulation, however, the force can not be decomposed in such a form since the linear superposition is not valid. Therefore in this work, the memory effect is retained directly through the solution of the wave patterns rather than a convolution of the response history.

In this thesis, studies of forced motion and free motion will be carried out. Forced motion is to restrict the ship to move in a prescribed mode, frequency and amplitude, so there is no need to solve the equation of motion. This allows for the comparison for the force coefficients between the extensive experimental data and numerical calculations so that the implementation of the method is validated. Free motion is to

allow the ship to move freely in six-degrees-of-freedom, so it requires the solution of the equation of motion. The ship motions in a steep wave are of course the ultimate goal of this study.

2.2.7 Time Derivatives

It is necessary to calculate the partial time derivatives of the velocity potentials throughout, i.e. in the dynamics of the free surface condition. This partial time derivatives could be evaluated by a finite difference formula, but numerical tests indicate that this often requires too small a time step to control the numerical error because panels are moving from one instant to another. To make the scheme more efficient, a boundary integral equation can be set up and solved for the partial time derivatives directly. This will incur some additional computational burden, but since it is not necessary to recompute the influence coefficients, it will offset the computation effort saved by the elimination of the need to decrease the time step if finite differences are used.

The Eulerian time derivatives of the velocity potentials $\partial\Psi/\partial t$ are, as a matter of fact, harmonic functions, therefore,

$$\nabla^2\Psi_t = 0, \tag{2.48}$$

where the subscript t indicates the partial derivative of time and Ψ here is just a symbol for velocity potential. Green's theorem is therefore directly applicable.

$$2\pi\Psi_t + \iint_{S_F\cup S_B} \Psi_t(\vec{\xi},t)\frac{\partial G(\vec{x},\vec{\xi})}{\partial n_\xi}dS_\xi = \iint_{S_F\cup S_B} \frac{\partial \Psi_t(\vec{\xi},t)}{\partial n_\xi}G(\vec{x},\vec{\xi})dS_\xi. \tag{2.49}$$

Numerical experiments show that the partial time derivative of the basis flow Φ is actually the most crucial and needs special care, while the partial time derivative of the wave flow ψ does not cause as much error. Thus the boundary integral equation (2.49) is used only for the calculation of Φ_t and a finite difference scheme is employed for the evaluation of ψ_t. The reason is that even though there is no need to set up the

left-hand side separately for the boundary integral equation (2.49), the calculation of the matrix still incurres some computational cost.

Consider the equality,

$$\frac{\partial}{\partial t}\frac{\partial \Phi}{\partial n} = \frac{\partial}{\partial t}(\nabla \Phi \cdot \vec{n}) = \nabla \Phi_t \cdot \vec{n} + \nabla \Phi \cdot \vec{n}_t. \tag{2.50}$$

Note that the normal vector $\vec{n}$ is a function of time, i.e.

$$\frac{\partial}{\partial t}\frac{\partial \Phi}{\partial n} \neq \frac{\partial}{\partial n}\frac{\partial \Phi}{\partial t}. \tag{2.51}$$

From (2.50), it follows that

$$\frac{\partial}{\partial n}\frac{\partial \Phi}{\partial t} = \frac{\partial}{\partial t}\frac{\partial \Phi}{\partial n} - \nabla \Phi \cdot \vec{n}_t. \tag{2.52}$$

The normal velocity of the basis flow Φ_n on the free surface equals zero because of the instantaneous no-flux condition, thus,

$$\frac{\partial}{\partial n}\frac{\partial \Phi}{\partial t} = -\nabla \Phi \cdot \vec{n}_t, \tag{2.53}$$

where the partial time derivative of the normal vector $\vec{n}_t$ may be easily computed since the free surface is prescribed by a known incoming wave. On the other hand, the normal velocity of the basis flow on the body may as well be computed from the body boundary condition (2.22),

$$\frac{\partial \Phi_t}{\partial n} = (\vec{U} - \nabla \Phi) \cdot \vec{n}_t. \tag{2.54}$$

The instantaneous normal vector $\vec{n}_t$ on the body surface is defined as,

$$\vec{n}_t = \mathbf{T}(t)\, \vec{n}_s. \tag{2.55}$$

where $\vec{n}_s$ is the time-independent normal vector to the hull and $\mathbf{T}(t)$ is the nonlinear rotational matrix defined in (2.37). With the knowledge of $\partial \Phi_t / \partial n$, the solution of the

boundary integral equations allows for the computation of the partial time derivative of the basis flow on the free surface and on the body surface.

Experience also shows that the following approximation does greatly improve the accurate evaluation of the partial time derivative. At each time step, the panels adjust their positions according to the ship motions and incident wave elevation. This displacement of panels is the most significant on the submerged body surface.

Define the so-called panel velocity $\vec{U}$,

$$\vec{U} = \frac{\vec{X} - \vec{X}_0}{\delta t}, \tag{2.56}$$

where $\vec{X}$ is the position of the ship at the present time and $\vec{X}_0$ is the position of the ship at the previous time step. Then, the Eulerian time derivative follows as:

$$\frac{\partial}{\partial t} = \frac{\partial}{\partial t}/_{panel} - \vec{U} \cdot \nabla, \tag{2.57}$$

$\frac{\partial}{\partial t}/_{panel}$ might be approximated by a finite difference scheme. This scheme improves the accuracy of the results while not increasing the computational burden.

Chapter 3

Numerical Algorithms

3.1 Rankine Panel Method

The Rankine Panel Method (RPM), which will be outlined in this chapter, was first designed for frequency domain linear solution for the interactions between a free surface and a steadily translating vessel, as originally developed by Sclavounos and Nakos [61], and, Nakos and Sclavounos [43]. It was later extended to time domain linear solution of the same problem by Nakos, Kring and Sclavounos [44]. The scheme has proven robust and accurate for linear solution in the above work. This linear time-domain method will in this thesis be improved and implemented for the solution of the nonlinear time-domain simulations of free surface ship waves.

Panel Methods, in general, are a subset of the boundary element method. The method takes advantage of Green's theorem to enforce the Laplace equation and results in the solution of a boundary integral equation, which governs the unknowns over the domain boundaries. Therefore it is only necessary to subdivide the boundary surfaces rather than the whole volume of the fluid domain. After obtaining the quantities of interest such as velocity potentials and normal velocities on the boundary surfaces, the quantities in the fluid domain are readily computed by an additional application of Green's identity.

On the discretized boundary surfaces, a distribution of singularities accounts for

the influence of the physical boundary. There are many choices for the Green function. Among the most commonly used are the free surface Green function and the Rankine Green function. The free surface Green function satisfies exactly the free surface conditions and the radiation conditions. One of the benefits is that only the submerged body surface boundary needs discretization. But it is very difficult to extend its success in linear problems to nonlinear problems because of the extreme complexity of the nonlinear free surface Green functions. One alternative is to distribute the so-called Rankine sources and dipoles on all boundary surfaces. This allows flexibility in the formulation of the free surface conditions so that nonlinear effects can be included efficiently. The disadvantage is that the free surface must be discretized as well, which introduces questions about numerical dispersion and dissipation, and also casts doubt on the enforcement of the radiation conditions. Because the goal in this work is to study the nonlinear free surface interactions with the translating body, the Rankine Panel Method, which is a panel method employing Rankine sources/dipoles as the Green function, is naturally chosen to be the numerical tool. The concerns about numerical dispersion, dissipation and radiation conditions will be addressed in later sections.

The time domain Rankine Panel Method consists also of a temporal integration of the free surface conditions to advance the wave simulation. At each time step, the so-called Emplicit scheme is used to integrate the free surface conditions (2.18)(2.19) to obtain the wave elevation and velocity potential over the free surface. The Emplicit scheme applies an explicit integration to the kinematic and implicit integration to the dynamic free surface condition. This combination of explicit and implicit schemes is shown in Vada and Nakos [70] to be stable and accurate. For a free motion simulation of a ship freely floating in six-degrees-of-freedom, the equation of motion is also numerically integrated to obtain the ship motion responses, by using the fourth order Adam-Bashford-Moulton (ABM) scheme with the fourth order Runge-Kutta scheme for the first four time steps. Kring and Sclavounos [28] proved that the scheme was stable and accurate as long as the ratio of time step and grid size is within a stability criterion.

3.1.1 Geometric Approximation

The numerical solution of a continuous problem entails the discretization of the fluid domain and proper representation of the unknown quantities on each individual grid point, or in this case, panel. As discussed above, only the fluid boundary surfaces need to be discretized by a collection of quadrilateral panels of mean spacings (h_x, h_y). The corner points of each panel are mapped to the plane that is determined by the mid-points of the line segments connecting the corner points. The panel is therefore a flat quadrilateral and geometrically constant. But the variation of the unknowns on the panel is expressed by a B-Spline scheme which enjoys great success in the field of Computer-Aided-Design (CAD). The unknown $\phi(x,y)$ (just a symbol, not necessarily the velocity potential) is approximated by a higher order polynomial in terms of basis function $B_j(x,y)$ with a finite number of degrees of freedom a_j:

$$\phi(x,y) \approx \sum_{j=-\infty}^{+\infty} a_j B_j^{(m,n)}(x,y) = \sum_{j=-\infty}^{+\infty} a_j b_j^{(m)}(x) b_j^{(n)}(y), \tag{3.1}$$

where the summation is carried over the vector index $j = (j_x, j_y)$, and $B_j^{(m,n)}$ is the two-dimensional basis function defined as the product of the basis functions in $x-$ and $y-$directions. The lowest order of the basis function $b^{(0)}(x)$ is defined as:

$$b^{(0)}(x) = \begin{cases} 1, & |x| \le h_x/2, \\ 0, & \text{otherwise.} \end{cases} \tag{3.2}$$

Higher order basis function $b^{(m)}(x)$ may be obtained from the convolution property (Trefethen [67]):

$$b^{(m)}(x) = \frac{1}{h_x} \int_{-\infty}^{\infty} d\xi \; b^{(m-1)}(\xi) \; b^{(0)}(x-\xi), \qquad \text{for } m \ge 1. \tag{3.3}$$

Using this representation for the solution $\phi(x,y)$, derivatives may be calculated analytically by differentiating m times in the $x-$direction and n times in the $y-$direction. This avoids the inaccurate and expensive finite difference approximation. In wave resistance and seakeeping problems, it is important to compute accurately the deriva-

tives up to the second order. Therefore, the bi-quadratic basis function $B^{(2,2)}(x,y)$ $(m = 2, n = 2)$, which provides the lowest order of approximation needed in this formulation, is chosen. The quadratic basis function $b^{(2)}(x)$ is written out as follows:

$$b^{(2)}(x) = \begin{cases} \frac{1}{2h_s^2}(x + \frac{3h_s}{2})^2, & -3h_s/2 < x < -h_s/2, \\ \frac{1}{h_s^2}(-x^2 + \frac{3h_s^2}{4}), & -h_s/2 < x < h_s/2, \\ \frac{1}{2h_s^2}(-x + \frac{3h_s}{2})^2, & h_s/2 < x < 3h_s/2. \end{cases} \tag{3.4}$$

It is important to note that the higher order approximation for the solution is being carried out on the grid with only one unknown corresponding to each panel. This is possible because the basis function is required to be a function of not only the unknown on the panel but also those on the neighboring panels. The higher the order of the basis function becomes, the more neighboring panels are needed. It is interesting to see that employment of $B^{(0,0)}(x,y)$ as the basis function will reduce the scheme to a piecewise constant approximation of the solution, which has been widely used since the days of Hess and Smith [18]. More details about this Rankine Panel Method can be found in the doctoral thesis of Nakos [42].

A typical computational grid is shown in Figure 3-1. It consists of panels on the submerged body surface, which is determined by the incident wave profile and the instantaneous position of the body, and the elevated free surface, which is prescribed by the incident wave profile. The panels are mostly flat quadrilaterals, but could also be triangular, especially near the ship ends. The original ship is shown with the bold line to demonstrate how much/little the ship might be wetted by water during the course of its movement. There are three spline sheets for each of the three unknowns on each panel, the velocity potential ϕ, the normal velocity ϕ_n and the wave elevation ζ, and they are defined as:

$$\phi(\vec{x},t) = \sum_{j=1}^{9} (\phi)_{(j)}(t) B_j^{(2,2)}(\vec{x}), \tag{3.5}$$

$$\phi_n(\vec{x},t) = \sum_{j=1}^{9} (\phi_n)_{(j)}(t) B_j^{(2,2)}(\vec{x}), \tag{3.6}$$

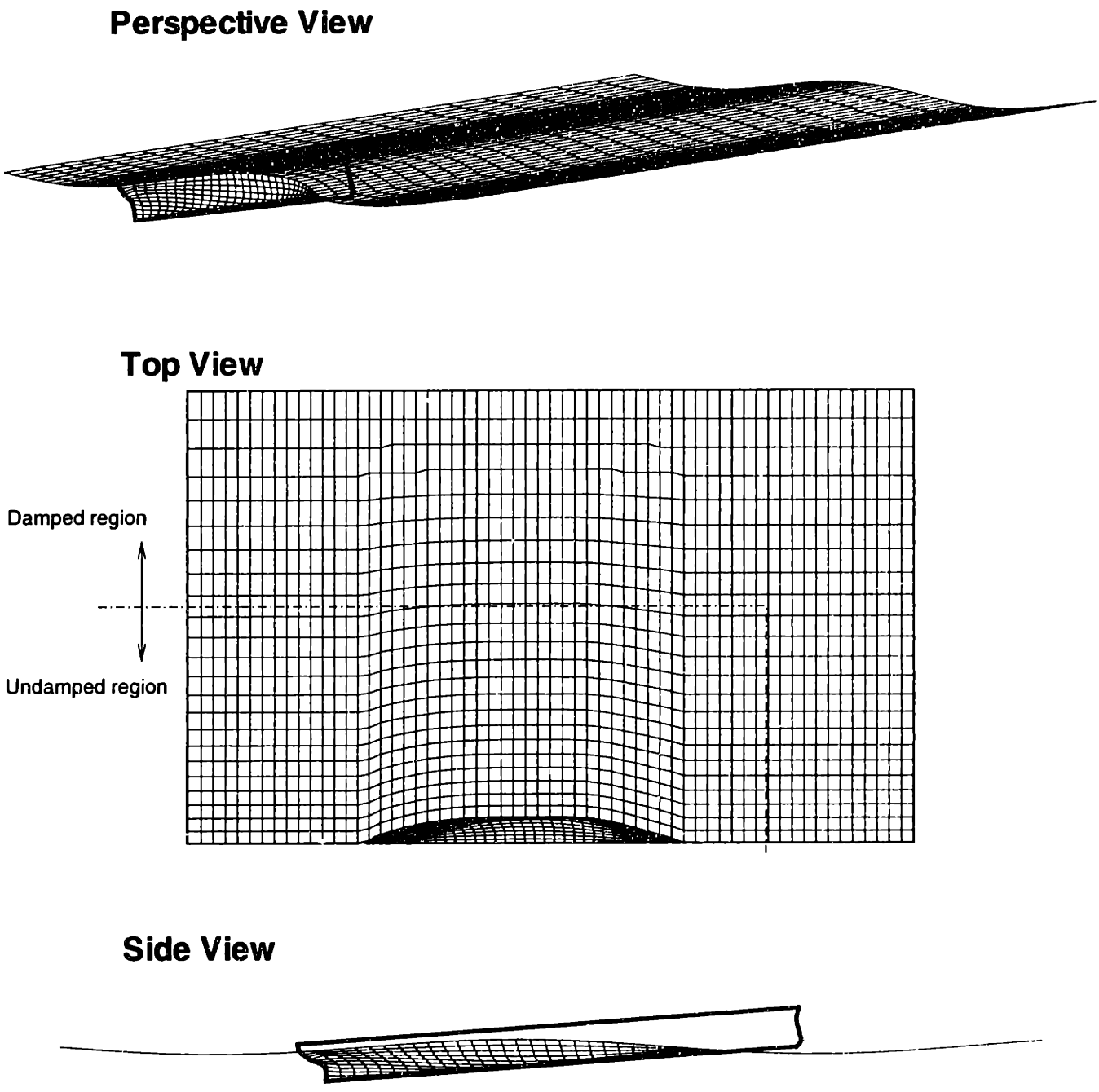

Figure 3-1: Typical Rectangular Computational Grid

$$\zeta(\vec{x},t) = \sum_{j=1}^{p}(\zeta)_{(j)}(t)B_j^{(2,2)}(\vec{x}), \tag{3.7}$$

where $(\phi)_j$, $(\phi_n)_j$ and $(\zeta)_j$ are the time-dependent spline coefficients for the unknowns and are the solutions of the system of linear equations. The spline representation of the unknowns may be stretched and twisted according to the panel shapes, so it is applicable for general shapes of body geometry. One additional strip of panels is used at each boundary edge to supply the necessary end conditions that close the spline representation of the solution.

While the fluid domain is presumed to extend to infinity, in numerical computations, the computation domain obviously has to be truncated to a finite extent to limit the computational cost. The truncation points are decided by numerical experimentations to account for the ship translation speed and the incoming wave length. Numerical cooling beaches are used to ensure minimum reflection of the disturbance waves at the truncated boundaries, and subsequently, the satisfaction of the radiation conditions. The mechanism of the numerical beach will be discussed in more detail later.

3.1.2 Oval-Type Grid Approximation

Previous versions of the SWAN program and the majority of other computer codes in this field are written for rectangular free surface grids as shown in Figure 3-1. The rectangular free surface grid is a most natural and popular selection because of its ease of setup and its accuracy in representing the trailing wave behind the ship. However according to numerical experience, the cluster of far-field panels near the centerline do not have large effects on the pressure integration over the hull surface. Hence, those far-field panels are not strictly necessary if only the computation of the forces on the ship is required, especially for short waves. This inspires the use of the so-called oval-type of free surface discretization, despite the fact that the system is elliptic. Chapter 4 will show that the rectangular grid and the oval-type grid virtually give the same predictions in terms of forces on the ship exerted by the flowing water

to justify the use of the oval-type grid.

Saving	Panel #	Ratio	CPU (hrs)	Ratio	Memory (MB)	Ratio
Rec. Grid	1954	1.30	52	1.93	94.1	1.47
Oval Grid	1504		27		63.9	

Table 3.1: Savings of CPU hours and Memory storage between oval-type grid and rectangular grid.

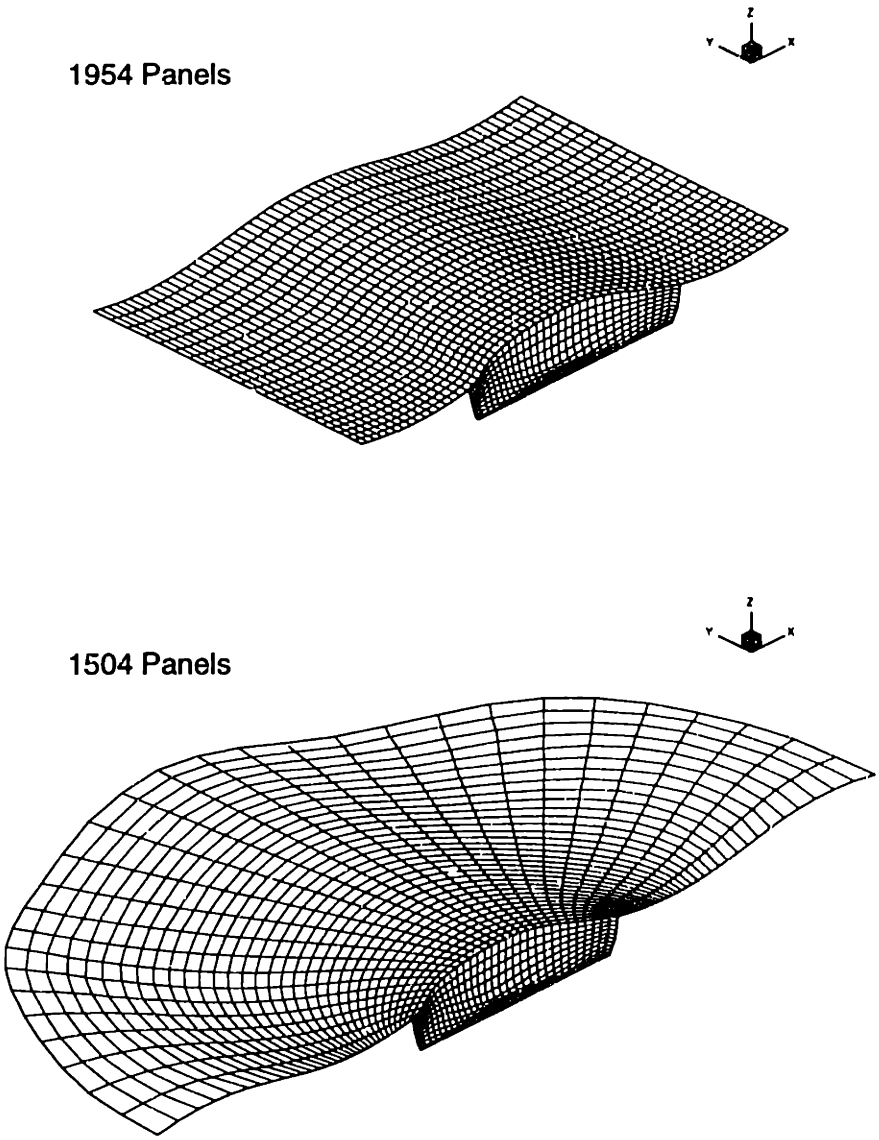

Figure 3-2: Oval and rectangular grid.

The idea of the oval-type grid is that in the vicinity of the ship, there is a higher density of panels to accurately simulate the fluid flow near the ship, while far from

the ship, there is a lesser density of panels. The grid spacings for panels expand from the ship. The whole free surface is divided into a constant panel inner region and varied-size panel outer region. The inner region is where the spacing of the panel is kept constant, while the outer region is where the spacing of the panel is exponentially varied according to an expansion ratio in a monotonic manner. A typical oval-type grid representation of the free surface is shown in Figure 3-3. The generation of the oval-type grid is discussed in Appendix B and more detail may be found in the book by Thompson, Warsi and Mastin [65].

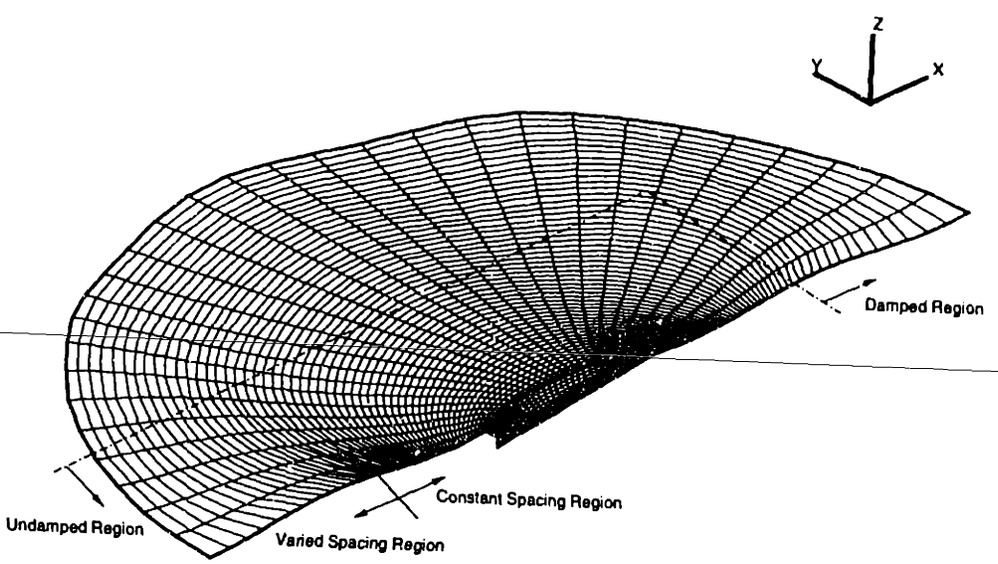

Figure 3-3: Typical Oval-Type Computational Grid

Table 3.1 demonstrates the benefit of the oval-type grid in terms of CPU cost and memory requirement. To attain the same accuracy in the solution, $N = 1954$ panels are needed on half of the computational domain if using the rectangular grid, only $N = 1504$ panels are needed (about 30% less) if using the oval-type grid. The saving in CPU usage is 93%, because the CPU requirement is in the order of between $\mathcal{O}(N^2)$ and $\mathcal{O}(N^3)$. The oval-type grid requires less memory by about 50% as well. For convergent results, more panels may be necessary and the savings of the oval-type

grid would be even more impressive. Therefore the oval-type grid should be adopted.

3.1.3 Numerical Issues

Discretization of the geometric domain will introduce a variety of numerical difficulties which call for careful treatment to prevent inaccurate solutions. The satisfaction of radiation conditions and the propagation of spurious wave components are among the most imperative. This section is going to address these two important numerical issues.

TRUNCATED DOMAIN AND RADIATION CONDITION

The computational domain has to be truncated some distance away from the wave-making source in order to keep the computational effort finite. As shown in Figures 3-1 and 3-3, the computation domain is truncated upstream, downstream and to the side. The extent of the domain is decided by numerical experimentation to model the ship flow over long time simulations and at the same time to minimize the computation cost. Any errors that might be introduced by this truncation in the form of wave reflections from the domain edges must be prevented from contaminating and eventually destroying the solution.

Because of the truncation of the computational domain, the Rankine Panel Method presents the difficulty of implementing radiation conditions, that require that disturbance waves be radiated outwards from the wave-making source. There are several ways to remedy the problem. One of them is adopted by Lin and Yue [34] in their body-exact solution of ship wave problems. The linearized free surface Green function satisfies exactly the linear free surface conditions and radiation conditions. So there is no need to distribute panels on the free surface $z = 0$. Consequently the radiation conditions are enforced automatically. But as pointed out before, the nonlinear free surface Green function is extremely complicated and difficult to evaluate by numerical means. It is therefore not suitable for the solution of nonlinear ship wave problems. A matching scheme could also be used by dividing the computational domain into two

parts, an inner nonlinear domain near the ship and an outer linear domain far from the ship. The reasoning for this scheme is that in the neighborhood of the ship the nonlinear effects are prominent and non-negligible, while away from the ship the nonlinear effects are largely diminished because three-dimensional waves would dissipate at the rate of $\mathcal{O}(\sqrt{R})$, where R is the radial distance between the field point and the ship. Thus it is conceivable to use the known linear solution to enforce the radiation conditions in the outer domain. Nevertheless, it is not easy at all to apply appropriate matching conditions at the matching boundaries and to deal with the reflection from the matching boundaries. The computational effort associated with such a hybrid scheme may be very significant. Hence numerical beaches will be adopted instead.

Numerical beaches were first proposed by Israeli and Orszag [19]. They were later successfully applied to the two-dimensional solution by Baker, Meiron & Orszag [1] and Cointe, Geyer, King, Molin & Tramoni [6], and three-dimensional ship wave problems by Nakos, Kring & Sclavounos [44]. A numerical beach functions exactly like the damping beach in a towing tank and absorbs disturbance waves keeping them from reflecting back. Numerically, a Newtonian cooling term is applied to the kinematic free surface condition to damp out all waves of wavelengths less than about twice the extent of the numerical beach. The cooling term physically corresponds to a mass sink over the free surface in order to minimize the waves near the edges of the domain. A Rayleigh viscosity term is also applied to eliminate artificial dispersive effects.

The scheme may be illustrated by considering only a linear solution. The linear flow ϕ within the beach section of the truncated free surface domain is the sum of the corresponding linear flow φ over the infinite free surface and a wave reflection error flow χ, of which φ satisfy the linearized free surface conditions,

$$\phi = \varphi + \chi, \tag{3.8}$$

and over the beach section of the truncated free surface space, it may be considered

as covered by a horizontal rigid lid, such that,

$$\phi_z = \varphi_z + \chi_z = 0. \tag{3.9}$$

Apply the linearized free surface condition to φ,

$$\chi_z = -\varphi_z = \frac{\varphi_{tt}}{g} = \frac{\phi_{tt} - \chi_{tt}}{g}. \tag{3.10}$$

Then the linearized free surface condition for the reflection flow χ within the beach section of the truncated free surface is derived as,

$$\chi_{tt} + g\chi_z = p_t, \qquad \text{with} \quad p(t) = \phi_t. \tag{3.11}$$

It is therefore clear that the wave reflection is present in the form of a pressure distribution $p(t)$.

Consider the linearized kinematic and dynamic free surface conditions, with artificial damping being added,

$$\phi_t = -g\zeta, \tag{3.12}$$

$$\zeta_t = \phi_z - 2\nu\zeta, \tag{3.13}$$

which results in the dispersion relationship relating wave frequency ω with the wavenumbers u and v in the x and y directions, respectively,

$$\omega = i\nu \pm (g\sqrt{u^2 + v^2} - \nu^2)^{1/2}, \tag{3.14}$$

where, ν denotes the Newtonian cooling strength with uniform distribution. Compared with the wave frequency without the cooling term,

$$\omega = g\sqrt{u^2 + v^2}, \tag{3.15}$$

it is evident that the cooling term ν basically introduces a shift to the wave frequency ω off the real axis in the complex domain and subsequently adds the time oscillation term $i\omega t$ with an exponential decay behaviour (when $\nu > 0$), whereby the wave is damped.

$$e^{i\omega t} = e^{-\nu t} \cdot e^{\pm i(g\sqrt{u^2+v^2}-\nu^2)^{1/2}t}. \tag{3.16}$$

There is also a shift in the real component of the wave frequency which causes a (higher-order) change in wave dispersion. This can be remedied by the addition of an artificial Rayleigh viscosity term and the free surface conditions finally read,

$$\left\{ \begin{array}{l} \phi_t = -g\zeta \\ \zeta_t = \phi_z - 2\nu\zeta + \frac{\nu^2}{g}\phi \end{array} \right\} \Longrightarrow \omega = i\nu \pm (g\sqrt{u^2+v^2})^{1/2}. \tag{3.17}$$

The Newtonian cooling term is physically interpreted via the modified kinematic free surface condition as the mass flux through the free surface, directed outside the fluid domain when $\zeta > 0$ and inside it when $\zeta < 0$. In view of this formulation, ν may now be considered as the Rayleigh viscosity used in the frequency domain solution of the problem for the enforcement of the radiation conditions. For free surface flows with forward speed, the modified free surface condition directly follows by the substitution of $\partial/\partial t$ with $\partial/\partial t + U\partial/\partial x$ if using only the free stream as the basis flow. The nonlinear free surface conditions fall out in the same fashion.

The variation of the cooling strength over the damping zone is quadratic, following the recommendations of Israeli and Orszag [19], with zero value and slope along the inside edges of the zone,

$$\nu(\rho) = 3\frac{C_s}{C_w^3}(\rho - \rho_0)^2, \qquad 0 \geq \rho - \rho_0 \geq C_w, \tag{3.18}$$

where ρ denotes the radial distance from the wave-making source, with the damping zone beginning from $\rho = \rho_0$ and extending to $\rho = \rho_0 + C_w$, and C_s is the overall cooling strength. Even though there exists an optimal Newtonian cooling strength, numerical experience dictates that any strength in the neighborhood of the optimal value will

suffice for the purpose. The damping zone width C_w plays a much more important role in damping out the waves. For usual problems, waves of all frequencies are present and the damping device can only be tuned to damp out the waves of wavelength $\lambda < 1.5C_w$. This suggests that large portion of the wave reflection ceases to exist when $C_w = \lambda$, where λ is the typical wavelength. For zero speed and low speed problems, disturbance waves propagate slowly towards all directions. Consequently it usually takes a longer time and stronger damping to attain steady state. For high forward speed problems, however, disturbance wave propagates out downstream so rapidly that implementation of damping beaches is not necessary behind the ship.

3.1.4 Temporal Integration

The free surface conditions (2.18)(2.19) are integrated to update the wave elevation and the wave velocity potential at each time step. Also, the equation of motion (2.46) is integrated in time to obtain the ship motion response. It is therefore crucial to acquire a stable, accurate and efficient time integration scheme. In what follows, the time integration schemes for the free surface evolution and ship motion response are discussed separately.

TIME INTEGRATION OF FREE SURFACE CONDITIONS

Time integration of the free surface conditions is a crucial step towards the solution. Vada and Nakos [70] expanded the error analysis, which Sclavounos and Nakos [61] developed for the frequency domain problem, to transient free surface flows and discussed the merits of a variety of numerical integration schemes. This section summarizes their key conclusions. The Emplicit-Euler integration scheme, which he recommended, will be adopted in this nonlinear solution of time-domain free surface problems. Extensive numerical tests have been carried out to validate the scheme.

Consider the model problem of a fluid flow around a transient wave-making source,

with oscillating strength,

$$\hat{R}(\vec{x},t) = \begin{cases} 0, & t < 0, \\ \frac{\cos(\omega t)}{|\vec{x}-\vec{x}_0|}, & t \geq 0, \end{cases} \tag{3.19}$$

where $\vec{x}_0$ is the location of the source and ω is the frequency of its oscillation. The linearized continuous formulation is restated for the problem with the uniform stream as the basis flow that implies the Neumann-Kelvin formulation,

$$\left\{ \begin{array}{l} \frac{\partial\phi}{\partial t} + U\frac{\partial\phi}{\partial x} = -g\zeta \\ \frac{\partial\zeta}{\partial t} + U\frac{\partial\zeta}{\partial x} = \frac{\partial\phi}{\partial z} \end{array} \right\} \quad \text{on} \quad z = 0, \tag{3.20}$$

coupling with the boundary integration equation:

$$\phi(\vec{x},t) - \iint_{S_F} \frac{\partial\phi}{\partial n}(\vec{\xi},t)G(\vec{x};\vec{\xi})d\vec{\xi} = R(\vec{x},t), \tag{3.21}$$

where $R(\vec{x},t)$ is the right-handed-side forcing term, obtained by integrating the source term (3.19) over the free surface. The solution of the velocity potential over the linearized free surface $z = 0$, subject to the Laplace equation, the linearized free surface condition (3.20) and the proper radiation condition, accepts in terms of Fourier transformation,

$$\phi(x,y,t) = \frac{1}{(2\pi)^3} \int d\omega \int_{-\infty}^{+\infty} du \int_{-\infty}^{+\infty} dv \, \frac{\tilde{f}(u,v,\omega)}{\mathcal{W}(u,v,\omega)} \, e^{-i(ux+vy-\omega t)}, \tag{3.22}$$

where $\tilde{f}$ is the Fourier spectrum of the forcing, which is assumed to decay fast enough to make the integral finite as $(u,v,\omega) \to \infty$. $\mathcal{W}$ denotes the dispersion relationship as obtained from (3.20),

$$\mathcal{W}(u,v,\omega) = -(\omega - Uu)^2 + g\sqrt{u^2+v^2} = 0. \tag{3.23}$$

In response to each wave component ω, the dispersion relationship (3.23) has two or four roots, which means that two or four waves are propagating in the system,

depending upon whether the reduced frequency $\tau = \omega U/g$ is smaller or larger than the critical value $\tau_{cr} = \frac{1}{4}$. Each wave component is propagating in the direction suggested by the group velocity,

$$\vec{V}_g = -\frac{(\frac{\partial W}{\partial u}, \frac{\partial W}{\partial v})}{\frac{\partial W}{\partial \omega}}. \tag{3.24}$$

As the reduced frequency τ approaches the critical value $\frac{1}{4}$, the corresponding group velocity V_g reduces to zero, which signifies wave energy is not propagating outwards, and eventually the wave disturbance may become singular. This demonstrates the inadequacy of the linear solution and Liu and Yue [35] discussed this difficulty extensively.

Using the basis functions defined in the previous section, the discrete formulation for the problem (3.21) and (3.20) takes the form,

$$(\phi)_j B_{ij} - (\phi_j)_j S_{ij} = R_i, \tag{3.25}$$

$$\frac{d(\zeta)_j}{dt} B_{ij} + U(\zeta)_j D_{ij} = (\phi_j)_j B_{ij}, \tag{3.26}$$

$$\frac{d(\phi)_j}{dt} B_{ij} + U(\phi)_j D_{ij} = -g(\zeta)_j B_{ij}, \tag{3.27}$$

where R_i is the right-handed-side forcing, D_{ij} and S_{ij} are defined as,

$$D_{ij} = \frac{\partial B_j}{\partial x}(\vec{x}_i), \tag{3.28}$$

$$S_{ij} = \iint_{-\infty}^{+\infty} B_j(\vec{\xi}) G(\vec{x}_i; \vec{\xi}) d\xi. \tag{3.29}$$

The explicit Euler scheme integrates the kinematic free surface condition to obtain the new wave elevation at each time step, according to the expression,

$$\frac{\zeta^{n+1} - \zeta^n}{\Delta t} B_{ij} + U(\zeta)_j^n D_{ij} = (\phi_z)_n^j B_{ij}, \tag{3.30}$$

and the implicit Euler scheme integrates the dynamic free surface condition to acquire

the new velocity potential on the free surface.

$$\frac{\phi^{n+1}-\phi^{n}}{\Delta t}B_{ij}+U(\phi)_j^{n+1}D_{ij}=-g(\zeta)_j^{n+1}B_{ij}, \tag{3.31}$$

where Δt is the time step. The discrete dispersion relationship is,

$$W=(\beta^2-i\beta F_h\mathcal{D})z^2-(2\beta^2+F_h^2\mathcal{D}^2-\mathcal{S})z+(\beta^2+i\beta F_h\mathcal{D})=\mathcal{W}+\mathcal{O}(h^3,\Delta t). \tag{3.32}$$

The whole scheme is referred to as the Emplicit-Euler integration scheme. Appendix A presents other integration schemes, and, concludes on the basis of an error and stability analysis [70] that this Emplicit scheme is the most efficient and stable.

TIME INTEGRATION OF THE EQUATION OF MOTION

A stable, accurate and efficient scheme is needed to integrate the equation of motion (2.46) in order to obtain the ship motion response to a particular sea state at each time step. The global numerical error, which is the difference between the exact solution and the approximate solution, must not be allowed to grow with time, otherwise the solution will be contaminated by error and become untrustworthy. In the early development of this numerical solution of time domain free surface problems, the stability characteristics were not entirely understood and the produced solutions were not physically resonable, until it was found that the problem has to be solved in a natural way and the impulsive forces be separated from the total excitation forces. Therefore it is absolutely essential to conduct a thorough error analysis for the numerical integration scheme before embarking on any serious solution of the problem.

Consider the homogeneous equation of motion,

$$(M+a_0)\ddot{\vec{\xi}}(t)+b_0\dot{\vec{\xi}}(t)+(C+c_0)\vec{\xi}(t)+\int_0^t d\tau K(t-\tau)\dot{\vec{\xi}}=0. \tag{3.33}$$

Note that a_0, b_0 and c_0 are the added mass, damping and restoring coefficients, respectively, which are derived from the time impulsive local forces. The convolution

integral retains the "memory" of the free surface flow and also contains part of the added mass and wave damping. This kind of second order Ordinary Differential Equation (ODE) is usually decomposed into a system of linear equations (twelve equations in this formulation) for numerical calculations.

$$\frac{d\vec{y}}{dt} = \vec{f}(t), \tag{3.34}$$

where

$$\vec{y}(t) = \left\{ \begin{array}{c} \vec{y}_1(t) \\ \vec{y}_2(t) \end{array} \right\} = \left\{ \begin{array}{c} \dot{\vec{\xi}}(t) \\ \vec{\xi}(t) \end{array} \right\}, \tag{3.35}$$

and

$$\vec{f}(t) = \left\{ \begin{array}{c} \vec{f}_1(t) \\ \vec{f}_2(t) \end{array} \right\} = \left\{ \begin{array}{c} -[M + a_0]^{-1} \left(b_0 \vec{y}_1(t) + (C + c_0)\vec{y}_2(t) + \int_0^t d\tau K(t-\tau)\vec{y}_1(\tau)\right) \\ \vec{y}_1(t) \end{array} \right\}. \tag{3.36}$$

An error function is defined as,

$$\vec{\varepsilon}(t) = \vec{y}(t) - \tilde{\vec{y}}(t), \tag{3.37}$$

where $\vec{y}(t)$ is the exact solution and $\tilde{\vec{y}}(t)$ is the numerical approximate solution. Then a system of linearized error equations results in the solutions of the error functions (3.37). In order to deal with the convolution integral, the equations are examined in the Laplace domain. The application of the von-Neumann analysis scheme to the error equation leads to a stability polynomial, while the boundary locus method produces the regime of absolute stability. Combination of the stability polynomial and the absolute stability renders the restrictions (upper and lower bounds) for the time step size. More details for the analysis may be found in Kring and Sclavounos [28].

In this work, the fourth order Adam-Bashford-Moulton (ABM) predictor-corrector method is chosen for the solution of the equation of motion, with the fourth order Runge-Kutta scheme for the first four time steps. The schemes are defined below,

Fourth-order Adam-Bashford-Moulton method:

$$\text{predictor:} \qquad y_5 = y_4 + \frac{h}{24}(55\dot{y}_4 - 59\dot{y}_3 + 37\dot{y}_2 - 9\dot{y}_1) + \mathcal{O}(h^5), \tag{3.38}$$

$$\text{corrector:} \qquad y_5 = y_4 + \frac{h}{24}(9\dot{y}_5 + 19\dot{y}_4 - 5\dot{y}_3 + \dot{y}_2) + \mathcal{O}(h^5). \tag{3.39}$$

Fourth-order Runge-Kutta method:

$$y_2 = y_1 + \frac{k_1}{6} + \frac{k_2}{3} + \frac{k_3}{3} + \frac{k_4}{6}, \tag{3.40}$$

where

$$k_1 = h\ \dot{f}(t_1, y_1), \tag{3.41}$$

$$k_2 = h\ \dot{f}(t_1 + \frac{h}{2}, y_1), \tag{3.42}$$

$$k_3 = h\ \dot{f}(t_1 + \frac{h}{2}, y_1 + \frac{k_2}{2}), \tag{3.43}$$

$$k_4 = h\ \dot{f}(t_1 + h, y_1 + k_3), \tag{3.44}$$

where h indicates the time step size Δt. Both schemes are standard integration algorithms for ODEs. The stability regime of an optimal scheme must overlap with the stability properties of the scheme used to evolve the free surface disturbance. Therefore the scheme having the largest stability regime is not necessarily the most efficient. The fourth order Runge-Kutta algorithm is one example. It is the most stable, but is prohibitively expensive because it needs to evaluate the function, f, four times at each time step. The fourth order ABM, on the other hand, has a large enough stability regime for all practical problems studied and requires only two evaluations of the function, f, at each time step. It is therefore the most ideal integration scheme for this formulation.

The stability depends also upon the shape of the hull and its forward speed. So whenever stability problems are encountered, this analysis can be revisited to isolate the reasons for the instability. Thus it is extremely important to gain a thorough

understanding on the numerical stability properties.

3.1.5 Numerical Filtering

Discretization of the free surface not only presents difficulties in enforcing radiation conditions, but also induces spurious wave modes, which could interfere with the physical waves and eventually destroy the credibility of the solution completely. This purely numerical phenomenon was first revealed and discussed by Longuet-Higgins and Cokelet [36] in their two-dimensional solution of nonlinear free surface waves. They found that saw-tooth like waves were superimposed on the physical waves such that the waves are zigzag alike if no preventive measure is taken. The 5-point Chebyshev smoothing (filtering) formula was used to remove the saw-tooth instability. The general consensus on the causes of the problem is that there is high concentration of fluid particles with high speed in certain regions especially near the water crests. The same problem was later encountered by the three-dimensional solution as well (Xü & Yue [73]).

In the present formulation, there exists a spurious short-wavelength disturbance propagating in the system. These small spurious waves sometimes deviate from the propagation of the physical wave systems and even travel upstream, especially for the small waves of less than five-panel-lengths. Without proper treatment, these small waves could strongly impede the convergence of the numerical solutions. Nevertheless, because of the size of the waves, it is believed that not much energy would be taken out from the physical system if a low-pass numerical filter over the free surface is applied to filter out these small erroneous wave components. A general filtering involves a series of operations: translation of the solution into the Fourier domain, multiplication by the filter shape, inversion back to the physical space. Alternatively, the filtering may be performed directly in the physical space via discrete convolution, as follows,

$$\bar{f}_i = \sum_{j=-\infty}^{+\infty} w_j f_{i-j}, \tag{3.45}$$

where $\bar{f}_i$ is the filtered of the solution and w_j is the weight function, which Fourier

transform is the desired filter shape. The energy taken out by the filtering process should be kept at a minimum. In other words, the smart filter should retain the physical wave, which are accurately presented by the numerical solution, and weed out numerical noise, which is detrimental to the numerical solution. Longuet-Higgins and Cokelet [36] introduced 5- and 7-point filters and demonstrated the superiority of the former one. However even the 5-point filter is not ideal for the present formulation because it significantly alters the waves which are accurately resolved especially in the neighborhood of $uh_x/2\pi = 0.2$, where u is the x-component of wave numbers and h_x is the panel dimension in the x direction. So Nakos [45] devised a modified 7-point filter:

$$w_0 = 0.701207, \quad w_{\pm 1} = 0.230639, \quad w_{\pm 2} = -0.100604, \quad w_{\pm 3} = 0.019361. \quad (3.46)$$

And the corresponding Fourier transform is:

$$H(u) = w_0 + 2w_{\pm 1}\cos u - 2w_{\pm 2}\cos 2u + 2w_{\pm 3}\cos 3u. \quad (3.47)$$

These three filter shapes are shown in Figure 3-4. The filtering scheme inevitably removes some energy. Therefore the frequency of the application of filtering during the simulation process should be minimized to prevent an excessive removel of energy. Otherwise, it may be presented as smaller damping coefficients and consequently larger body motions. Numerical results must eventually be shown to be insensitive to the frequency of the application of the filtering process and some results in Chapter 4 will demonstrate just that. Practically one application of the filter for every 20 time steps has been found not to affect the body forces and yet to produce smooth wave patterns for all cases tested.

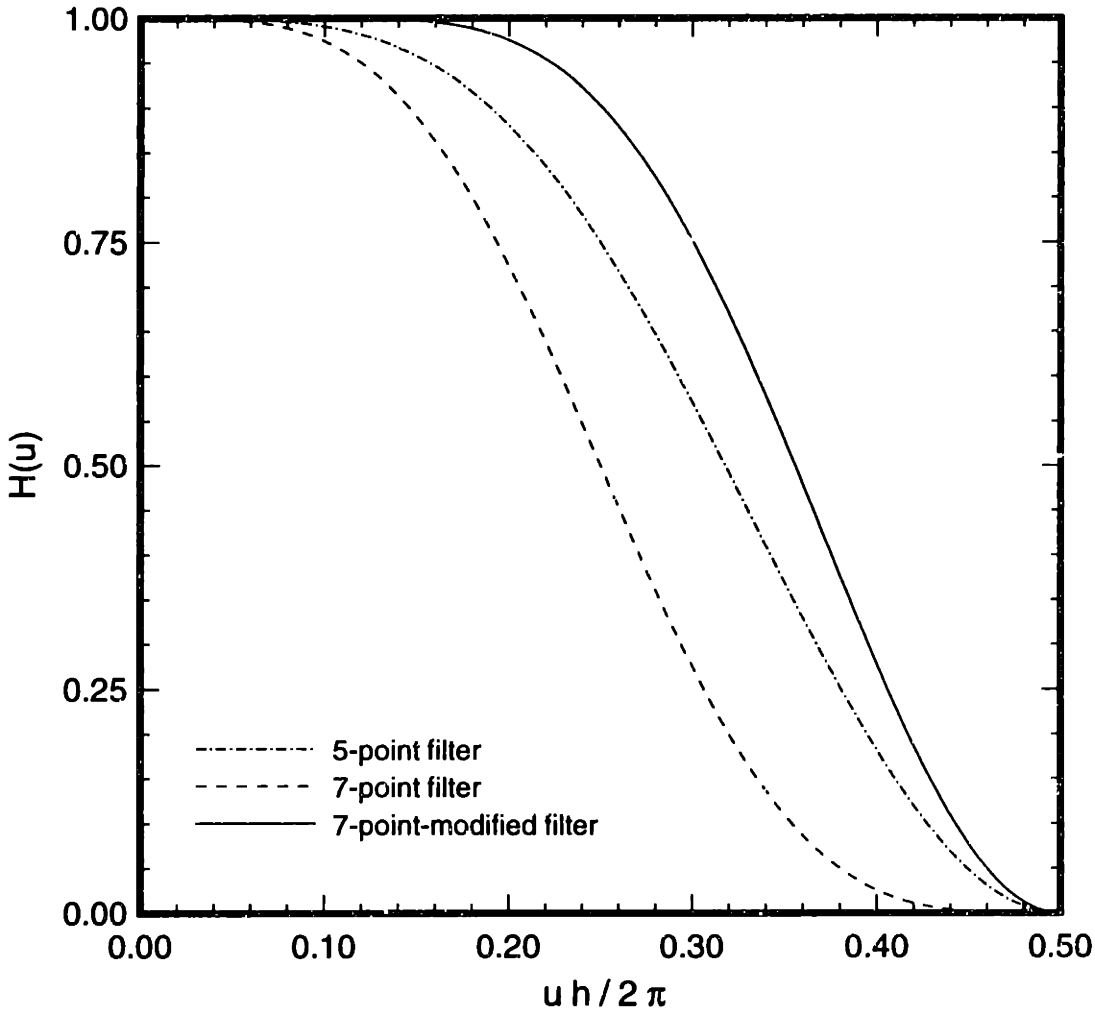

Figure 3-4: Low-pass filters for spatial smoothing. The 7-point-modified filter is used in the present study

Chapter 4

Numerical Results

4.1 Computer Implementation

The theory and the algorithms discussed in the previous two chapters are written into a modular FORTRAN77 computer program, referred to as SWAN (Ship Wave ANalysis). The SWAN program has been continuously developed for almost a decade. Past work includes the linear frequency domain version SWAN1 (progress documented in Sclavounos & Nakos [61], Sclavounos, Nakos & Huang [63] and Nakos & Sclavounos [46]) and the linear time domain version SWAN2 (first reported in Nakos, Kring & Sclavounos [44] and recently in Kring, Huang, Sclavounos, Vada & Braathen [30]). The Weak-Scatterer version of the code, which is a major contribution of this thesis, represents the logical evolution of the SWAN project.

This version of the program is designed to efficiently simulate the nonlinear time domain ship motions of a steadily translating ship either oscillating at a prescribed frequency (dubbed as forced motion) or freely floating in the presence of an incoming wave (dubbed as free motion). Because the basis flow is time-dependent, the Weak-Scatterer version of SWAN carries out the setup and solution of the linear system of equations at each time step, unlike the linear time domain SWAN2, which is divided into setup and solve procedures in order to save computational time. The solution at each time step mainly consists of:

- regridding of the free surface and submerged hull surface.
- evaluation of influence coefficients.
- solution of a mixed boundary value problem for basis flow quantities.
- solution of a mixed boundary value problem for time-local flow quantities.
- evolution of the free surface conditions to obtain the updated values of wave elevation and velocity potential on the free surface.
- solution of a mixed boundary value problem for disturbance flow quantities.
- updating of the flow quantities.

Figure 4-1 shows the detail work flow of the code.

The execution of the Weak-Scatterer program represents a significant computational effort. For a computational domain consisting of 2000 total panels, it takes about 48 hours to attain a steady state solution on a DEC Alpha 600 Workstation. The majority of the cost is associated with the solution of the mixed boundary value problems, especially the evaluation of the influence coefficients, which accounts for about 50% of the total cost. The solution of the resulting full, dense linear system of equations also requires a significant computational expense. The solution of the evolution equations constitutes only relatively minor computational costs since the equations are sparse and narrow-banded. An improved **LU** decomposition is used in the solution of the linear system of equations and requires between $\mathcal{O}(N^2)$ and $\mathcal{O}(N^3)$ floating point operations, with N denoting as the total number of panels. The Multipole, a $\mathcal{O}(N)$ scheme, and pre-corrected-FFT accelerated iterative methods, a $\mathcal{O}(N \log N)$ scheme, (Nabors, Phillips, Korsmeyer & White [41]), might in the future be used to reduce the computational time. At this stage, the oval-type grid described in the previous chapter is used to improve the efficiencies of the computational algorithm.

Between the forced and the free motion simulation, the latter is twice as expensive since two functional evaluations for the hydrodynamic wave forces are required by the

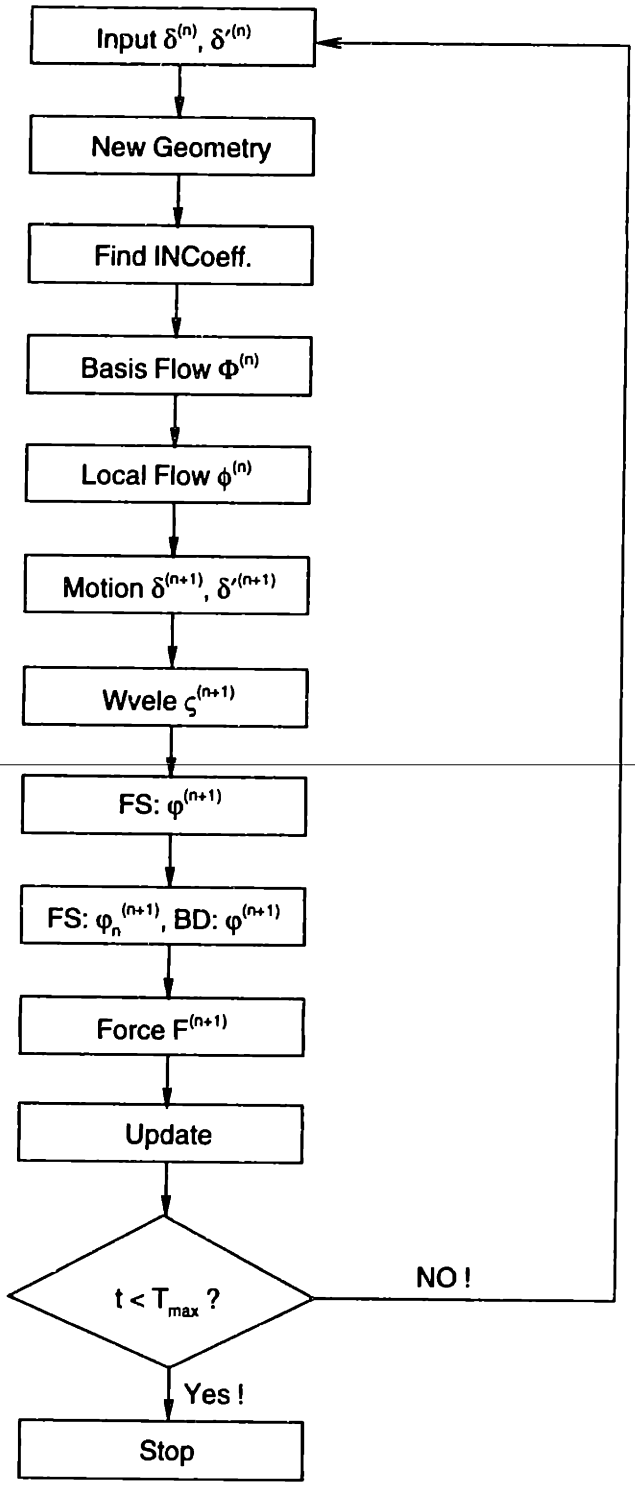

Figure 4-1: Work Flow Chart for the Weak-Scatterer Version of the SWAN2 Program.

ABM predictor-corrector scheme which integrates the equations of motions for the motion responses.

4.2 Feasibility Study

The nonlinearities associated with steep ambient waves and large amplitude body motions are essential for the accurate solution of free surface ship flows. It is however very expensive to solve even a partially nonlinear solution based on the Weak-Scatterer hypothesis. Hence it is wise to assess the feasibility of the proposed Weak-Scatterer solution.

The linear version of the SWAN2 program provides an intermediate tool to achieve this objective. First of all, the linear time domain solution from the computer code SWAN2 renders a measuring stick for any meaningful development in the nonlinear solution, while experimental results serve as another. Then, the linear method has developed a variation, referred to hereafter as quasi-nonlinear SWAN2, to account for some nonlinear effects of hydrostatic and Froude-Krylov forces, while keeping the hydrodynamic problem still solved by a purely linear approach. In other words, the hydrodynamic solution is achieved by solving a boundary value problem over the free surface which is still defined as a flat surface $z = 0$ and the wetted body surface which is the surface intercepted by calm water. The nonlinear hydrostatic effects are however included by adding the difference in hydrostatic forces between what is obtained by integrating the hydrostatic pressure over an instantaneous submerged hull surface and what is obtained by integrating the hydrostatic pressure over an calm-water submerged hull surface. And the nonlinear Froude-Krylov force is obtained by the integration of incident wave pressure over the instantaneous, instead of the calm-water wetted hull surface. So the forces exerted on the body by the fluid are the sum of linear hydrostatic forces, linear hydrodynamic forces, and the forces the pure linear theory does not account for such as the nonlinear hydrostatic force components and nonlinear Froude-Krylov forces. The approach is of course not at all physically consistent and scientifically rigorous, nevertheless it provides the evidence that nonlinearities of steep

incoming waves and large body motions are indeed crucial for accurate predictions of motion responses for many practical applications.

4.2.1 Series60 (Block Coefficient 0.7)

The free motion tests on the Series 60 hull in head seas serve to validate this quasi-nonlinear method. Because the Series60 hull does not have significant waterline geometric changes, and it can be considered as a linear seakeeping hull. The nonlinearities introduced by the nonlinear hydrostatic and Froude-Krylov forces are expected not to cause the quasi-nonlinear predictions to deviate much from the linear computational results, and more importantly, the experimental measurements. Figures 4-2 and 4-3 display the results for a Series60 ($C_b = 0.7$) hull for a wide range of incoming waves at a Froude number $\mathcal{F} = U/\sqrt{gL} = 0.2$, where U is the ship speed in the $x-$direction, g is the gravitational acceleration and L is the ship length between its perpendiculars. The comparisons of heave and pitch Response Amplitude Operators (RAO) between the linear SWAN2 computational results, the linear SWAN2 with nonlinear hydrostatic and Froude-Krylov correction predictions and the experimental measurements are satisfactory, as expected. The experiment was carried out by Gerritmma, Beukelman and Glansdorp [16]. Here, the RAOs calculated are actually the first-harmonic amplitude of the heave and pitch signals.

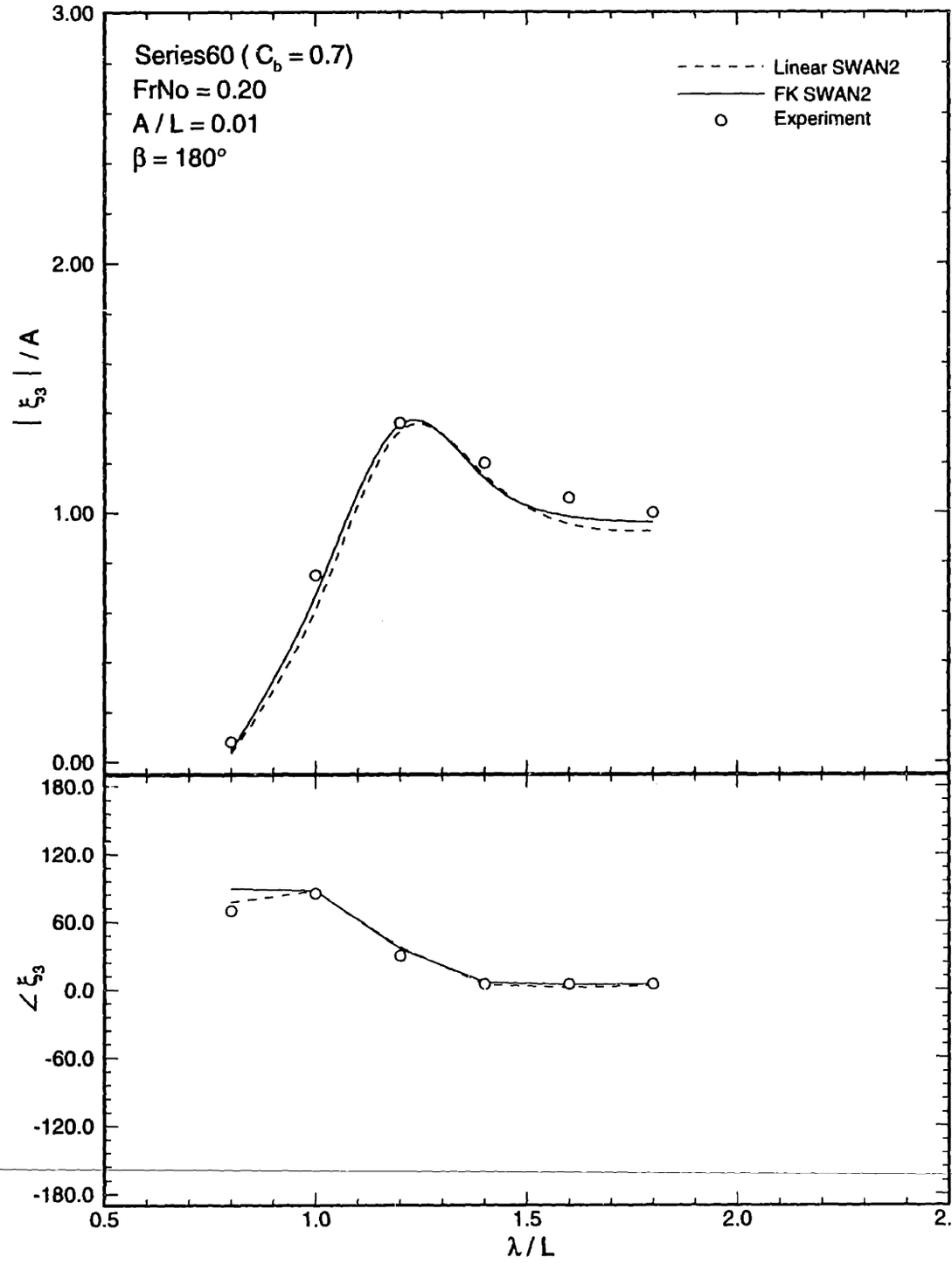

Figure 4-2: Amplitude and phase of the heave response amplitude operator (RAO) for a Series60 ($C_b = 0.7$) hull at $\mathcal{F} = 0.2$ in head seas.

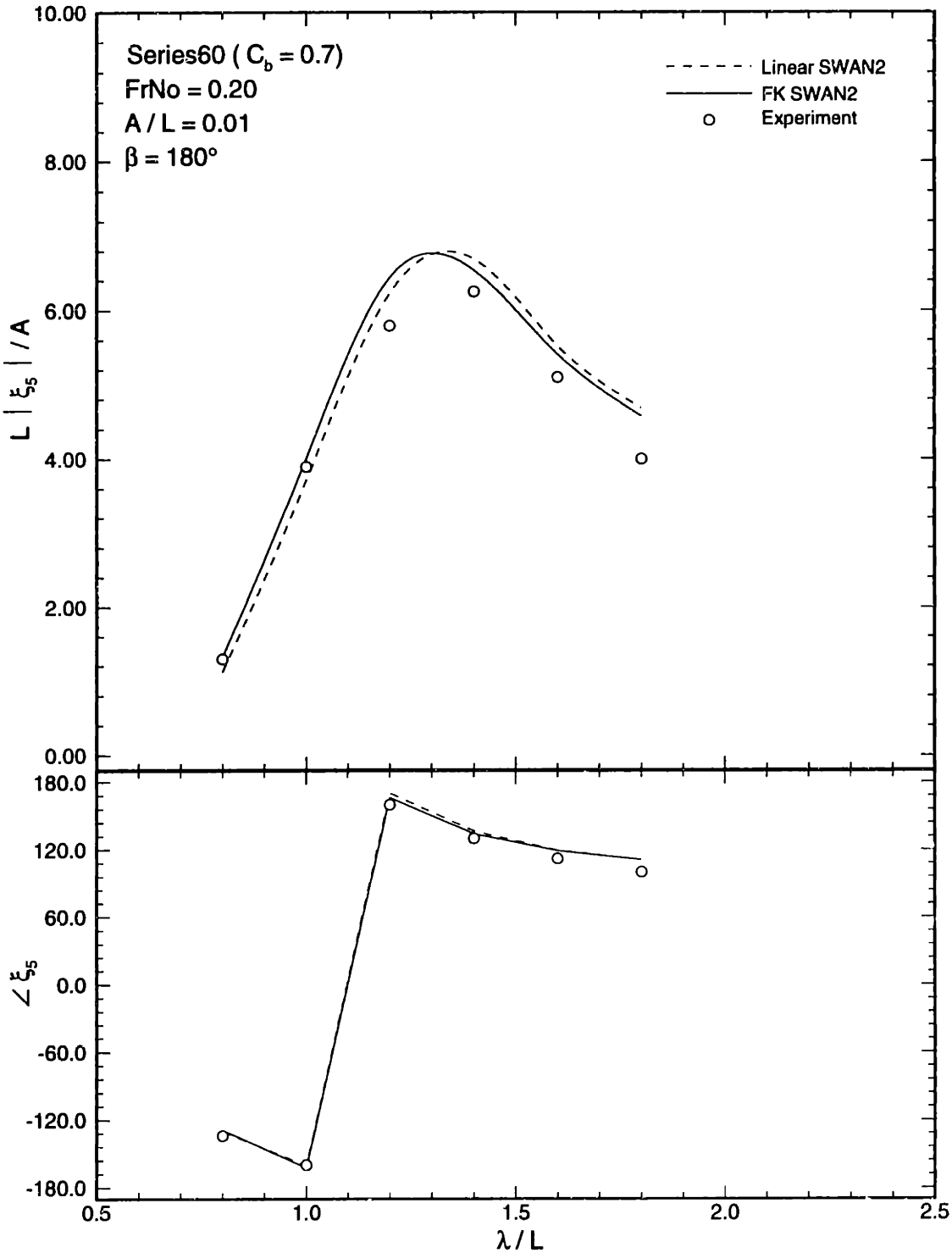

Figure 4-3: Amplitude and phase of the pitch response amplitude operator (RAO) for a Series60 ($C_b = 0.7$) hull at $\mathcal{F} = 0.2$ in head seas.

4.2.2 SnowDrift (Ballast)

The tests on the SnowDrift hull are carried out to demonstrate that the nonlinearities associated with the hydrostatic and Froude-Krylov forces do have a strong influence on the motion responses, especially at the resonance. The SnowDrift hull is a slender body container vessel with moderate bow flare and stern counter. Figure 4-4 shows its body plan. At the ballast condition (8 meter draft), the counter stern is just above the calm waterline, and apparently it will be in and out of the water while the vessel actually travels in ambient waves. Thus, the quasi-nonlinear approach is expected to be useful in this case. Figures 4-6 and 4-7 show comparisons of the motion RAO's between the linear and quasi-nonlinear calculations and experimental data. The predictions of the quasi-nonlinear scheme based on the combination of the nonlinear hydrostatic and Froude-Krylov forces and linear hydrodynamic coefficients are superior to those of the linear computational method, especially near the resonance. This is not surprising since at resonance, the larger motion amplitude of the vessel causes deeper submergence of the counter stern and consequently alters significantly the hydrostatic characteristics. It is also noteworthy that the nonlinearities are more important on the pitch than on heave motion.

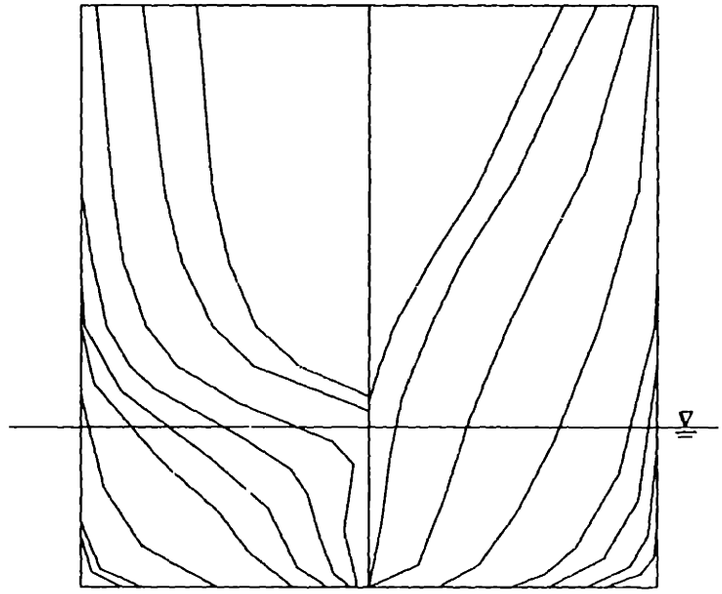

Figure 4-4: Body Plan for a Slender Container Vessel: SnowDrift.

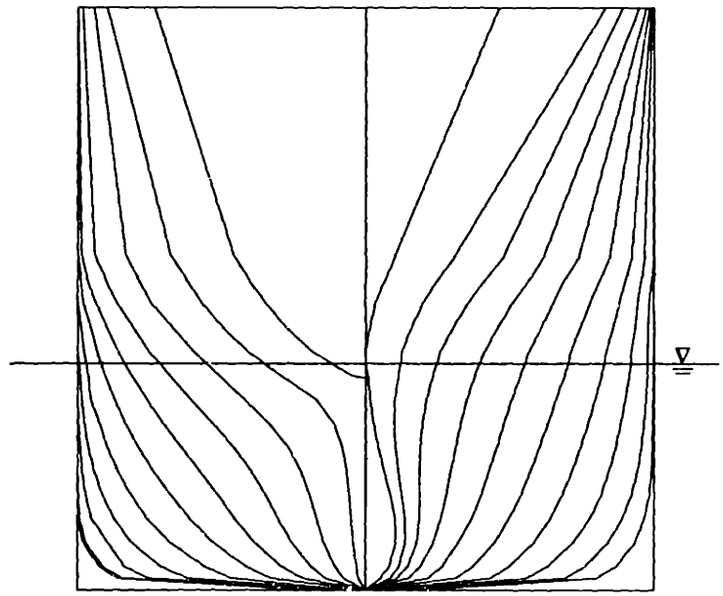

Figure 4-5: Body Plan for a Container Vessel: S7-175.

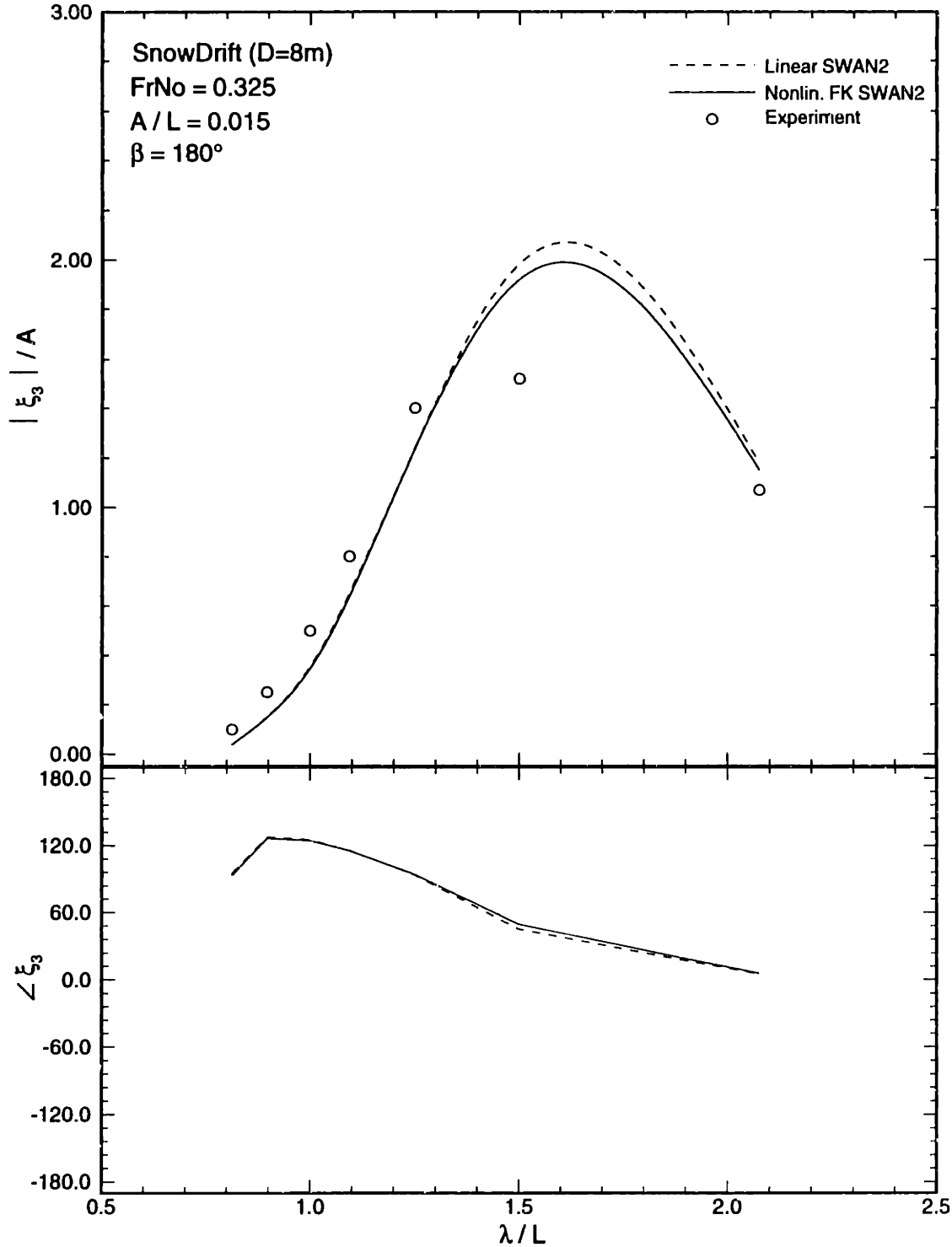

Figure 4-6: Amplitude and phase of the heave response amplitude operator (RAO) for the SnowDrift ($D = 8(m)$) hull at $\mathcal{F} = 0.325$ in head seas. Demonstrates the importance of the nonlinearities associated with the nonlinear hydrostatic and Froude-Krylov forces.

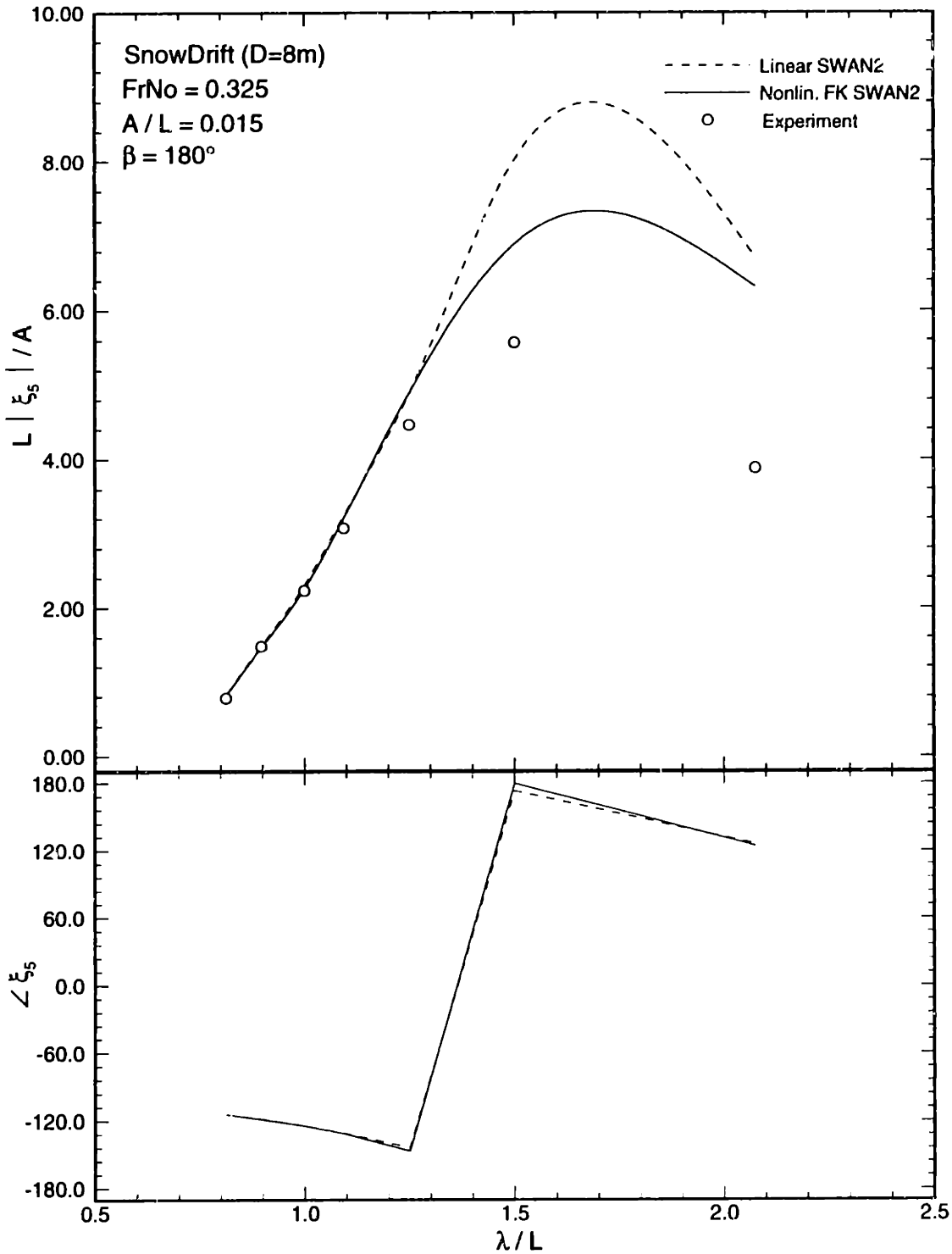

Figure 4-7: Amplitude and phase of the pitch response amplitude operator (RAO) for the SnowDrift ($D = 8(m)$) hull at $\mathcal{F} = 0.325$ in head seas. Demonstrates the importance of the nonlinearities associated with the nonlinear hydrostatic and Froude-Krylov forces.

4.2.3 Steady Sinkage/Trim and Wave Elevation

Although the quasi-nonlinear scheme gives a better prediction of the motion response RAO's, there is still considerable discrepancy between the calculations and the experimental measurements. It is believed that this partially stems from the interactions between the steady and unsteady flows. For ships with significant bow flares and stern counters, the steady sinkage and trim are sometimes proven to be very important, (see for example the work of Sclavounos, Nakos and Huang [63]). The extra wetness of the bow flare and stern counter due to steady sinkage/trim and steady wave elevation that is not accounted for in the pure linear theory, often alters markedly the ship hydrostatic characteristics and consequently influences the unsteady oscillatory fluid flows around the vessel. Figure 4-8 and 4-9 display the importance of the steady sinkage and trim. The inclusion of the steady sinkage/trim and steady wave elevation, shows some improvement in the predictions of motion responses, particularly at resonance and for the pitch motion.

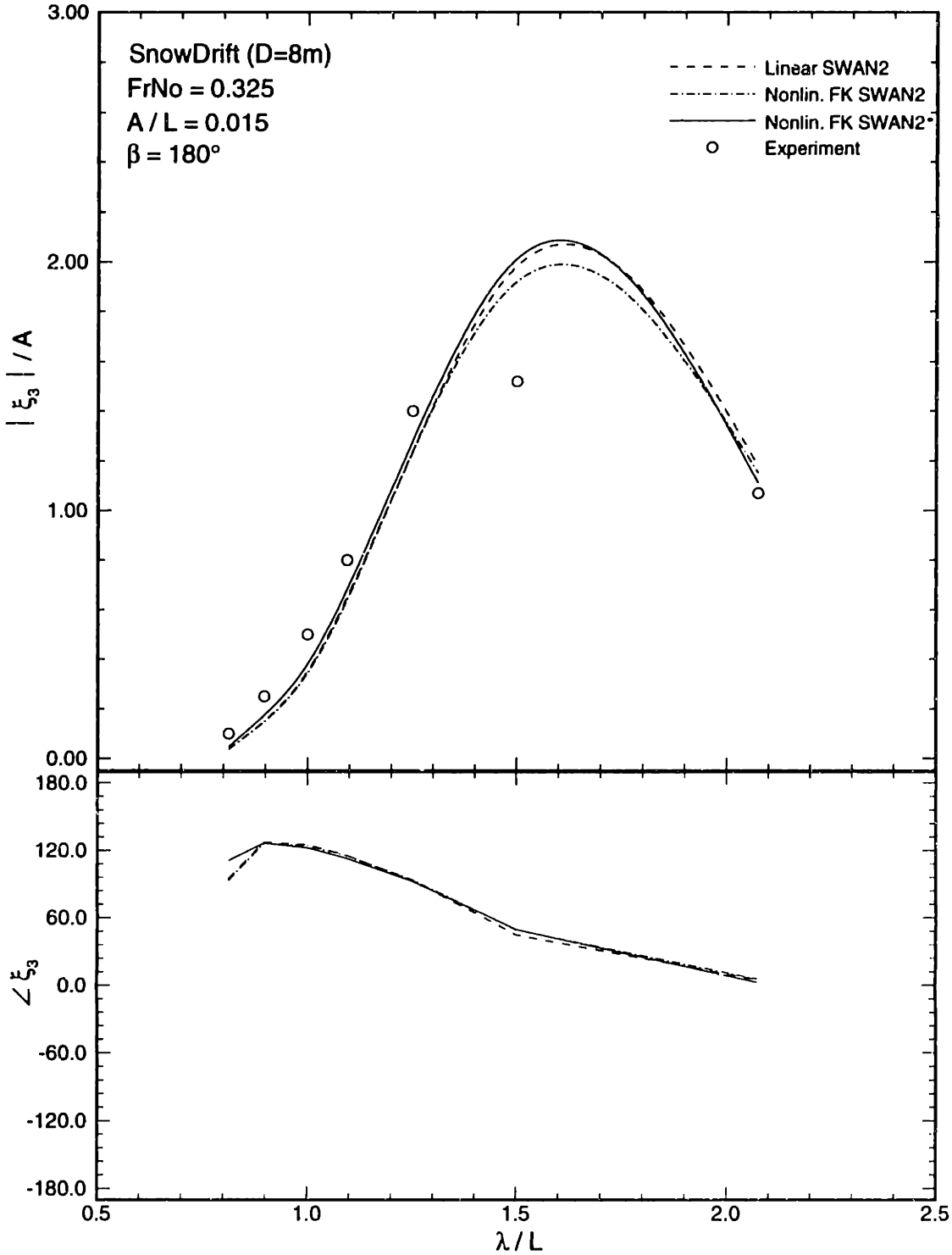

Figure 4-8: Amplitude and phase of the heave response amplitude operator (RAO) for the SnowDrift ($D = 8(m)$) hull at $\mathcal{F} = 0.325$ in head seas. Demonstrates the importance of the steady sinkage/trim and wave elevation.

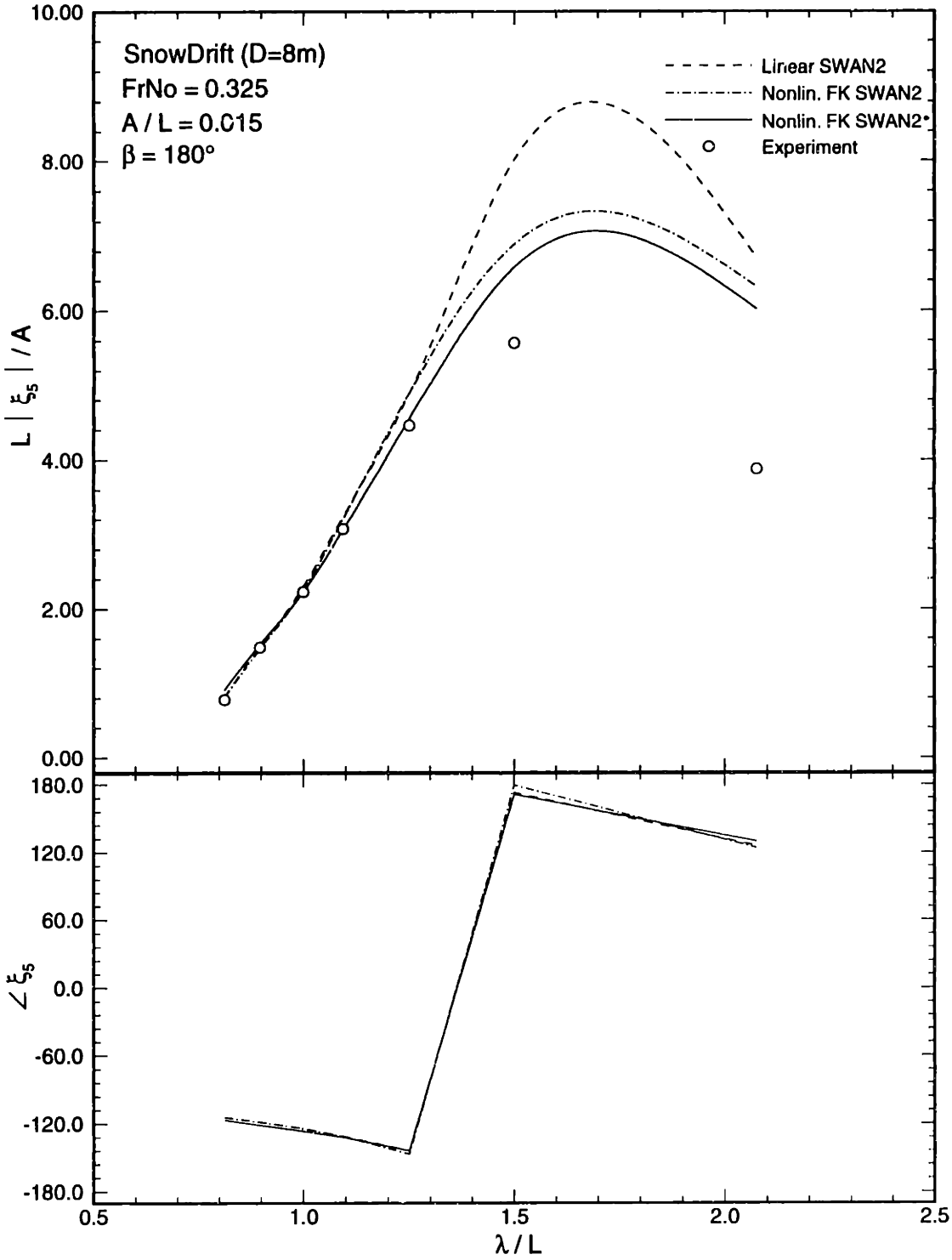

Figure 4-9: Amplitude and phase of the pitch response amplitude operator (RAO) for the SnowDrift ($D = 8(m)$) hull at $\mathcal{F} = 0.325$ in head seas. Demonstrates the importance of the steady sinkage/trim and wave elevation.

4.3 Weak-Scatterer Computation

4.3.1 Validation of Body Boundary Conditions

In the linear solution, the interactions between the steady and unsteady disturbances are accounted for by the so-called m-term, that was first derived by Timman and Newman [66]. Its non-negligible leading order importance was later stressed by Ogilvie and Tuck [54], who reduced it into a compact formula amenable to computation. The Neumann-Kelvin model has been shown to be inadequate precisely because of its poor treatment of m-terms. That is where double-body model really shows its strength (cf. Nakos and Sclavounos [43]).

In the Weak-Scatterer formulation, the exact body boundary conditions are enforced over the instantaneous body wetted surface. The m-term effects, directly result from the linearization of body boundary conditions, should be automatically included and the need for an explicit m-term in the body boundary conditions hence ceases to exist. To ensure this is the case, forced motion tests are conducted using the Weak-Scatterer SWAN program.

Forced motion simulations are performed for a Series60 (Block Coefficient 0.7) hull in order to compute the force coefficients such as added mass and damping coefficients. Extensive experimental data are available for both the force coefficients and motion responses. Therefore it is a good test to validate the algorithms, and in particular the compatibility of the linear SWAN2 predictions with those from the Weak-Scatterer algorithm.

The ship is assumed to undergo forced oscillations at a variety of prescribed frequencies ($\omega\sqrt{L/g} = 2.0 \rightarrow 5.0$, where ω is the oscillatory frequency nondimensionalized by the gravitational acceleration and ship length), while steadily translating at a Froude number $\mathcal{F} = 0.20$. Because there are no incoming waves, only the radiation problem is being studied. From the recorded force history, the force coefficients are extracted using a Fourier transform (FT). Figure 4-10 shows the comparison of the experimental measurements and the predictions of linear SWAN2 and the Weak-

Scatterer SWAN2 for the diagonal heave and pitch added mass and damping coefficients, while Figure 4-11 illustrates the correlation for the cross-coupling added mass and damping coefficients. All computational results are convergent with respect to panel number and time step. The results illustrated in the figures are calculated using 1800 panels over half of the computational domain (240 panels on the body surface) and 0.06 seconds as the time step. The agreement is generally satisfactory. As expected, the linear and Weak-Scatterer calculations are in good agreement because the Series60 hull is considered a slender and "linear" ship. This exercise serves to demonstrate that the m-term effects are adequately accounted for in the Weak-Scatterer program via the enforcement of the nonlinear body boundary condition.

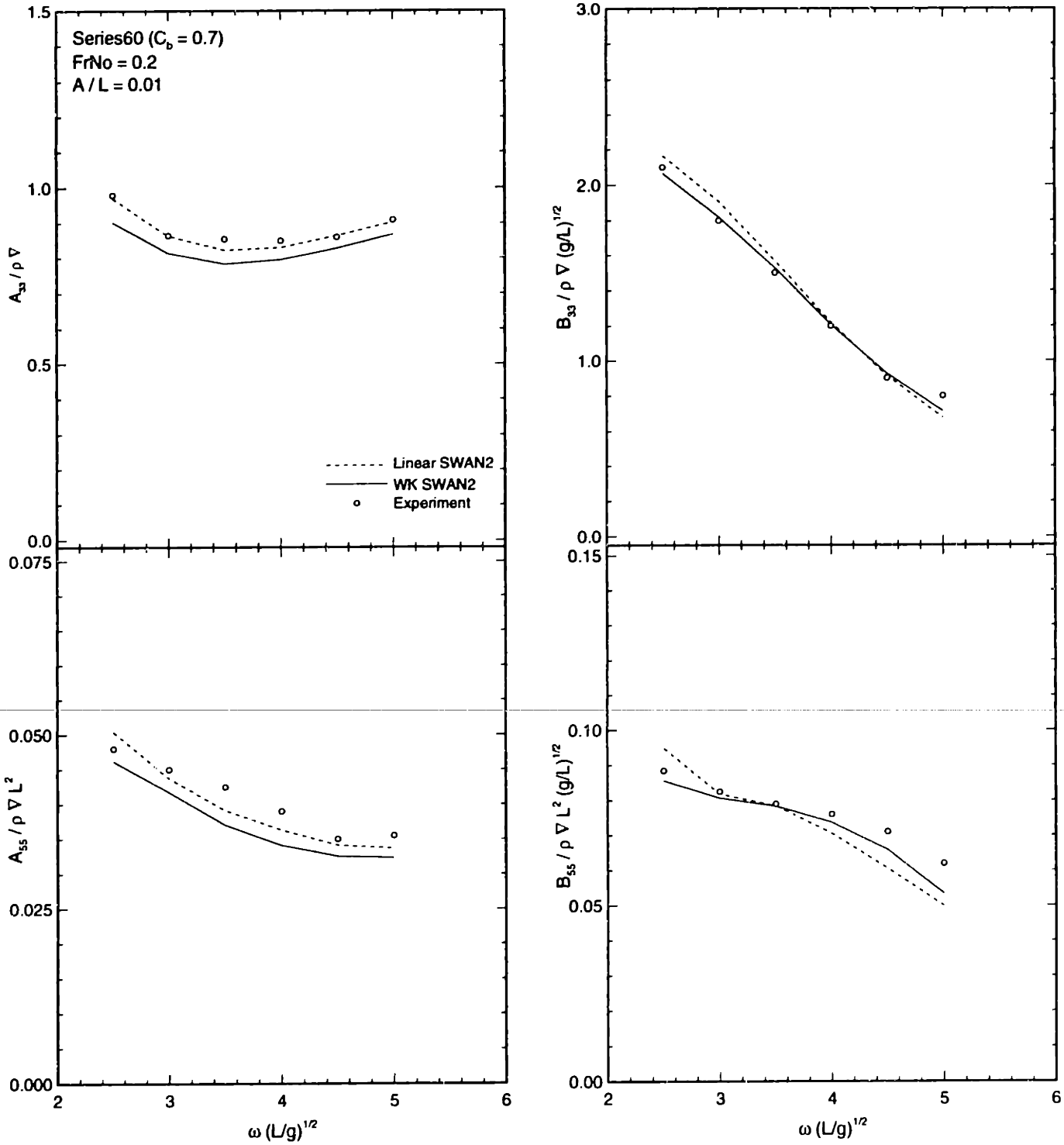

Figure 4-10: Diagonal added mass and damping coefficients for the Series60 (C_B = 0.7) at $\mathcal{F} = 0.2$.

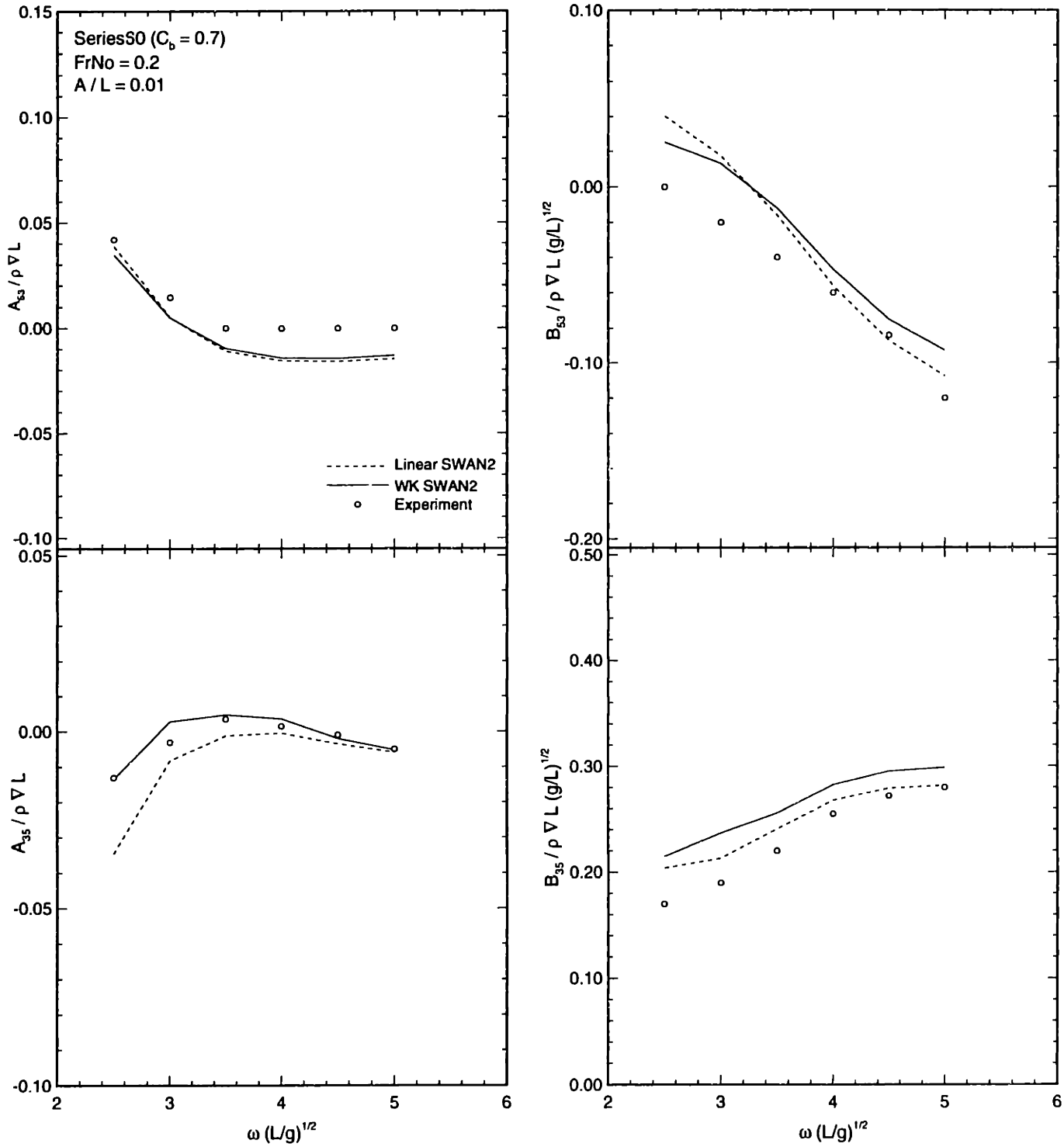

Figure 4-11: Cross-coupling added mass and damping coefficients for the Series60 ($C_B = 0.7$) at $\mathcal{F} = 0.2$.

4.3.2 Convergence Studies

For a time domain numerical scheme to become credible, it has to achieve both temporal and spatial convergence. Moreover, computations should not be sensitive to changes in the other parameters of the numerical algorithm as well, such as the filtering frequencies, the beach size and the cooling strength. This section sets out to validate the convergence properties of the algorithms and recommend values for these parameters.

In the following studies, the ship is traveling at $\mathcal{F} = 0.325$ in head seas at the encounter frequency of $\omega\sqrt{L/g} = 3.408$, or near the resonant peak. The incident wave amplitude is $A/L = 0.015$.

Figure 4-12 illustrates the convergence of the motion with respect to the spatial discretization. Using 30, 40 and 50 panels along the ship waterline with the total number of panels on half the body surface and free surface running from 1800, 3000, 4200 respectively, the spatial convergence is quite adequate with no obvious graphic difference between the two densest cases. Each discretization employs the same domain extent, numerical beach and girth-wise panel number (10 panels). Also, a common time-step of $t\sqrt{g/L} = 0.01$ was chosen that falls within the stability and convergence conditions for all these cases. It is interesting to note that the panel number required for convergence (150 MB memory size) is well within the computational capability of a personal engineering workstation.

The temporal convergence is demonstrated in Figure 4-13. With the same geometric discretizations, namely 30 panels along the ship waterline, tests are conducted to compare results for time step sizes of $\Delta t\sqrt{g/L} = 0.005, 0.010$ and 0.020 with one spatial filtering at every twenty time steps. Even though there would be actually more filtering applied for smaller time step size cases for the same period of time, the convergence is still considered good.

The panelization of the free surface introduces some artificial waves, which sometimes even travel upstream and could distort the numerical solution. In almost all

nonlinear free surface wave simulations, this type of numerical instability has been encountered and commonly solved by the application of filtering or smoothing scheme. The detailed filtering scheme is discussed in the previous chapter and herein it proves that the computation results are convergent with respect to the filtering frequency. Figure 4-14 shows sensitivity to the spatial filtering. Various filtering frequencies (one application of filtering per 20, 40, 80 time step) have been tested and the results are shown no obvious sensitivity to the filtering rate.

The discretization of the free surface presents another difficulty, namely the enforcement of the radiation condition or the wave reflection from the free surface boundary. This wave reflection works in a similar manner as the wave reflection from towing tank walls. Therefore a numerical beach similar to the physical beach in a towing tank is designed to minimize the wave reflection. Here the convergence of the algorithms for two major beach parameters: beach strength and beach size, is studied, and shows good beach-independence.

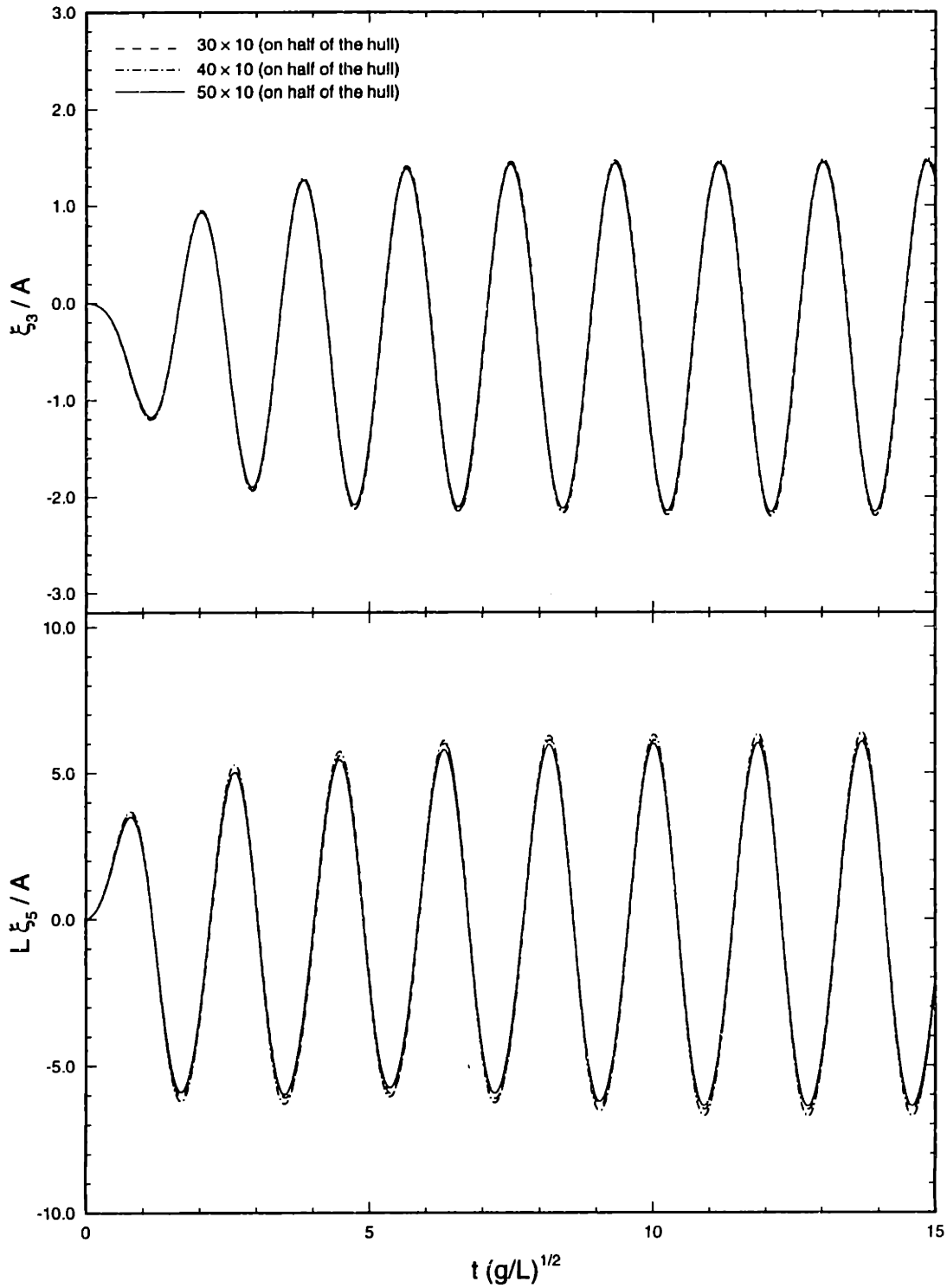

Figure 4-12: Spatial convergence of heave and pitch motions for the SnowDrift hull (D=8m) at $\mathcal{F} = 0.325$ in incident head seas, at an encounter frequency of $\omega(L/g)^{1/2} = 3.408$.

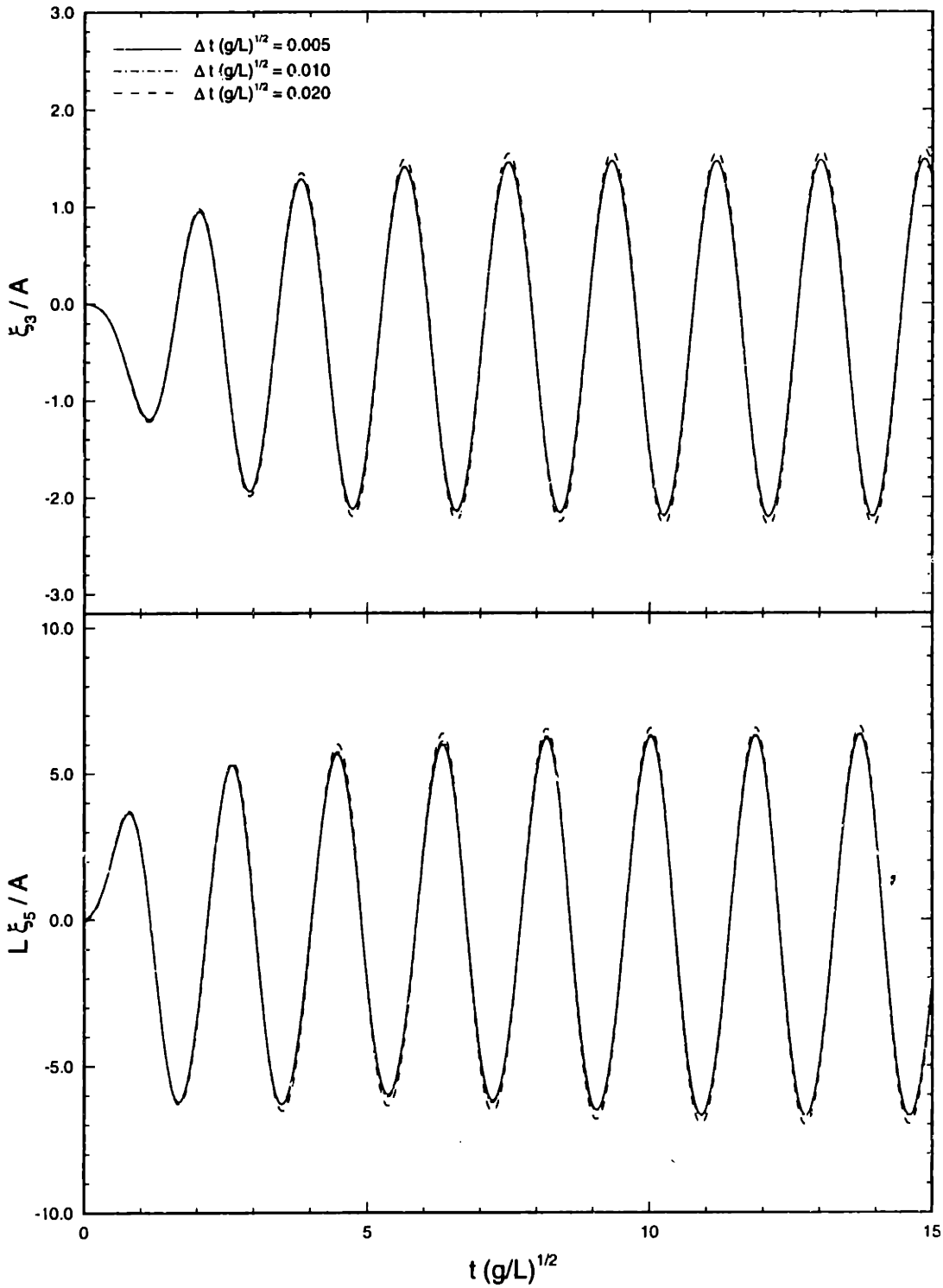

Figure 4-13: Temporal convergence of heave and pitch motions for the SnowDrift hull (D=8m) at $\mathcal{F} = 0.325$ in incident head seas, at an encounter frequency of $\omega(L/g)^{1/2} = 3.408$.

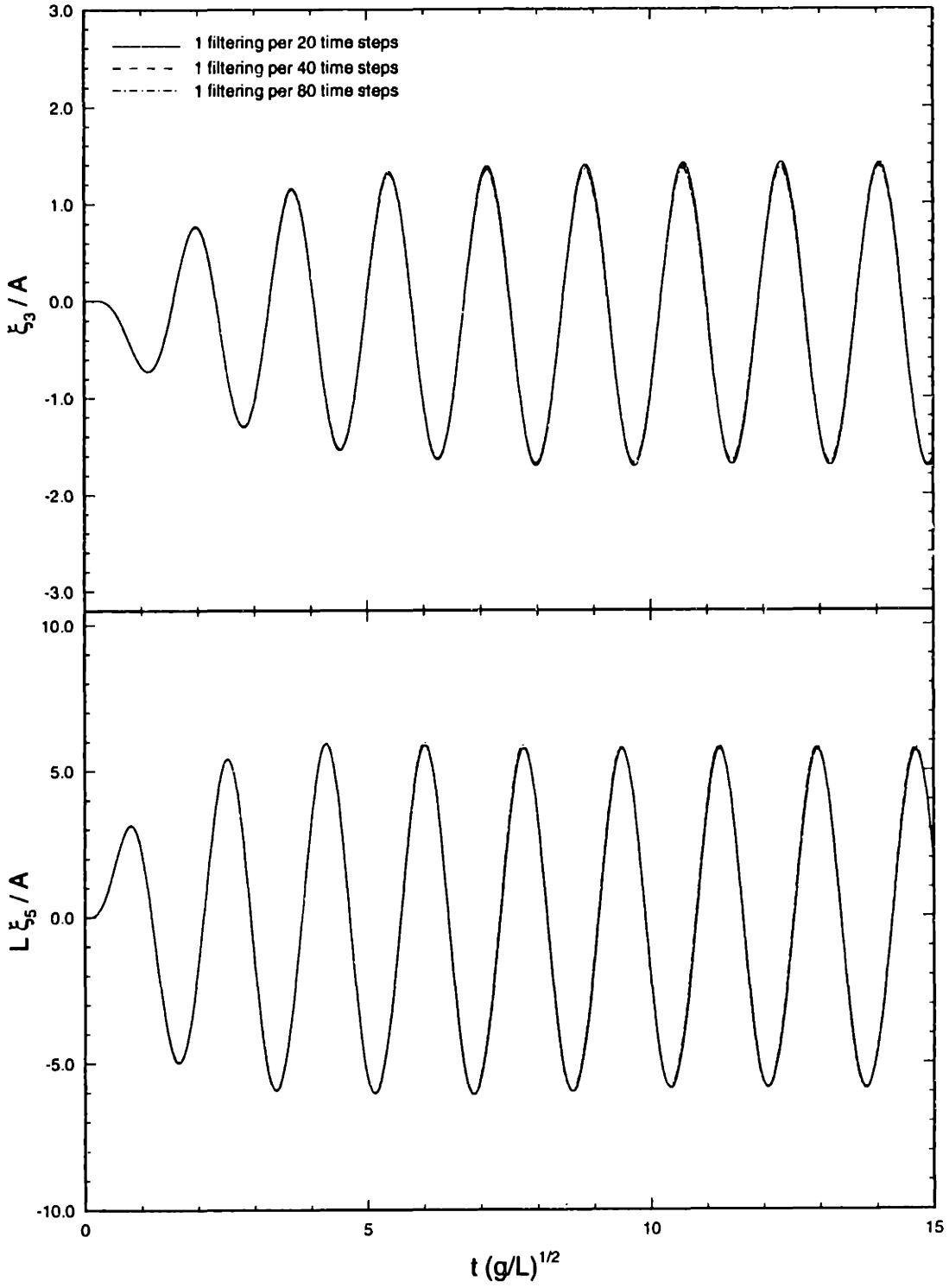

Figure 4-14: Convergence of heave and pitch motions with respect to filtering frequency for S7-175 at $\mathcal{F} = 0.275$ in incident head seas, at an encounter frequency of $\omega(L/g)^{1/2} = 3.628$.

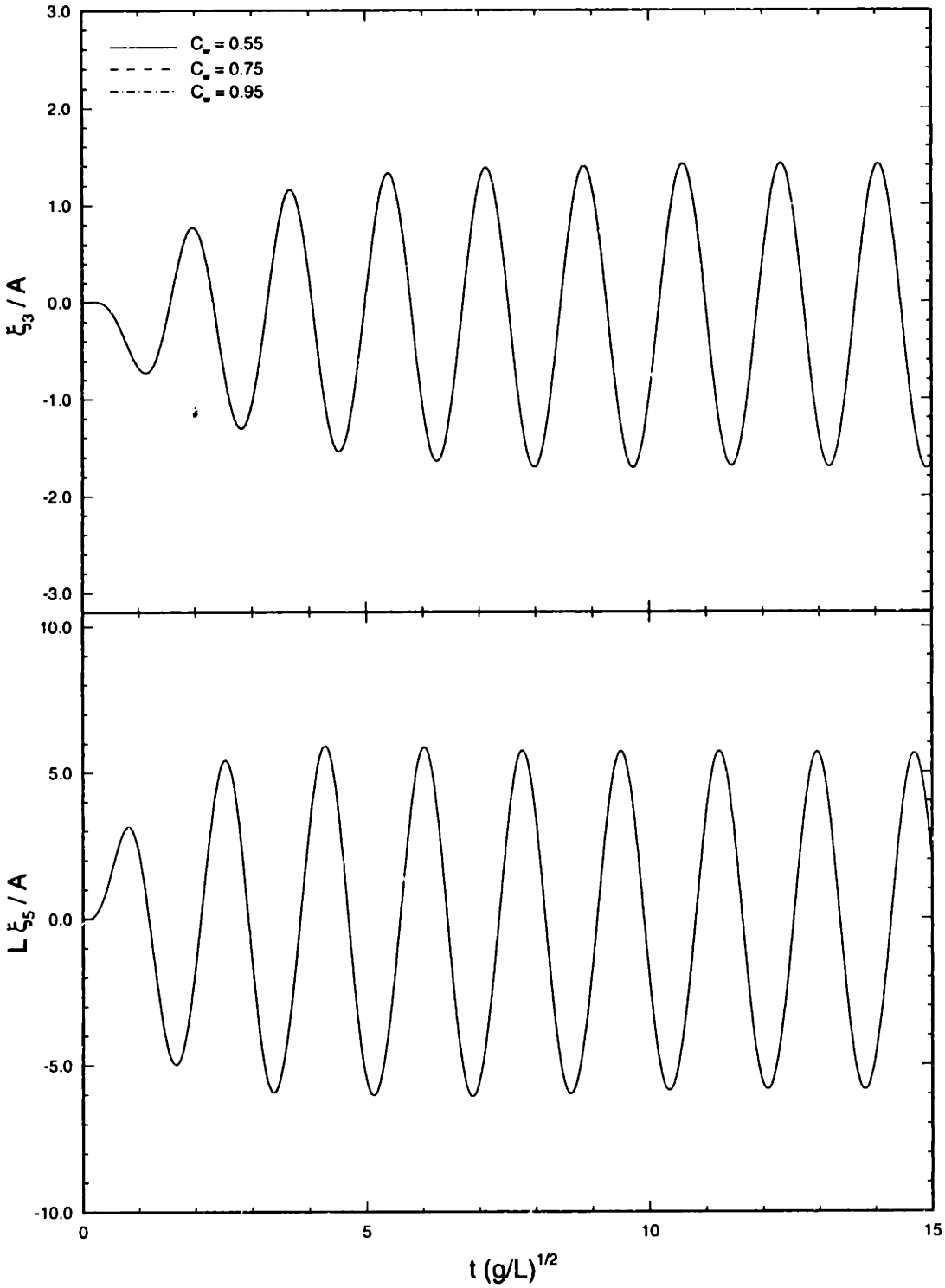

Figure 4-15: Convergence of heave and pitch motions with respect to beach size for S7-175 at $\mathcal{F} = 0.275$ in incident head seas, at an encounter frequency of $\omega(L/g)^{1/2} = 3.628$.

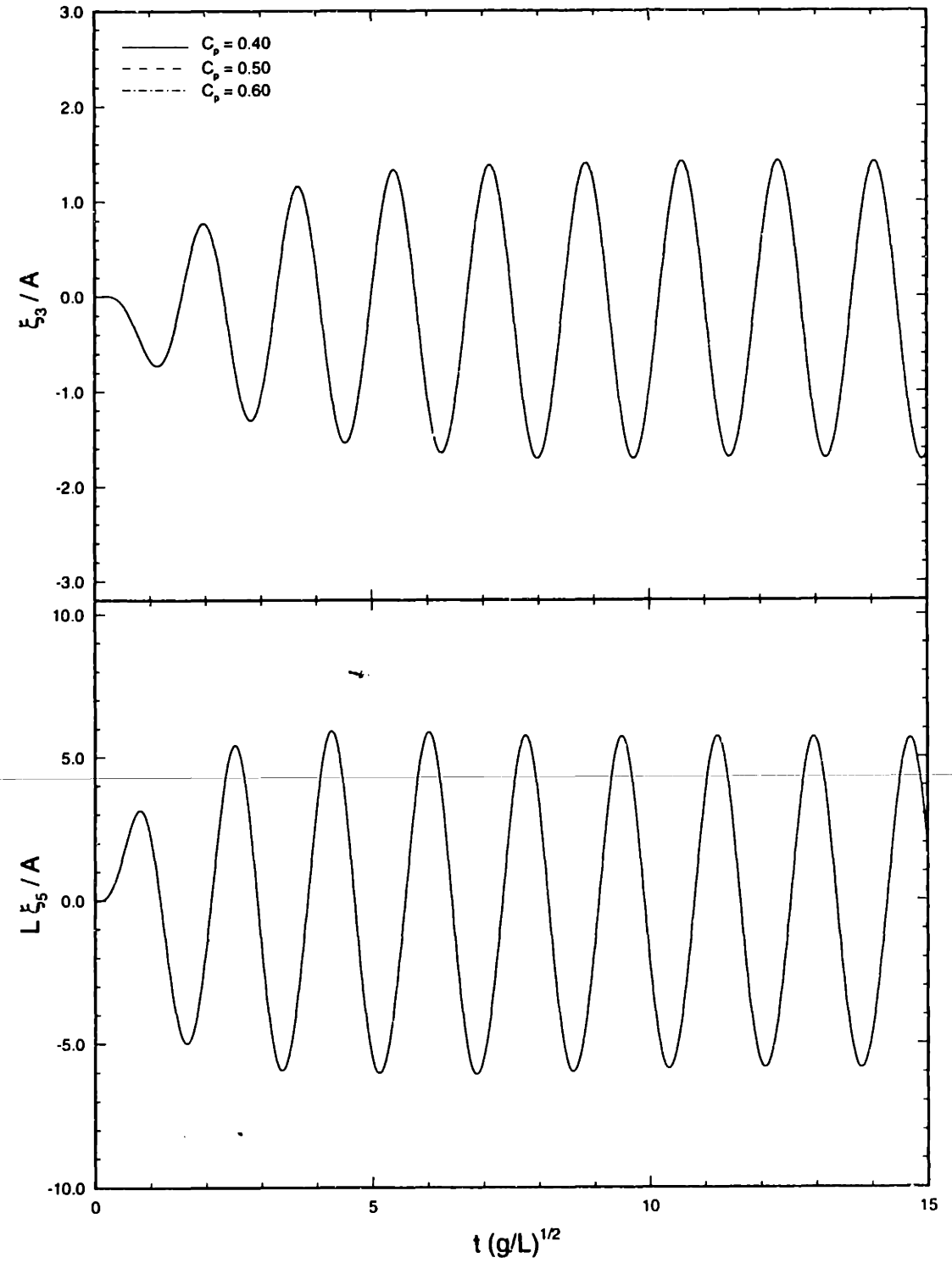

Figure 4-16: Convergence of heave and pitch motions with respect to beach starting point for S7-175 at $\mathcal{F} = 0.275$ in incident head seas, at an encounter frequency of $\omega(L/g)^{1/2} = 3.628$.

4.3.3 Oval-Type Grid

As discussed in the previous chapter, the oval-type free surface grid may lead to considerable savings in computational efforts in terms of both CPU hours and memory storage, often by as much as four times. But before any confidence is given in this type of geometric discretization, it is necessary to carry out careful tests on convergence and stability. Since the field problem being solved is elliptic, the coarse grid in the outer domain may have some effects on the pressure integration over the body. However the oval-type free surface grid, developed in this thesis, is found not to induce a large error.

As shown in Figure 3-3, the oval-type grid is determined primarily by three parameters: the width of constant spacing inner region, R_C, the width of the whole region, R_T, and the constant spacing in the inner region, Δ. Figures 4-17, 4-18 and 4-19 show that this oval type of geometric gridding is convergent with respect to all these parameters.

In Figures 4-20 and 4-21, the computational results between the oval type and the rectangular free surface grid are compared. The agreement for short waves is very satisfactory, but there are some discrepancies for long waves. It is believed that the differences come from the inadequate resolution in the far field which has far more influence for long waves. Another reason may be that the domain and beach are not large enough to accommodate long waves. Therefore for long waves, use of the rectangular free surface grid might be preferable.

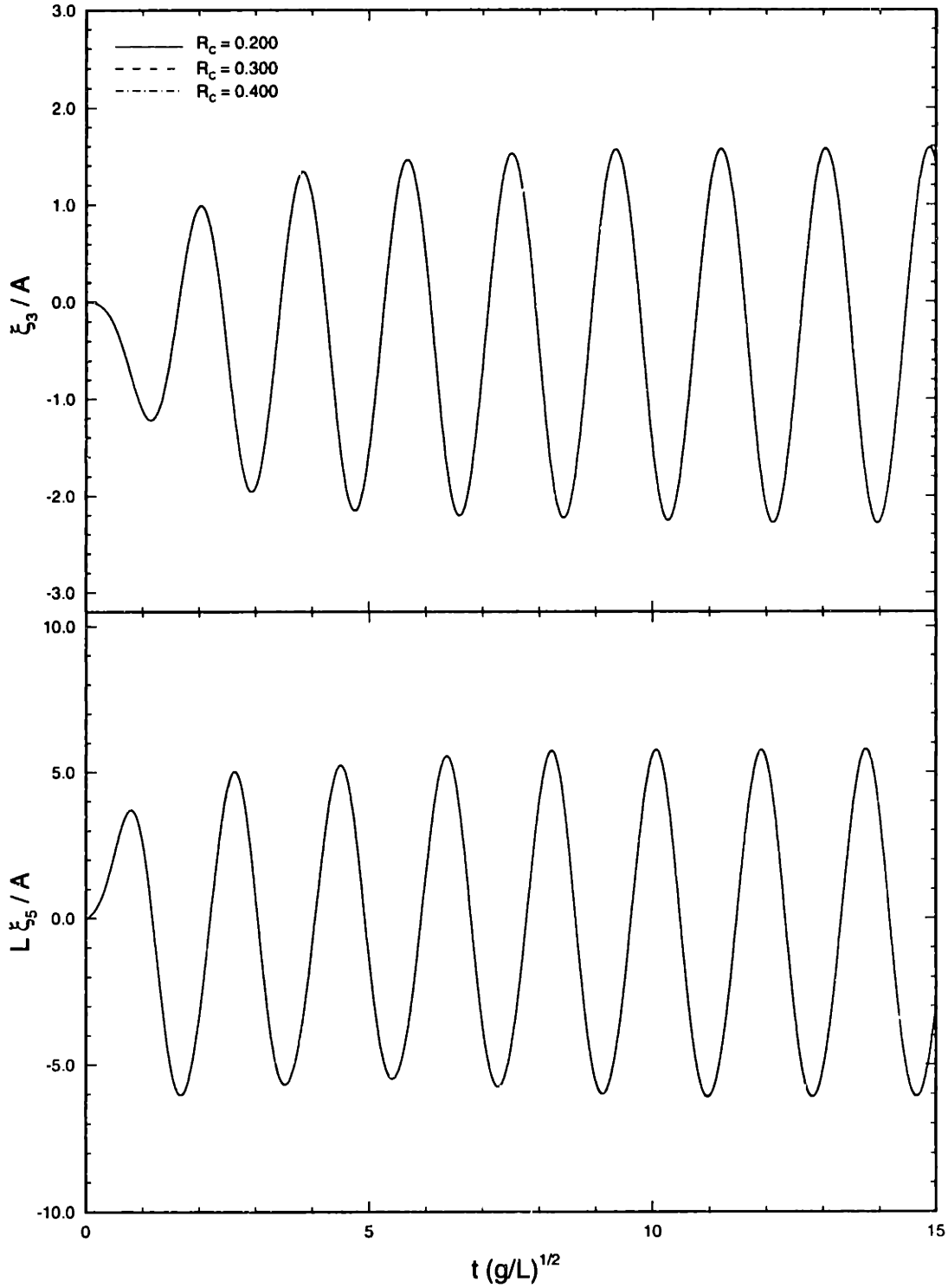

Figure 4-17: Constant domain width convergence of heave and pitch motions for the SnowDrift hull (D=8m) at $\mathcal{F} = 0.325$ in incident head seas, at an encounter frequency of $\omega(L/g)^{1/2} = 3.408$.

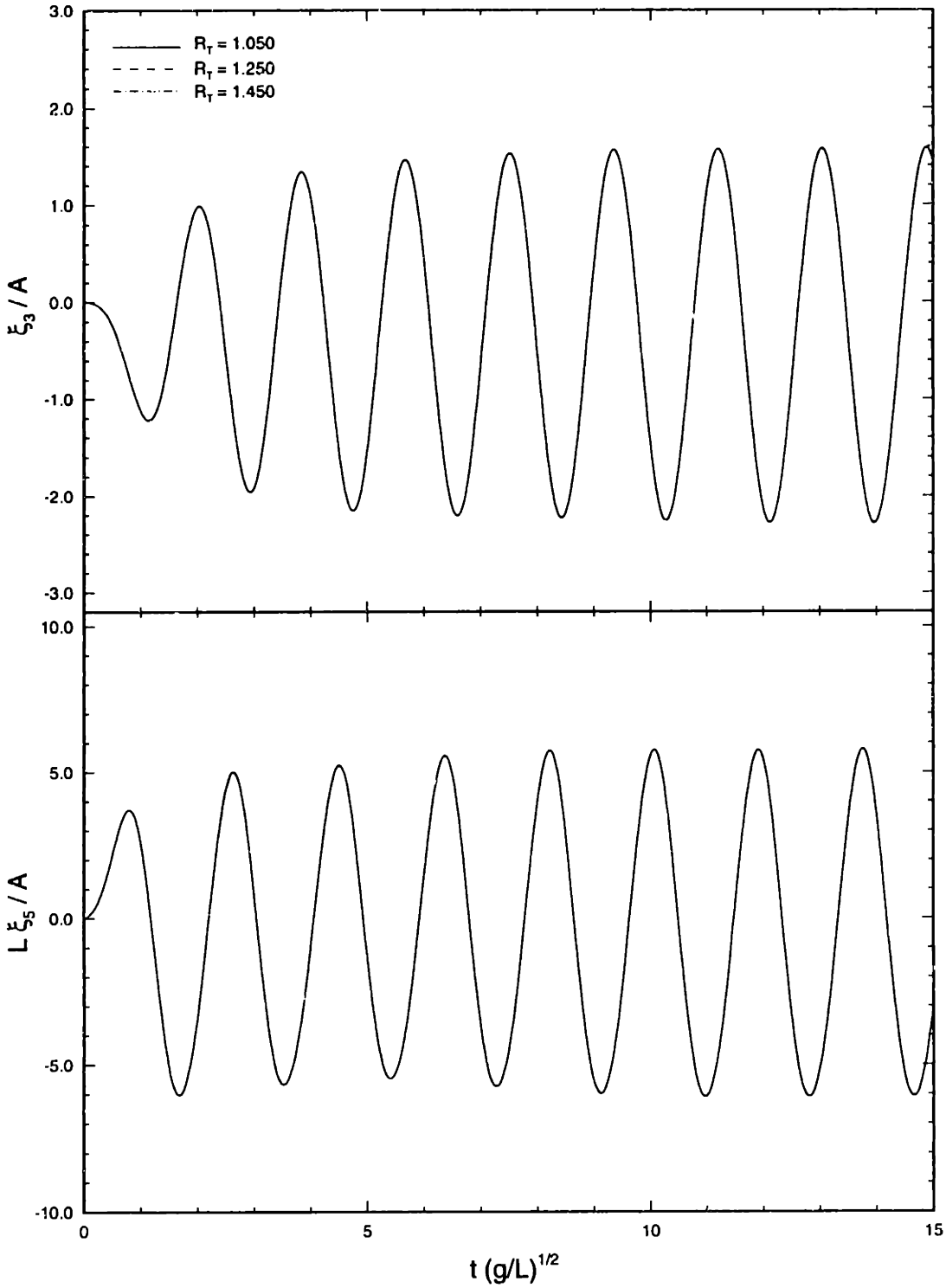

Figure 4-18: Whole domain width convergence of heave and pitch motions for the SnowDrift hull (D=8m) at $\mathcal{F} = 0.325$ in incident head seas, at an encounter frequency of $\omega(L/g)^{1/2} = 3.408$.

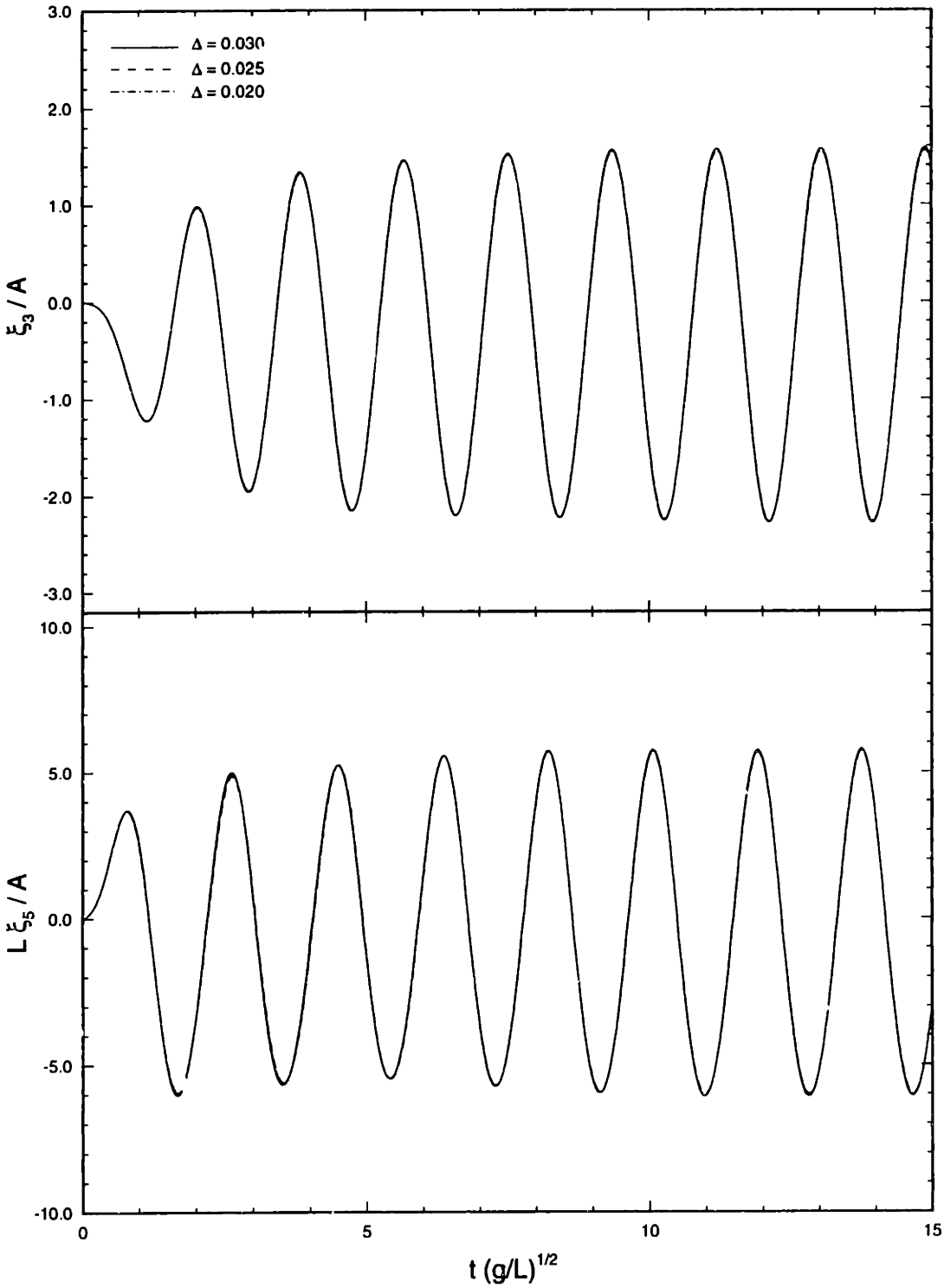

Figure 4-19: Constant domain spacing convergence of heave and pitch motions for the SnowDrift hull (D=8m) at $\mathcal{F} = 0.325$ in incident head seas at an encounter frequency of $\omega(L/g)^{1/2} = 3.408$.

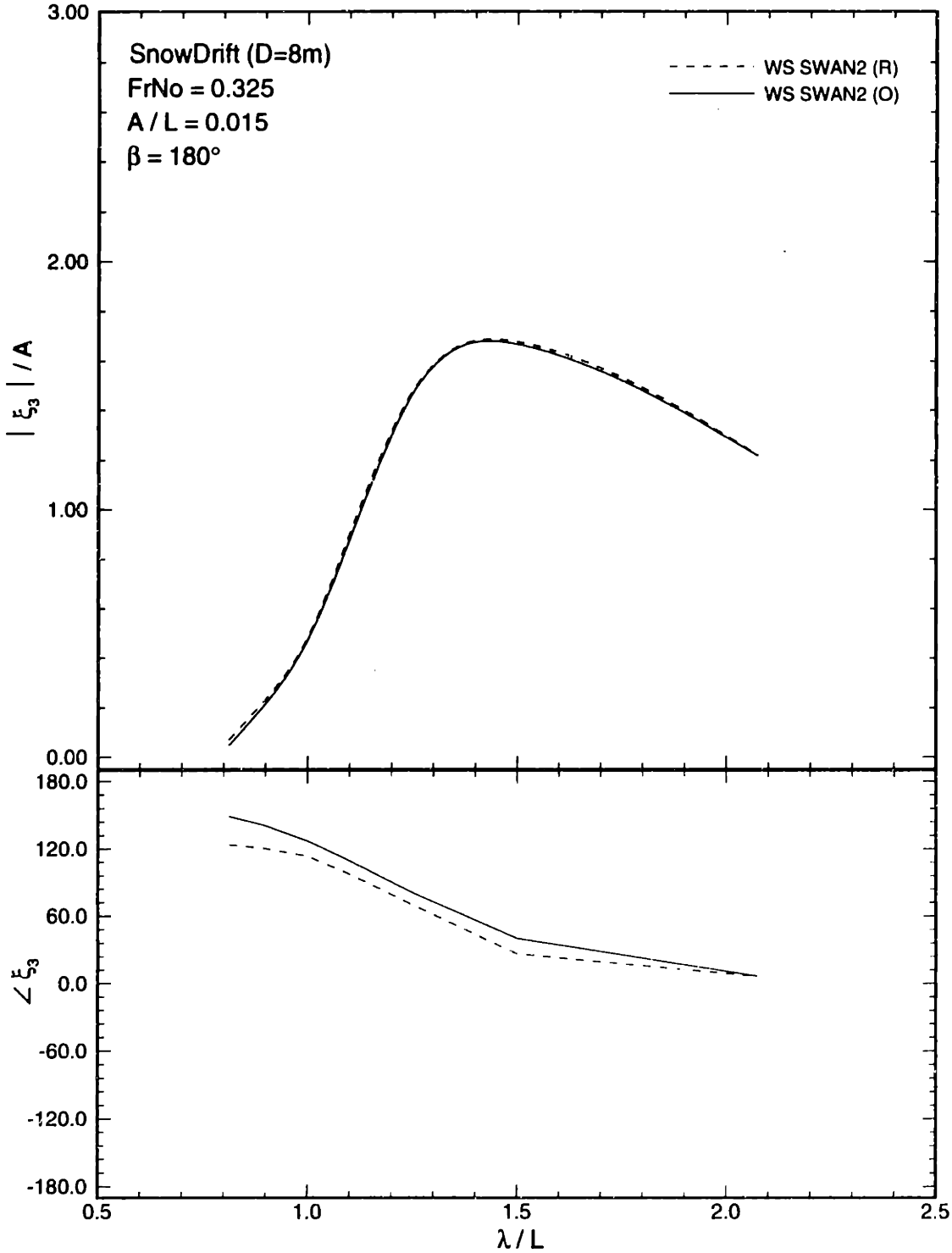

Figure 4-20: Comparison between rectangular and oval free surface grid of heave motions for the SnowDrift hull (D=8m) at $\mathcal{F} = 0.325$ in incident head seas at an encounter frequency of $\omega(L/g)^{1/2} = 3.408$.

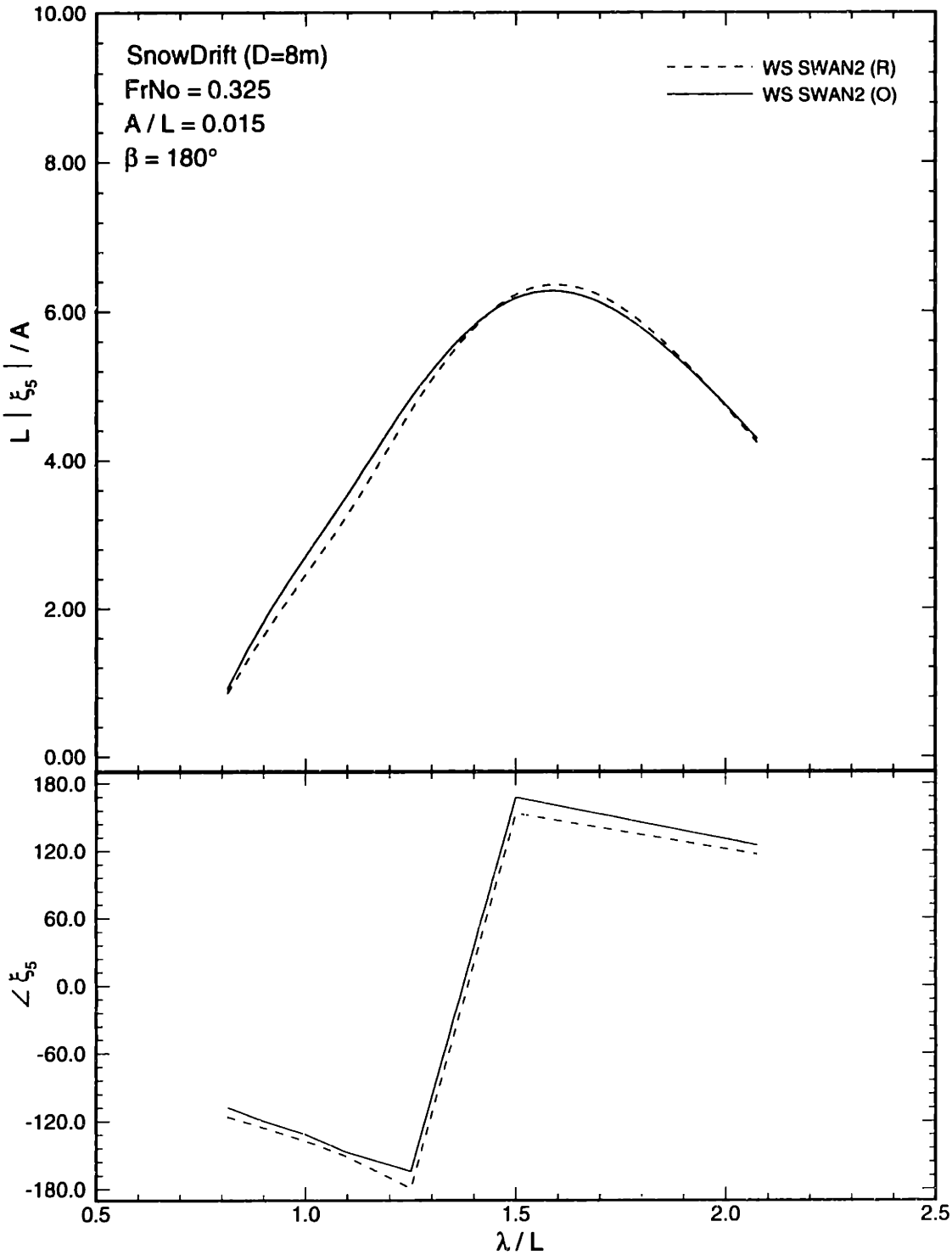

Figure 4-21: Comparison between rectangular and oval free surface grid of pitch motions for the SnowDrift hull (D=8m) at $\mathcal{F} = 0.325$ in incident head seas at an encounter frequency of $\omega(L/g)^{1/2} = 3.408$.

4.3.4 Series60 (Block Coefficient 0.7)

Again, before testing the program for more practical cases, this numerical method is tested for a Series60 ($C_b = 0.7$) hull. The nonlinear effects are expected not to be important for this type of hull, and the linear and nonlinear predictions of motion responses should be close. Figures 4-22 and 4-23 show comparisons between the linear, nonlinear computational results and experimental measurements. The agreement is satisfactory, as expected.

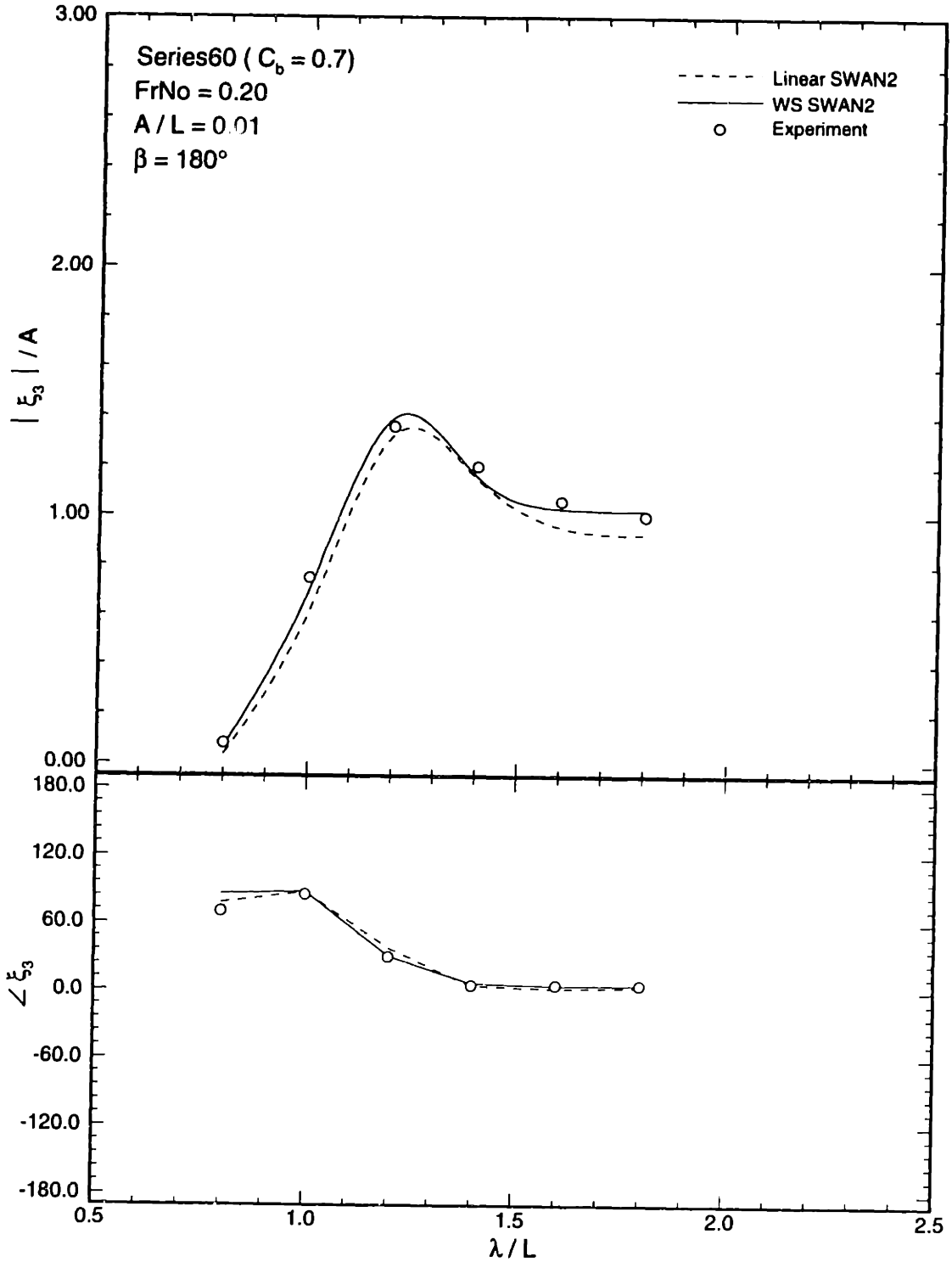

Figure 4-22: Amplitude and phase of the heave response amplitude operator (RAO) for the Series60 ($C_b = 0.7$) hull at $\mathcal{F} = 0.2$ in head seas.

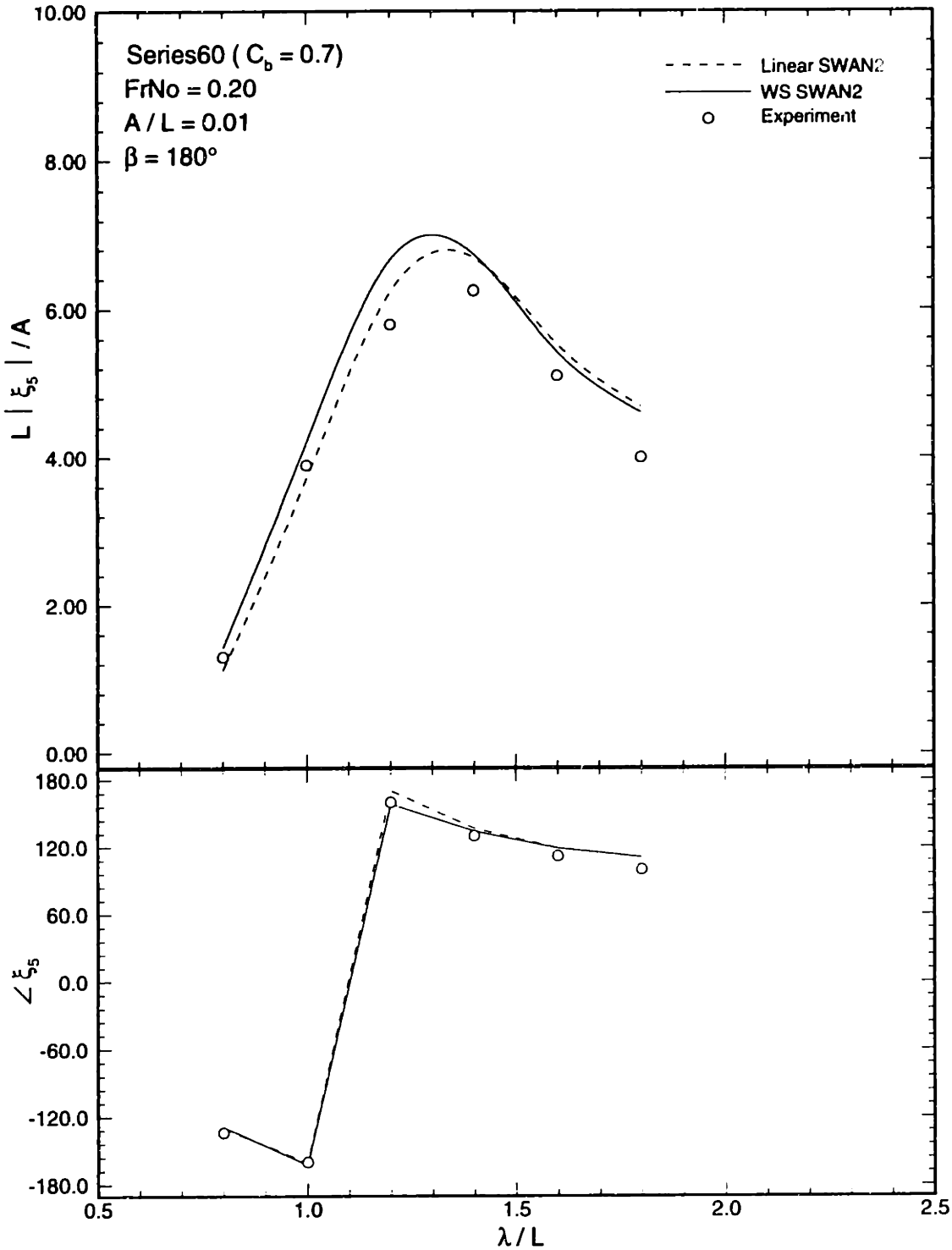

Figure 4-23: Amplitude and phase of the pitch response amplitude operator (RAO) for the Series60 ($C_b = 0.7$) hull at $\mathcal{F} = 0.2$ in head seas.

4.3.5 SnowDrift (Ballast)

The usefulness of the Weak-Scatterer version of SWAN2 program is demonstrated in Figures 4-24 and 4-25, which show the amplitude and phase of the head sea, motion response amplitude operators over the range of incident wavelengths for a slender-body containership: the SnowDrift hull in ballast condition. The computational results shown in previous sections are included to illustrate the progressive improvement in the numerical predictions relative to the experiment data by the gradual account of nonlinear effects. The predictions of the Weak-Scatterer SWAN2 are consistently better than all other calculations for both heave and pitch motions, compared with the experimental measurements.

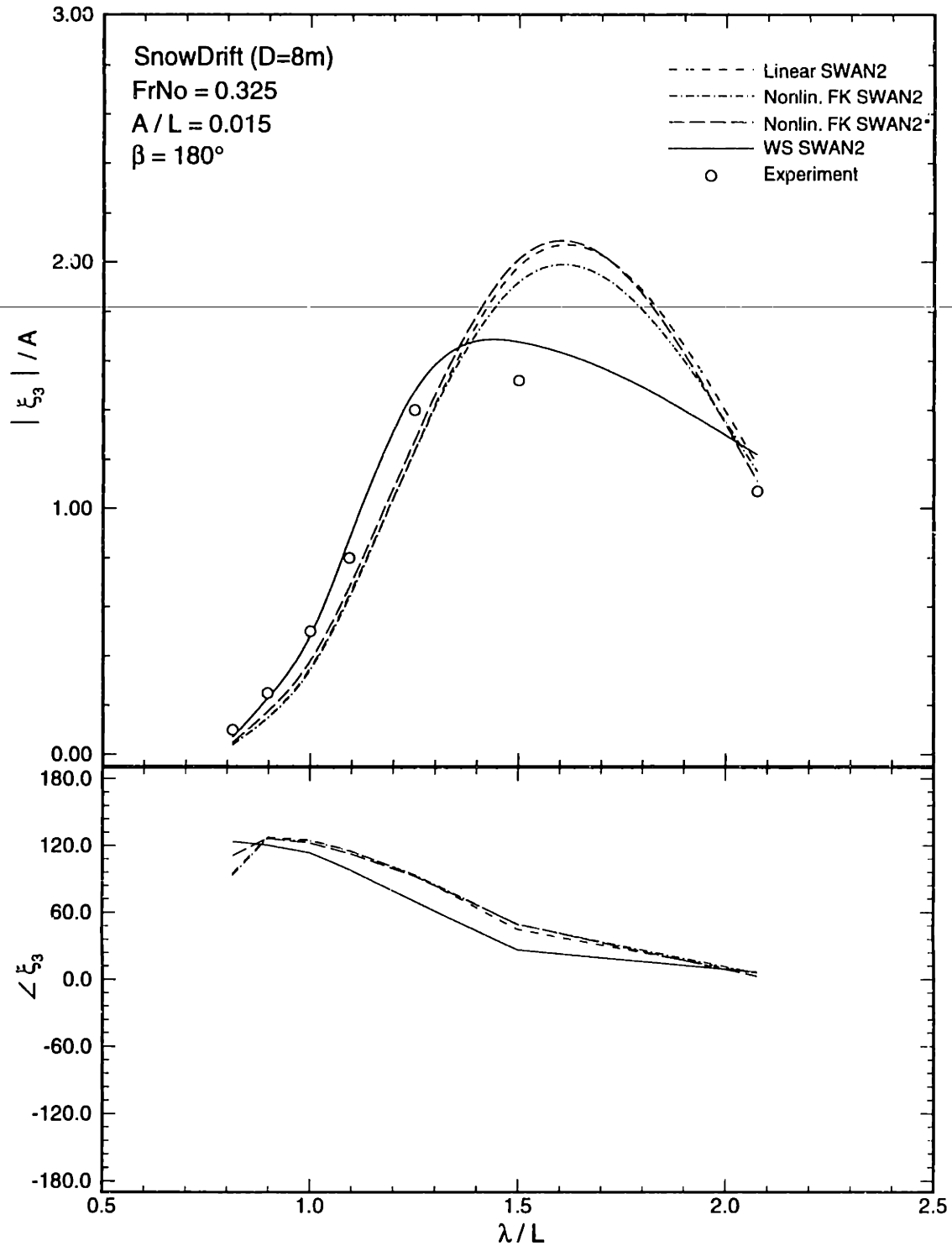

Figure 4-24: Amplitude and phase of the heave response amplitude operator (RAO) for the SnowDrift ($D = 8(m)$) hull at $\mathcal{F} = 0.325$ in head seas.

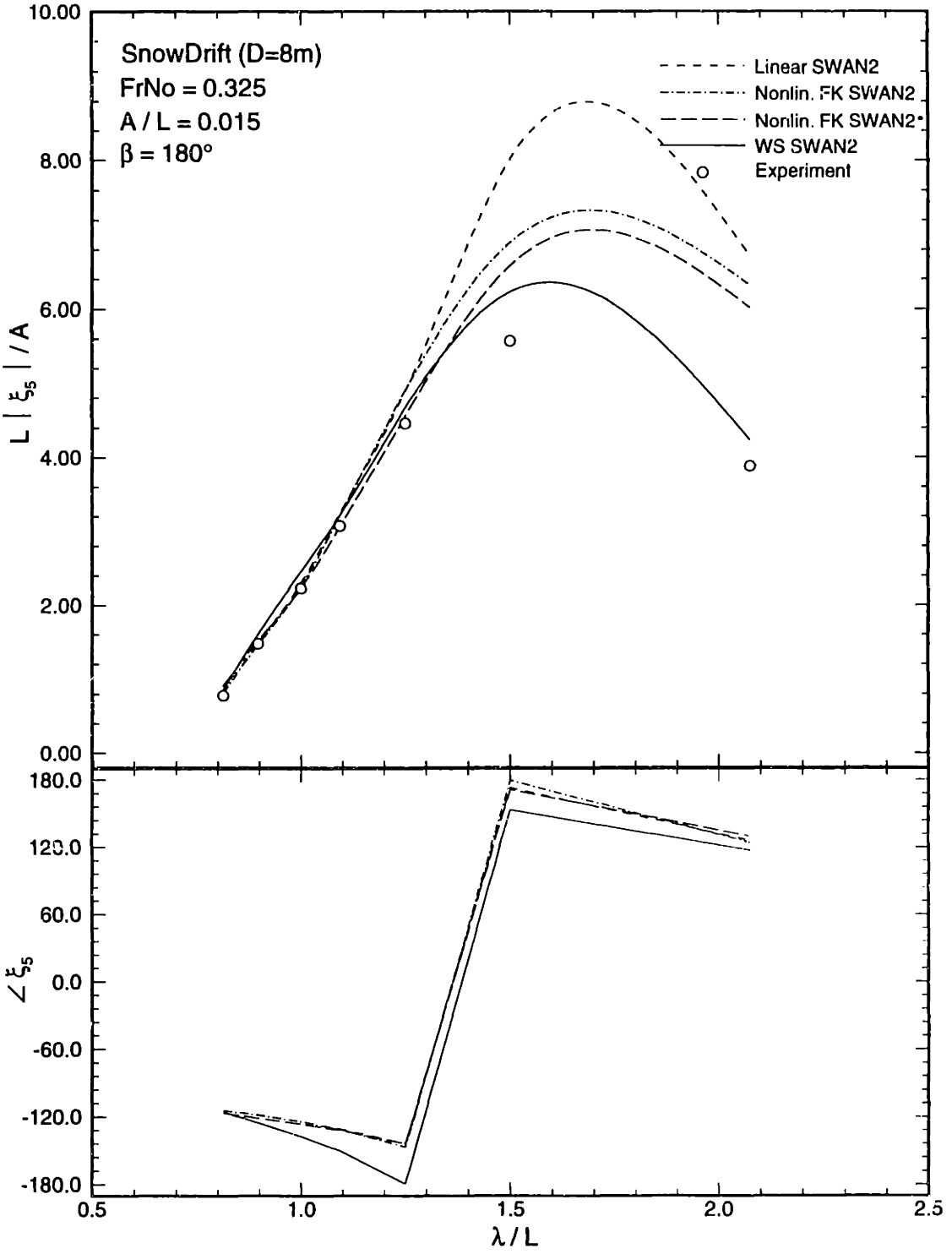

Figure 4-25: Amplitude and phase of the pitch response amplitude operator (RAO) for the SnowDrift ($D = 8(m)$) hull at $\mathcal{F} = 0.325$ in head seas.

4.3.6 S7-175 Containership

The Weak-Scatterer version of SWAN2 program is also tested for a more conventional containership S7-175, for which experimental data are available and trusted. Figure 4-5 shows its body plan. The output of the heave and pitch motion RAO's is shown along with results from the linear SWAN2, the quasi-nonlinear SWAN2 and experiment measurements, in Figures 4-26 and 4-27. The experiment was conducted by Dalzell, Thomas and Lee in 1986 [9]. The S7-175 hull is traveling at $\mathcal{F} = 0.275$ in head seas. Again, compared with those of the linear and quasi-nonlinear versions, the predictions of the Weak-Scatterer version are consistently better for both heave and pitch motions in correlation to the experimental results. The improvement is clear, particularly at the resonant peak, and it shows the importance in the inclusion of bow flares and stern counters in the calculations. The effects of the nonlinear Froude-Krylov forces, originally thought to be dominant, turn out to be less significant than the nonlinear hydrodynamic effects accounted for by the Weak-Scatterer formulation.

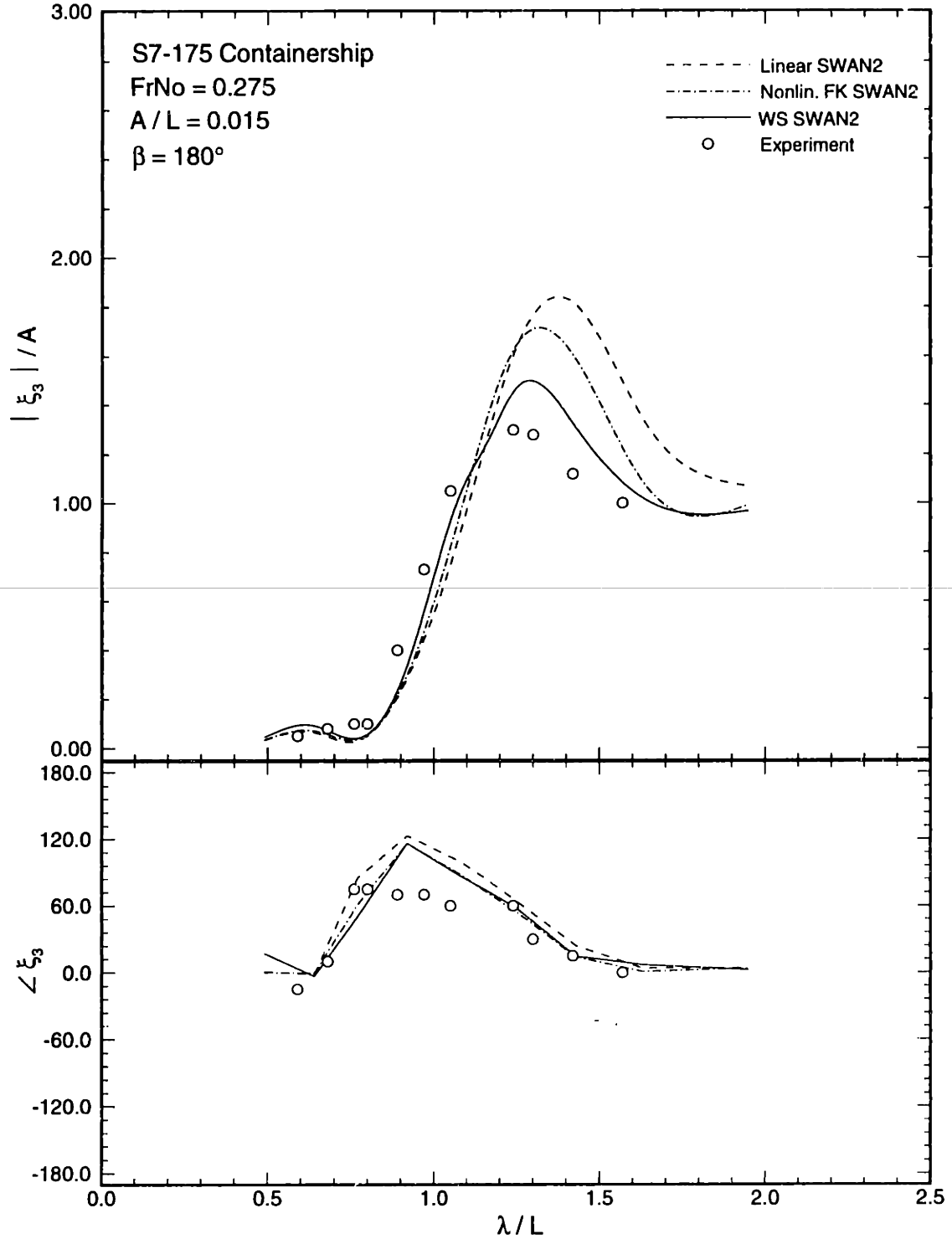

Figure 4-26: Amplitude and phase of the heave response amplitude operator (RAO) for the S7-175 Containership at $\mathcal{F} = 0.275$ in head seas.

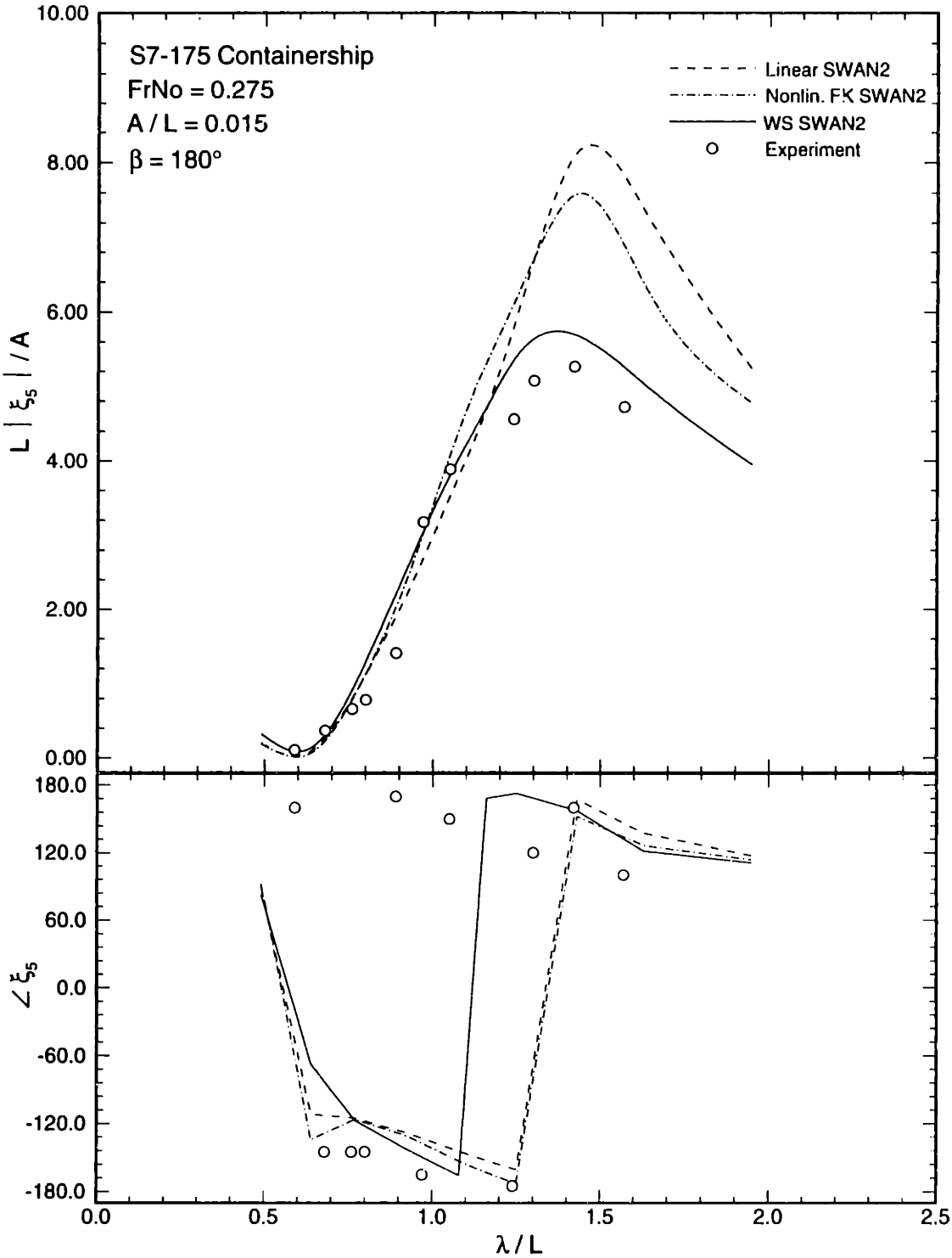

Figure 4-27: Amplitude and phase of the pitch response amplitude operator (RAO) for the S7-175 Containership at $\mathcal{F} = 0.275$ in head seas.

4.3.7 Nonlinearities and Wave Patterns

Figure 4-28 shows four snapshots of the hull positions relative to the ambient waves at different instants during the simulation. The S7-175 containership is translating at $\mathcal{F} = 0.275$ in head seas at the encounter wave frequency $\omega\sqrt{g/L} = 3.629$. The classical linear theory presumes the ship stays in the calm-water position (the top figure) at all times and consequently it misses the geometric nonlinear effects (bow flares and stern counters) while the ship is actually moving in and out of water, as demonstrated in the figure.

Figure 4-29 displays the sensitivities of the heave and pitch motion RAO to the incoming wave slopes. The Weak-Scatterer version of SWAN is tested for the S7-175 containership traveling at $\mathcal{F} = 0.275$ in head seas at the encounter wave frequency $\omega\sqrt{g/L} = 3.629$, and with increasing ambient wave amplitude. The heave and pitch motion RAO's show evident wave steepness dependency. The steeper the waves become, the lower the RAO's. This is understandable because larger waves presumably submerge more hull surface and therefore increase the hydrostatic restoring forces. It is also interesting to note that for small wave slope, the Weak-Scatterer prediction does converge to the linear result, thus demonstrating the consistency of the Weak-Scatterer formulation.

Figures 4-31 and 4-32 show the disturbance wave profiles for the SnowDrift (ballast) hull, traveling at $\mathcal{F} = 0.325$ in head seas with the ratio of the incoming wave wavelength over the ship length between perpendiculars $\lambda/L = 1.50$, at four instances. The corresponding disturbance wave patterns calculated by the linear version of SWAN2 are also included for comparison. The waves actually look quite similar, but there exist distinct differences in pressure distributions over the hull surface. This again shows the importance on the actual geometric positions of the ship. A snapshot of the disturbance wave pattern in the whole domain is provided as well.

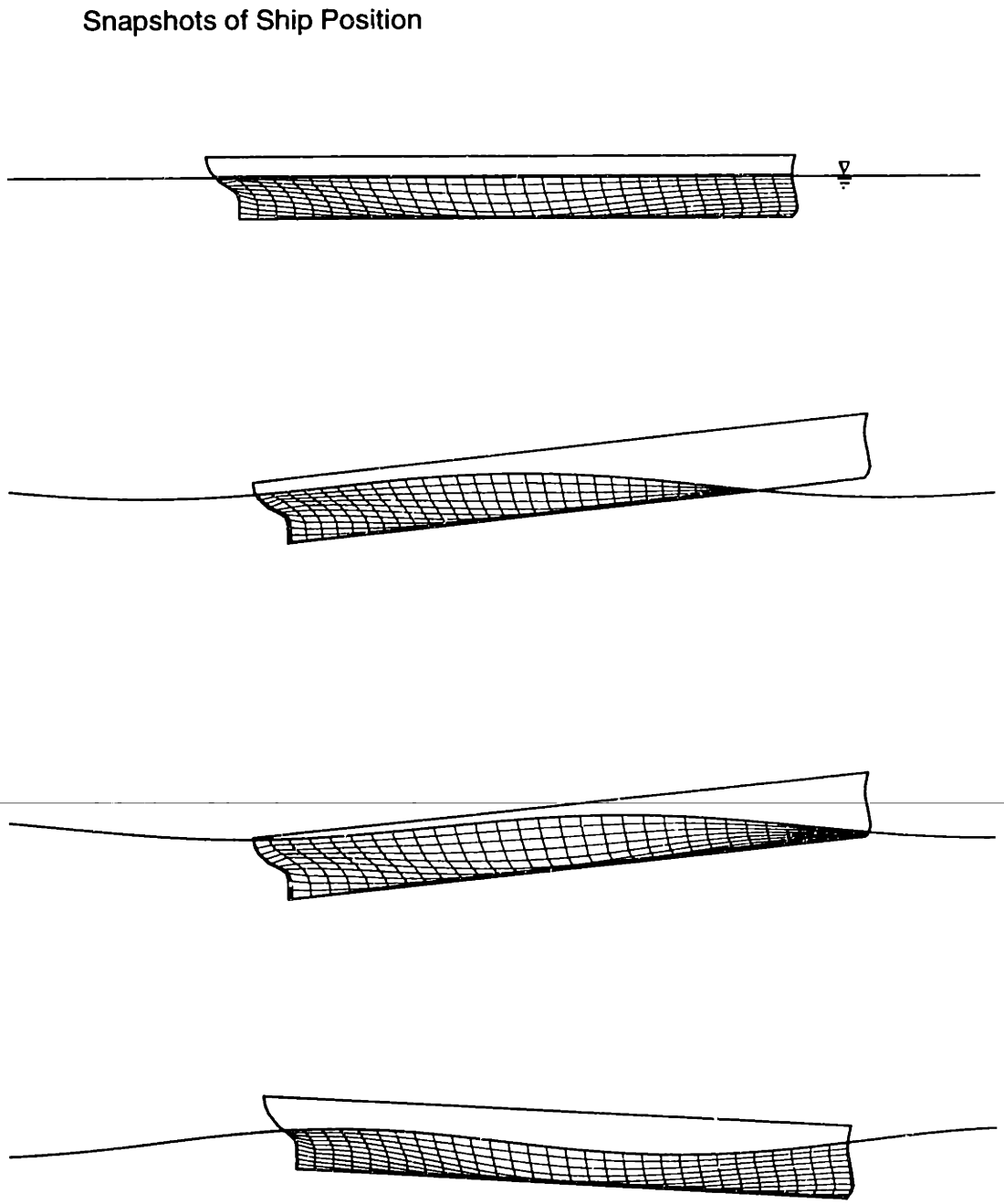

Figure 4-28: Snapshots of hull positions for the S7-175 containership at $\mathcal{F} = 0.275$ in head seas.

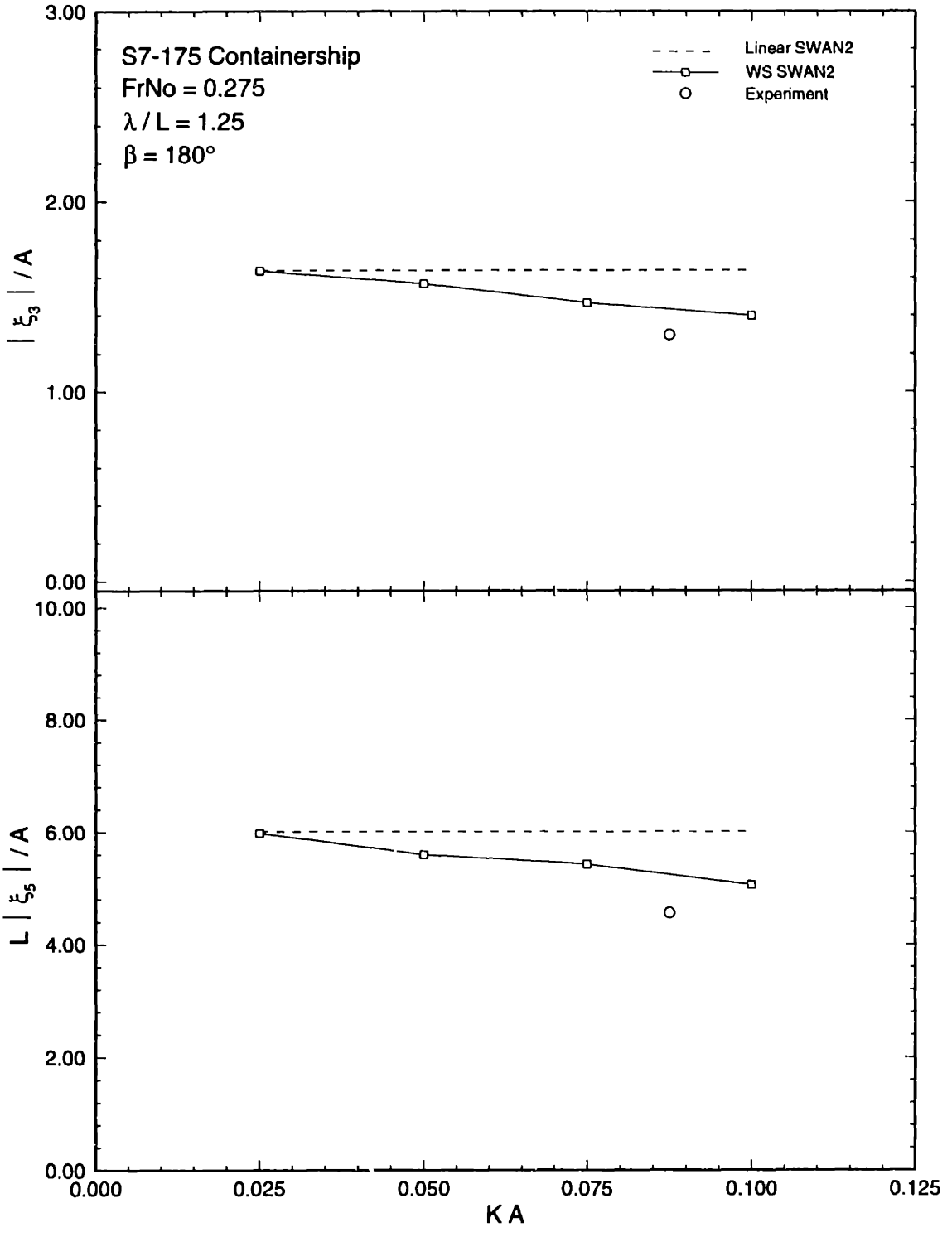

Figure 4-29: Nonlinearities of motion RAO's for the S7-175 containership at $\mathcal{F} = 0.275$ at different incoming wave slopes. In head seas with the ratio of the wavelength over ship length at 1.25.

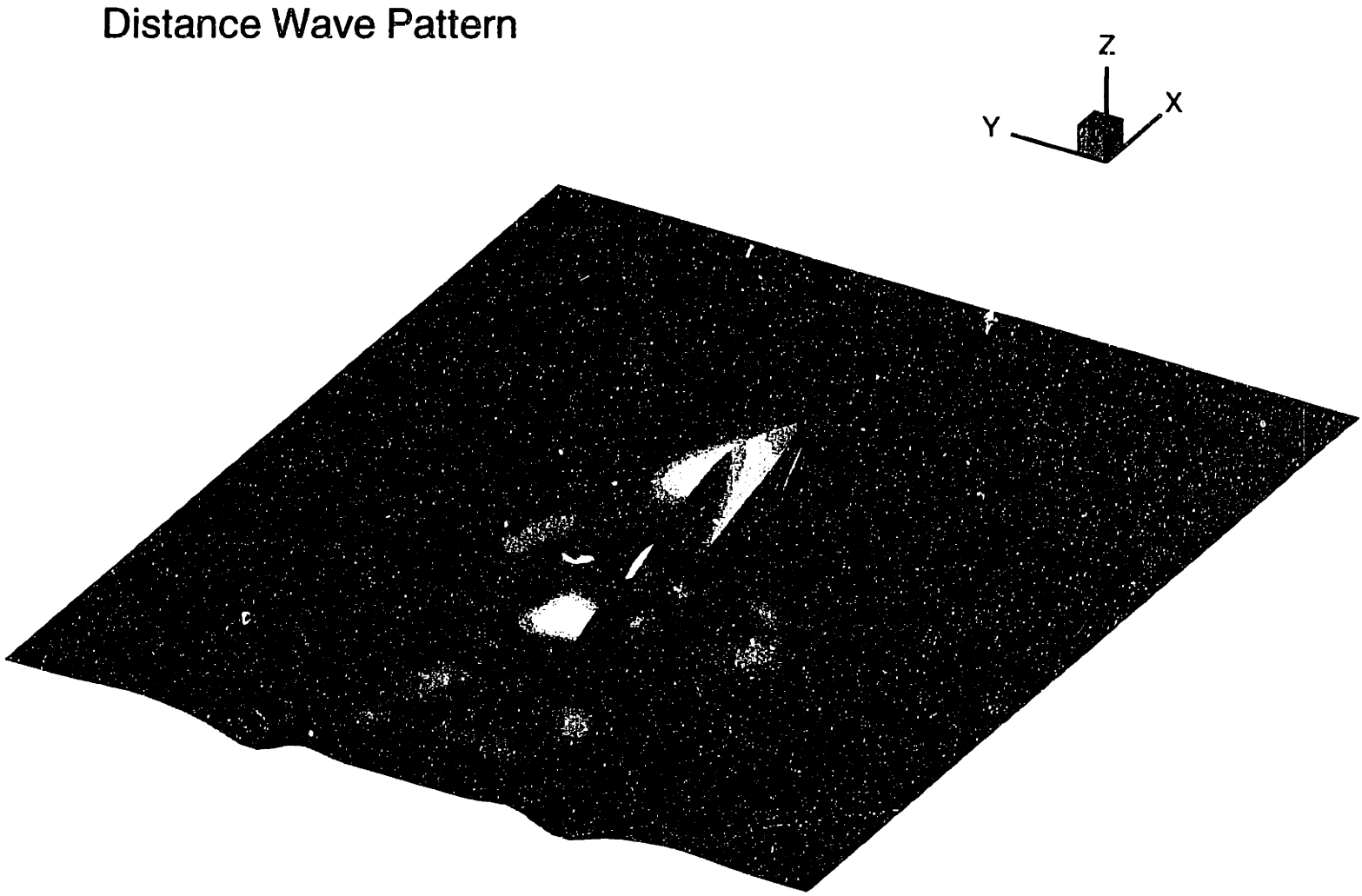

Figure 4-30: Disturbance wave patterns for the SnowDrift (ballast) containership at $\mathcal{F} = 0.325$. In head seas with the ratio of the wavelength over ship length $\lambda/L = 1.50$.

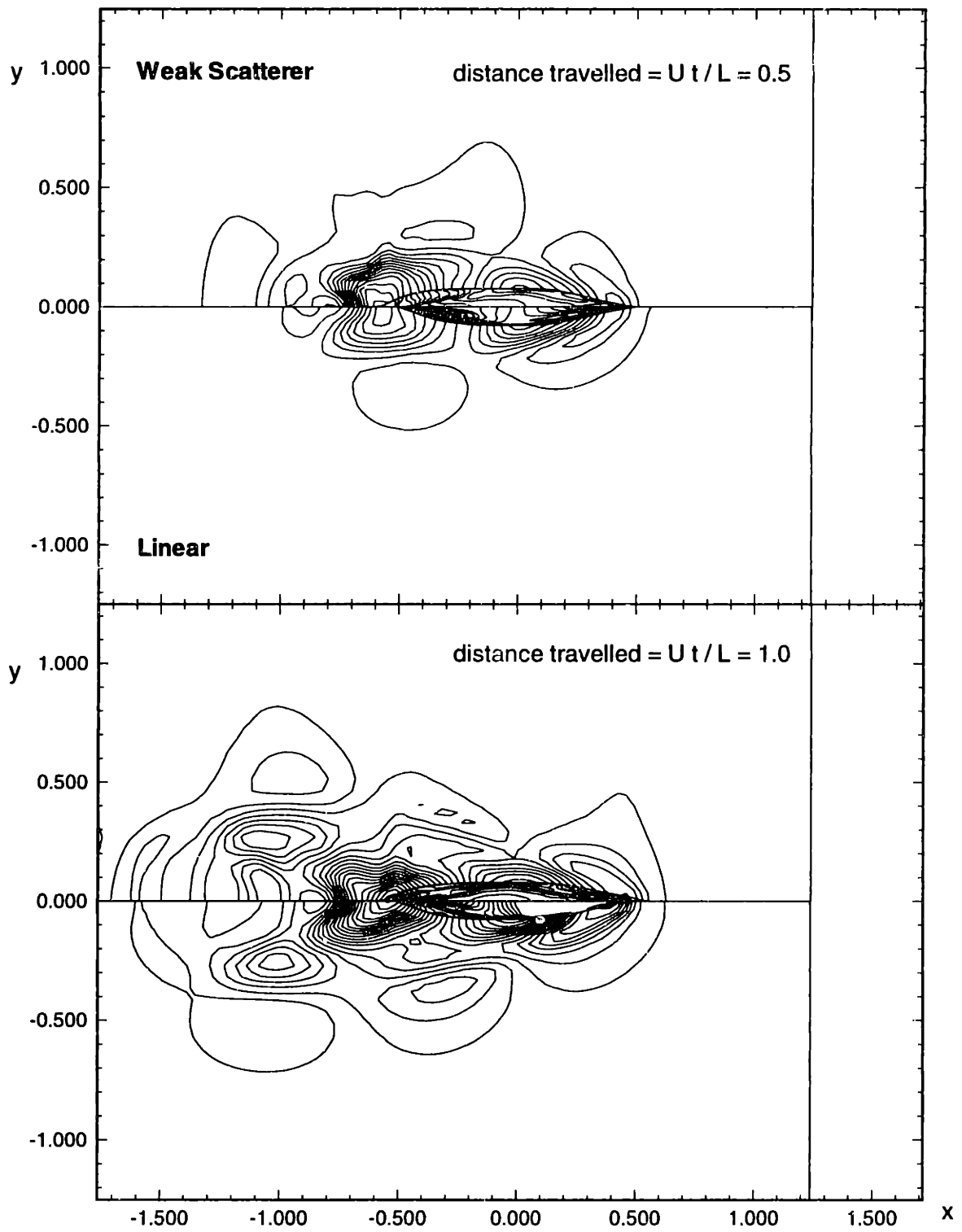

Figure 4-31: Disturbance wave patterns history for the SnowDrift (ballast) containership at $\mathcal{F} = 0.325$. In head seas with the ratio of the wavelength over ship length $\lambda/L = 1.50$.

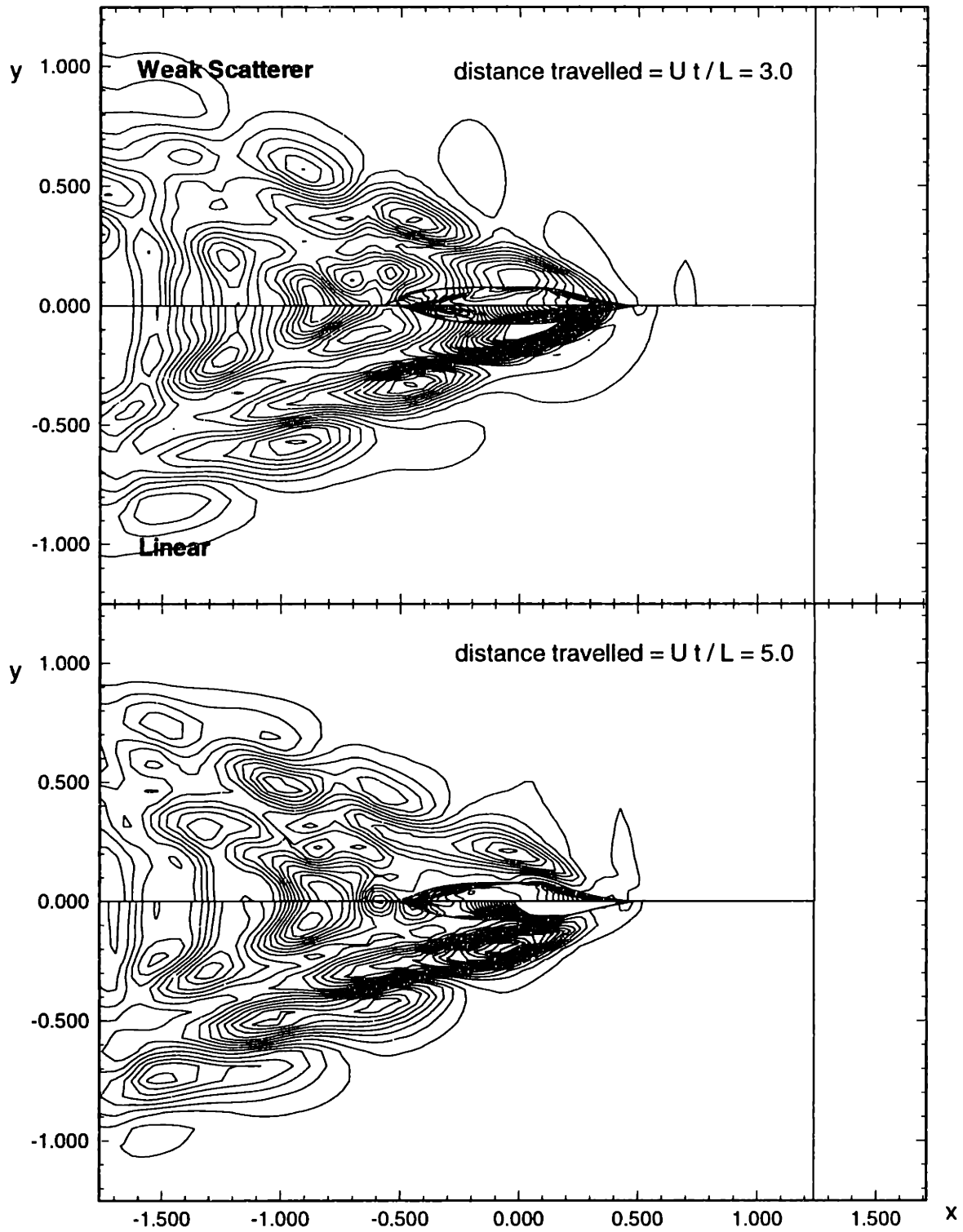

Figure 4-32: Disturbance wave patterns history for the SnowDrift (ballast) containership at $\mathcal{F} = 0.325$. In head seas with the ratio of the wavelength over ship length $\lambda/L = 1.50$.

Chapter 5

Conclusions and Future Work

In this thesis, a robust numerical algorithm has been developed to simulate the nonlinear free surface ship flows and compute the motion responses for a variety of ships in steep ambient waves. It serves as a numerical tank to differentiate among all kinds of nonlinearities embedded in the problem and eventually provides guidance in studying the exact fully nonlinear ship wave problems.

The numerical method is based on a carefully examined theory — the Weak-Scatterer hypothesis, which assumes a relatively small ship-generated disturbances even in the presence of steep incoming incident waves and large body motions. This represents a major step towards the complete solution of the exactly nonlinear problem. In classical linear theory, it is presumed that the incoming waves and wave-induced body motions are so small that all disturbances are linearizable over the forward speed effects. Although the linear theory has its applications and often produces reasonable results, it fails in many practical applications because it cannot properly handle complex ship geometry and the nonlinearities associated with steep ambient waves. The Weak-Scatterer theory, on the other hand, identifies accurately and consistently the nonlinearities of the ship geometry and incoming waves since it imposes the body boundary conditions over the exact instantaneous submerged body surface and the free surface conditions upon the incoming wave profile, therefore being a drastic departure from the linear theory. Classical linear theory enforces the body

boundary conditions on the calm-water body position and the free surface conditions on the calm water free surface plane. Even though the Weak-Scatterer theory invokes certain approximations, in that it assumes that the ship-generated disturbances are comparatively small and it is not capable of modeling "local" extreme events such as wave breaking, slamming and deck-wetness. This thesis however has demonstrated that the theory is able to capture "global" nonlinearities and improve the predictions of motion responses for ships traveling in rough water and moderate Froude numbers.

The numerical method has evolved from a decade's experience in developing the frequency- and time-domain Rankine panel methods, originating from a solid foundation of linear programs — SWAN1 and SWAN2, and founded upon a thorough understanding of numerical stability and error propagation over free surface panel discretizations. The Rankine panel method discretizes both the free surface and the submerged hull surface, and requires the distribution of Rankine sources/dipoles over the discretized domains. It is not the most elegant method in enforcing the free surface conditions and the radiation conditions. It however has demonstrated a large degree of flexibility in adopting different kinds of free surface conditions (linear or nonlinear) in the linear programs and again in the present nonlinear extension. A bi-quadratic spline scheme is used for the spatial discretizations of all quantities of interest such as the velocity potentials, the normal velocities and the wave elevations, coupled with the temporal discretizations of the so-called Emplicit (Explicit-Implicit) Euler scheme. The algorithm has been developed through careful numerical error analysis and gained from the development of the linear methods. Numerical errors introduced by the discretization of the free surface are controlled by the modified 7-point spatial filter. The truncation of the free surface is made possible by the implementation of numerical beaches which damp out the wave reflections from the boundaries. A nonlinear equation of motion is derived and integrated by the fourth-order Adams-Bashford-Moulton scheme with the fourth-order Runge-Kutta scheme for the first four time steps. The time-step is selected from the stability criterion derived from a von-Neumann error analysis. An extensive set of calculations of motion responses has been carried out for realistic ship forms to demonstrate the accuracy and robustness

of the Weak-Scatterer method.

The numerical method in this thesis has been validated against exhaustive numerical experiments. First of all, the time-domain linear program (SWAN2) and its quasi-nonlinear variation are used to demonstrate the feasibility of the proposed study. Nonlinear hydrostatic forces and Froude-Krylov forces are included into the linear solution with the hydrodynamic problem treated linearly. This somewhat inconsistent extension proves the importance of the nonlinearities associated with the hydrostatics and incoming waves since it improves the predictions of the motion response RAO's over the classical linear theory. Secondly, forced motion tests have been conducted to validate the enforcement of the body boundary conditions over the exact instantaneous submerged hull surface. Force coefficients of a Series60 hull are calculated and compared to those from the linear computations and experimental measurements. Thirdly, free motion simulations have been carried out for a Series60 hull and two practical ships. Motion response RAOs in head seas and disturbance wave patterns are computed. All computational results from the Weak-Scatterer method demonstrably improves over those from the linear versions and quasi-nonlinear version of the SWAN program in comparison to experimental measurements. This new nonlinear extension of the method is therefore expected to serve as a valuable computer analysis and design tool for conventional ships.

Future developments are planned in the following directions.

- **Global structural load computations:** A safe design for a ship hinges upon accurate predictions of the global structural loads. This nonlinear method needs to be extended to compute the global forces.

- **Oblique wave applications:** At the present, the method can only simulate free surface flows in head seas. An oblique sea extension should be developed and eventually simulations in stochastic sea states should be integrated into the method.

- **Transom-stern ships:** Transom-stern ships progressively become more and

more popular. It would therefore be useful for the method to be able to handle transom-stern ships. There has already been some experience with the use of the linear method in dealing with transom sterns. Conditions of continuity in the wave elevations and pressures at the transom stern and the free surface have been enforced, and some promising results have been obtained. Extensions with the present nonlinear method would therefore be forthcoming.

- **Computational efficiency:** For a typical commercial ship application, the program currently is running at a ratio of computational simulation time to real time in the order of 1000:1, with the linear programs in the order of 10:1. It is therefore important to improve the computational efficiency so that the program could be used in the actual designs of commercial ships. Previous chapters have discussed candidate schemes to increase the efficiency of the method, such as an $\mathcal{O}(N)$ algorithm for solving the boundary value problems or a matching scheme. Further research in these directions is necessary.

- **Six-degrees-of-freedom:** It should not be hard to extend the code to solve the fully nonlinear equation of motion in six-degrees-of-freedom. The lingering question would be whether the inclusion of the nonlinear terms in the equation of motion affects the numerical stability properties of the integration algorithms.

- **Slamming:** Slamming is a highly local nonlinear effect which evidently cannot be handle by this Weak-Scatterer approximation. Most studies to date treat the two-dimensional problem (cf. Zhao, Faltinsen and Aarsnes [76]). The study of a three-dimensional slamming model is needed. This could be derived from the present nonlinear ship motion method combined with the development of a localized three-dimensional treatment of the slamming region along the lines suggested in the above reference.

In conclusion, this work produces a robust and accurate numerical tool for naval architects at the analysis stage of designing a variety of ships. And it also provides the guidance in further development for more complex problems encountered in constructing modern commercial ships.

Appendix A

Discrete Integration Schemes and their Dispersion Relations

Consider a linearized free surface wave problem, that is governed by the linear free surface conditions,

$$\left\{ \begin{array}{l} \frac{\partial \phi}{\partial t} + U\frac{\partial \phi}{\partial x} = -g\zeta \\ \frac{\partial \zeta}{\partial t} + U\frac{\partial \zeta}{\partial x} = \frac{\partial \phi}{\partial z} \end{array} \right\}, \qquad \text{on} \quad z = 0, \tag{A.1}$$

and the Laplace equation, which is enforced by applying the Green's theorem,

$$\phi(\vec{x},t) - \iint_{S_F} \frac{\partial \phi}{\partial n}(\vec{\xi},t) G(\vec{x};\vec{\xi}) d\vec{\xi} = R(\vec{x},t), \tag{A.2}$$

where ϕ is the unknown and $R(\vec{x},t)$ is the right-handed forcing.

To solve these equations numerically, various schemes might be used. The discrete integration schemes and their related numerical dispersion relations are derived, and reproduced as follows,

- Fully Explicit Euler Scheme:

$$(\phi)_j^n B_{ij} - (\phi_z)_j^n S_{ij} = R_i^n, \tag{A.3}$$

$$\frac{(\phi)_j^{n+1} - (\phi)_j^n}{\Delta t} B_{ij} + U(\phi)_j^n D_{ij} = -g(\eta)_j^n B_{ij}, \tag{A.4}$$

$$\frac{(\eta)_j^{n+1}-(\eta)_j^n}{\Delta t}B_{ij}+U(\eta)_j^nD_{ij} = (\phi_z)_j^nB_{ij}. \quad (A.5)$$

$$W=\beta^2z^2-2(\beta^2+i\beta F_h\mathcal{D})z+(\beta^2+2i\beta F_h\mathcal{D}-F_h^2\mathcal{D}^2+\mathcal{S})=\mathcal{W}+\mathcal{O}(h^3,\Delta t). \quad (A.6)$$

- Fully Implicit Euler Scheme:

$$(\phi)_j^nB_{ij}-(\phi_z)_j^nS_{ij} = R_i^n, \quad (A.7)$$

$$\frac{(\phi)_j^{n+1}-(\phi)_j^n}{\Delta t}B_{ij}+U(\phi)_j^{n+1}D_{ij} = -g(\eta)_j^{n+1}B_{ij}, \quad (A.8)$$

$$\frac{(\eta)_j^{n+1}-(\eta)_j^n}{\Delta t}B_{ij}+U(\eta)_j^{n+1}D_{ij} = (\phi_z)_j^{n+1}B_{ij}. \quad (A.9)$$

$$W=(\beta^2-2i\beta F_h\mathcal{D}-F_h^2\mathcal{D}^2+\mathcal{S})z^2-2(\beta^2+i\beta F_h\mathcal{D})z+\beta^2=\mathcal{W}+\mathcal{O}(h^3,\Delta t). \quad (A.10)$$

- Emplicit Euler Scheme:

$$(\phi)_j^nB_{ij}-(\phi_z)_j^nS_{ij} = R_i^n, \quad (A.11)$$

$$\frac{(\phi)_j^{n+1}-(\phi)_j^n}{\Delta t}B_{ij}+U(\phi)_j^{n+1}D_{ij} = -g(\eta)_j^{n+1}B_{ij}, \quad (A.12)$$

$$\frac{(\eta)_j^{n+1}-(\eta)_j^n}{\Delta t}B_{ij}+U(\eta)_j^nD_{ij} = (\phi_z)_j^nB_{ij}. \quad (A.13)$$

$$W=(\beta^2-i\beta F_h\mathcal{D})z^2-(2\beta^2+F_h^2\mathcal{D}^2-\mathcal{S})z+(\beta^2+i\beta F_h\mathcal{D})=\mathcal{W}+\mathcal{O}(h^3,\Delta t). \quad (A.14)$$

- Trapezoidal Scheme:

$$(\phi)_j^nB_{ij}-(\phi_z)_j^nS_{ij} = R_i^n, \quad (A.15)$$

$$\frac{(\phi)_j^{n+1}-(\phi)_j^n}{\Delta t}B_{ij}+U\frac{(\phi)_j^{n+1}+(\phi)_j^n}{2}D_{ij} = -g\frac{(\eta)_j^{n+1}+(\eta)_j^n}{2}B_{ij}, \quad (A.16)$$

$$\frac{(\eta)_j^{n+1}-(\eta)_j^n}{\Delta t}B_{ij}+U\frac{(\eta)_j^{n+1}+(\eta)_j^n}{2}D_{ij} = \frac{(\phi_z)_j^{n+1}+(\phi_z)_j^n}{2}B_{ij}. \quad (A.17)$$

$$W=(\beta^2-i\beta F_h\mathcal{D}-\frac{F_h^2\mathcal{D}^2-\mathcal{S}}{4})z^2-(2\beta^2+\frac{F_h^2\mathcal{D}^2-\mathcal{S}}{4})z + (\beta^2+i\beta F_h\mathcal{D}-\frac{F_h^2\mathcal{D}^2-\mathcal{S}}{4})=\mathcal{W}+\mathcal{O}(h^3,\Delta t^2). \quad (A.18)$$

Appendix B

Generation of the Oval-Type Grid

The oval-type grid is a subset of the boundary-conforming grid system. The generation of such a system is accomplished by the determination of the curvilinear coordinates in the interior of a physical region from specified values (and/or slopes of the coordinates lines intersects the boundary) on the boundary of the physical region. In this study, the physical region is the free surface and the boundary is the ship waterline.

The field values of a function from prescribed boundary values may be obtained in a variety of ways, e.g., by interpolation between the boundaries. The solution of such a boundary-value problem, however, is a classic example of partial differential equations. Therefore, it is logical to take the coordinates to be the solutions of a system of partial differential equations. Since in this problem, the coordinates (and/or slopes) are specified on the entire closed boundary of the waterline hull surface, the equation must be elliptic.

The simplest elliptic partial differential system and one that does exhibit considerable smoothness is the Laplace equation:

$$\xi_{xx} + \xi_{yy} = 0, \tag{B.1}$$

$$\eta_{xx} + \eta_{yy} = 0, \tag{B.2}$$

where (x, y) is the grid point in the physical domain and (ξ, η) is the corresponding grid point in the computational domain. This Laplace system is essentially to control the mapping between the physical and transformed domains. And this one-to-one mapping is guaranteed by the extreme principles, i.e., that extrema of solutions cannot occur within the field, which are exhibited by elliptic systems. The Laplace system, however, lacks control on the coordinate line distribution in the field.

Another elliptic system, the Poisson equation:

$$\xi_{xx} + \xi_{yy} = P(\xi, \eta), \tag{B.3}$$

$$\eta_{xx} + \eta_{yy} = Q(\xi, \eta), \tag{B.4}$$

is able to exercise some degree of control on the spacing and orientation of the grid lines by specifying the control function (P, Q). Equations (B.3) and (B.4) are then transformed to the computational domain by interchanging (x, y) and (ξ, η). This yields a system of two elliptic equations in the form of,

$$\alpha x_{\xi\xi} - 2\beta x_{\xi\eta} + \gamma x_{\eta\eta} = -J^2(P x_\xi + Q x_\eta), \tag{B.5}$$

$$\alpha y_{\xi\xi} - 2\beta y_{\xi\eta} + \gamma y_{\eta\eta} = -J^2(P y_\xi + Q y_\eta), \tag{B.6}$$

where

$$\alpha = x_\eta^2 + y_\eta^2 \tag{B.7}$$

$$\beta = x_\xi x_\eta + y_\xi y_\eta \tag{B.8}$$

$$\gamma = x_\xi^2 + y_\xi^2 \tag{B.9}$$

$$J = \frac{\partial(x, y)}{\partial(\xi, \eta)} = x_\xi y_\eta - y_\xi x_\eta \tag{B.10}$$

This system of equations is solved on a uniformed-spaced grid (ξ, η) in the computational space for (x, y) coordinates of each point in the physical space. The derivatives are approximated by finite difference schemes and the system of equations are solved by an iterative algorithm.

Bibliography

[1] Baker, G.H., Meiron, D.I. and Orszag, S.A., (1981) "Application of a generalized vortex method to free surface flows", Proceedings of the *3rd International Conference on Numerical Ship Hydrodynamics*, Paris, France.

[2] Beck, R.F. and Magee, A.R., (1990) "Time domain analysis for predicting ship motions", Proceedings of the *IUTAM Symposium on Dynamics of Marine Vehicles and Structures in Waves*, London, UK.

[3] Beck, R.F., Cao, Y. and Lee, T.H., (1993) "Fully nonlinear time-domain computations of water waves problems using the desingularized method", Proceedings of the *6th International Conference on Numerical Ship Hydrodynamics*, Iowa City, IA.

[4] Bingham, H.B., Korsmeyer, F.T., Newman, J.N. and Osborne, G.E., (1993) "The simulation of ship motions", Proceedings of the *6th International Conference on Numerical Ship Hydrodynamics*, Iowa City, IA.

[5] Bingham, H.B., (1994) "Simulating ship motions in the Time domain", Ph.D. thesis, MIT.

[6] Cointe, R., Geyer, P., King, B., Molin, B. and Tramoni, M., (1990) "Nonlinear and linear motions of a rectangular barge in a perfect fluid", Proceedings of the *18th Symposium on Naval Hydrodynamics*, Ann Arbor, Michigan.

[7] Cummins, W.E., (1962) "The impulse response function and ship motions", *Schiffstechnik*, 9:101-109.

[8] van Daalen, E.F.G., (1993) "Numerical and theoretical studies of water waves and floating bodies", Ph.D. thesis, The University of Twente, The Netherlands.

[9] Dalzell, J.F., Thomas III, W.L. and Lee, W.T., (1986) "Correlations of model data with analytical load predictions for three high speed ships", *Department Report*, Ship Hydrodynamics Department, Naval Surface Warfare Center.

[10] Dawson, C.W., (1977) "A practical computer method for solving ship-wave problems", Proceedings of the *2nd International Conference on Numerical Ship Hydrodynamics*, Berkeley, CA.

[11] St. Denis, M. and Pierson, W.J., (1953) "On the motions of ships in confused seas", Transactions of the Society of Naval Architects and Marine Engineers, Vol. 61, pp. 280-357.

[12] Dommermuth, D.G. and Yue, D.K.P., (1987) "A high-order spectral method for the study of nonlinear gravity waves", *Journal of Fluid Mechanics*, Vol. 184, pp. 267-288.

[13] Fornberg, B. and Whitham, G.B., (1978) "A numerical and theoretical study of certain nonlinear wave phenomena", *Philosophical Transactions of the Royal Society*, Vol. A289, pp. 373-404.

[14] Froude, W. (1861) "On the rolling of ships", Transactions of the Institute of Naval Architecture, Vol. 2, pp. 180-229.

[15] Gadd, G.E., (1976) "A method of computing the flow and surface wave pattern around full forms", Transactions of Royal Association of Naval Architects, Vol. 113.

[16] Gerritsma, J., Beukelman, W. and Glansdorp, C., (1974) "The effects of beam on the hydrodynamic characteristics of ship hulls", Proceedings of the *10th Symposium on Naval Hydrodynamics*, Cambridge, MA.

[17] Grosenbaugh, M.A. and Yeung, R.W., (1989) "Nonlinear free-surface flow at a two-dimensional bow", *Journal of Fluid Mechanics*, Vol. 209, pp. 57-75.

[18] Hess, J.L. and Smith, A.M.O., (1962) "Calculation of non-lifting potential flow about arbitrary three-dimensional bodies", *Technical Report No. E.S. 40622*, Douglas Aircraft Co., Inc., Long Beach, CA.

[19] Israeli, M. and Orszag, S.A., (1981) "Approximation of radiation boundary conditions", *Journal of Computational Physics*, Vol. 41.

[20] Jensen, G., Bertram, V. and Söding, H., (1988) "Ship wave resistance computations", Proceedings of the *5th International Conference on Numerical Ship Hydrodynamics*, Hiroshima, Japan.

[21] Kim, M.H. and Yue, D.K.P., (1989) "The complete second-order diffraction solution for an axisymmetric body, Part 1: monochromatic incident waves", *Journal of Fluid Mechanics*, Vol. 200, pp. 235-264.

[22] Kim, M.H. and Yue, D.K.P., (1990) "The complete second-order diffraction solution for an axisymmetric body, Part 2: bichromatic incident waves and body motions", *Journal of Fluid Mechanics*, Vol. 211, pp. 557-593.

[23] King, B.W., (1987) "Time domain analysis of wave exciting forces on ships and bodies", *Technical Report 306*, The Department of Naval Architecture and Marine Engineering, The University of Michigan.

[24] King, B.W., Beck, R.F., and Magee, A.R., (1988) "Seakeeping calculations with forward speed using time domain analysis", Proceedings of the *17th Symposium on Naval Hydrodynamics*, The Hague, Netherlands.

[25] Korsmeyer, F.T., (1988) "The first and second-order transient free surface wave radiation problems", Ph.D. thesis, MIT.

[26] Korvin-Kroukovsky, B.V. and Jacobs, W.R., (1957) "Pitching and heaving motions of a ship in regular waves", Trans. SNAME, Vol. 65.

[27] Kring, D.C., (1994) "Time domain ship motions by a three-dimensional Rankine Panel Method", Ph.D. thesis, MIT.

[28] Kring, D.C. and Sclavounos, P.D., (1995) "Numerical Stability Analysis for Time Domain Ship Motion Simulations", *Journal of Ship Research*, Vol. 39, No. 4, pp 321-327.

[29] Kring, D.C., Huang, Y. and Sclavounos, P.D., (1995) "Time Domain Ship Motions with a Nonlinear Extension", Proceedings of the *10th International Workshop on Water Waves and Floating Bodies*, Oxford, UK.

[30] Kring, D.C., Huang, Y., Sclavounos, P.D., Vada, T. and Braathen, A., (1996) "Nonlinear Ship Motions and Wave Induced Loads by a Rankine Panel Method", Proceedings of the *21th Symposium on Naval Hydrodynamics*, Trondheim, Norway.

[31] Krylov, A., (1896) "A new theory of the pitching motion of ships on waves", Transactions of the Society of Naval Architects and Marine Engineers, Vol. 37, pp. 326-368.

[32] Lewis, F.M., (1929) "The inertia of water surrounding a vibrating ship", Transactions of the Society of Naval Architects and Marine Engineers, Vol. 37, pp. 1-20.

[33] Liapis, S.J. (1986) "Time domain analysis of ship motions", *Technical Report 302*, The Department of Naval Architecture and Marine Engineering, The University of Michigan.

[34] Lin, W.M. and Yue, D.K.P., (1990) "Numerical solutions for large-amplitude ship motions in time domain", Proceedings of the *18th Symposium on Naval Hydrodynamics*, Ann Arbor, Michigan.

[35] Liu, Y. and Yue, D.K.P., (1993) "On the solution near the critical frequency for an oscillating and translating body in or near a free surface", *Journal of Fluid Mechanics*, Vol. 254, pp. 251-266.

[36] Longuet-Higgins, M.S. and Cokelet, E.D., (1976) "The deformation of steep surface waves on water (I) — A numerical method of computation", Proceedings of *the Royal Society of London*, Series A, 350:1-26.

[37] Maruo, H., (1970) "An improvement of the slender body theory for oscillating ships with zero forward speed", Bulletin of The Faculty of Engineering at Yokohama National University, Japan.

[38] Maskew, B., (1992) "Prediction of nonlinear wave/hull interactions on complex vessels", Proceedings of the 19th Symposium on Naval Hydrodynamics, Seoul, Korea.

[39] Mastin, C.W. and Thompson, J.F., (1978) "Elliptic systems and numerical transformations", *Journal of Mathematical Analysis and Applications*, Vol. 62.

[40] Michell, J.H., (1898) "The wave resistance of a ship", Philos. Mag. [5], Vol. 45, pp. 106-123.

[41] Nabors, K., Phillips, J., Korsmeyer, F.T. and White, J., (1996) "Domain-based parallelism and problem decomposition methods in science and engineering", *SIAM*, edited by Keyes, D.E, Saad, Y. and Truhlar, D.G., Philadelphia, PA.

[42] Nakos, D.E., (1990) "Ship wave patterns and motions by a three dimensional Rankine Panel Method", Ph.D. thesis, MIT.

[43] Nakos, D.E., and Sclavounos, P.D. (1990) "Steady and unsteady ship wave patterns", *Journal of Fluid Mechanics*, Vol. 215.

[44] Nakos, D.E., Kring, D.C. and Sclavounos, P.D., (1993) "Rankine panel methods for transient free surface flows", Proceedings of the *6th International Conference on Numerical Ship Hydrodynamics*, Iowa City, IA.

[45] Nakos, D.E., (1993) "Stability of transient gravity waves on a discrete free surface", MIT Report.

[46] Nakos, D.E. and Sclavounos, P.D., (1994) "Kelvin wakes and wave resistance of cruiser- and transom-stern ships", *Journal of Ship Research*, Vol. 38, No. 1, pp. 9-29.

[47] Newman, J.N., (1961) "A linearized theory for the motion of a thin ship in regular waves", *Journal of Ship Research*, Vol. 3, pp. 1-19.

[48] Newman, J.N. and Tuck, E.O., (1964) "Current progress in the slender-body theory of ship motions", Proceedings of the 5th Symposium on Naval Hydrodynamics, Washington, DC.

[49] Newman, J.N., (1977) "Marine Hydrodynamics", The MIT Press, Cambridge, MA.

[50] Newman, J.N., (1978) "Wave radiation from slender bodies", Proceedings of the *Symposium on Applied Mathematics*, dedicated to the Late Professor: Dr. R. Timman., Sijthoff & Nordhoff, Groningen.

[51] Newman, J.N., (1978) "The theory of ship motions", *Advances in Applied Mechanics*, Vol. 18.

[52] Newman, J.N., (1986) "Distribution of sources and normal dipoles over a quadrilateral panel", *Journal of Engineering Mathematics*, Vol. 20.

[53] Ogilvie, T.F., (1964) "Recent progress toward to the understanding and prediction of ship motions", Proceedings of the *5th Symposium on Naval Hydrodynamics*, Bergen, Norway.

[54] Ogilvie, T.F. and Tuck, E.O., (1969) "A rational strip theory for ship motions", Part 1, *Technical Report 013*, The Department of Naval Architecture and Marine Engineering, The University of Michigan.

[55] Ogilvie, T.F., (1983) "Second-order hydrodynamic effects on ocean platforms", Proceedings of the *International Workshop on Ship and Platform Motions*, University of California, Berkeley.

[56] Pawlowski, J., (1992) "A nonlinear theory of ship motions in waves", Proceedings of the *19th Symposium on Naval Hydrodynamics*, Seoul, Korea.

[57] Peters, A.S. and Stoker, J.J., (1957) "The motion of a ship, as a floating rigid body, in a seaway", *Communications on Pure and Applied Mathematics*, Vol. 10, pp. 339-490.

[58] Raven, H.C., (1992) "A practical nonlinear method for calculating ship wavemaking and wave resistance", Proceedings of the *19th Symposium on Naval Hydrodynamics*, Seoul, Korea.

[59] Salvesen, N., Tuck, E. O. and Faltinsen, O., (1970) "Ship motions and sea loads", *Trans. SNAME*, Vol. 78.

[60] Sclavounos, P.D., (1984) "The unified slender-body theory: ship motions in waves", Proceedings of *15th Symposium on Naval Hydrodynamics*, Hamburg, Germany.

[61] Sclavounos, P.D. and Nakos, D.E., (1988) "Stability analysis of panel methods for free surface flows with forward speed", Proceedings of *17th Symposium on Naval Hydrodynamics*, Den Hague, The Netherlands.

[62] Sclavounos, P.D., (1988) "Radiation and diffraction of second-order surface waves by floating bodies", *Journal of Fluid Mechanics*, Vol. 196, pp. 65-91.

[63] Sclavounos, P.D., Nakos, D.E., and Huang, Y., (1993) "Seakeeping and wave induced loads on ship with flare by a Rankine Panel Method" Proceedings of the *6th International Conference on Numerical Ship Hydrodynamics*, Iowa City, IA.

[64] Sclavounos, P. D., (1995) "Computation of wave ship interactions" *Advances in Marine Hydrodynamics*, edited by M. Ohkusu, Computational Mechanics Publications.

[65] Thompson, J.F., Warsi, Z.U.A. and Mastin, C.W., (1985) "Numerical grid generation", North-Holland, Elsevier Science Publishing Co., Inc..

[66] Timman, R. and Newman, J.N., (1962) "The couples damping coefficients of symmetric ships", *Journal of Ship Research*, Vol. 5, No. 4.

[67] Trefethen, L.N., (1990) "Approximation theory and numerical linear algebra", *Algorithms for approximation II*, edited by Mason, J.C. and Cox, M.G., Chapman & Hall.

[68] Tulin, M.P., (1957) "The theory of slender surfaces planing at high speeds", *Schiffstechnik*, 4.

[69] Ursell, F., (1962) "Slender oscillating ships at zero forward speed", *Journal of Fluid Mechanics*, Vol. 19, pp. 496-516.

[70] Vada, T. and Nakos, D.E., (1993) "Time-marching schemes for ship motion simulations", Proceedings of the *8th International Workshop on Water Waves and Floating Bodies*, St. John's, Newfoundland, Canada.

[71] Vinje, T. and Brevig, P., (1981) "Nonlinear two-dimensional ship motion", Proceedings of the *3rd International Conference on Numerical Ship Hydrodynamics*, Paris, France.

[72] Wehausen, J.V. and Laitone, E.V., (1960) "Surface waves", *Handbook der Physic*, Vol. 9, pp. 446-778, Springer-Verlang, Berlin, Germany.

[73] Xü, H. and Yue, D.K.P., (1992) "Computations of fully-nonlinear three-dimensional water waves", Proceedings of the *19th Symposium on Naval Hydrodynamics*, Seoul, Korea.

[74] Xue, M. and Yue, D.K.P., (1995) "Fully nonlinear three dimensional interaction between water waves and a surface-piercing body", Proceedings of the *10th International Workshop on Water Waves and Floating Bodies*, Oxford, UK.

[75] Zakharov, V.E., (1968) "Stability of periodic waves of finite amplitude on the surface of a deep fluid", *Journal of Applied Mechanics and Technical Physics*, Vol. 9, pp. 190-194 (English Translation).

[76] Zhao, R., Faltinsen, O. and Aarsnes, J., (1996) "Water entry of arbitrary two-dimensional sections with and without flow separation", Proceedings of the *19th Symposium on Naval Hydrodynamics*, Trondheim, Norway.